

Study on Simplified Speed Sensorless Vector Control Systems for Induction Motors

February 2015

Graduate School of Engineering
Nagasaki University

Glanny Martial Christiaan Mangindaan

CONTENTS

Chapter 1 Introduction

1.1 Background	1
1.2 Content of Chapters	8

Chapter 2 Models of Induction Motor

2.1 Space Vector Representation of Induction Motor	10
2.2 $d - q$ Model	19
2.3 Electromagnetic Torque	23
2.4 Non – linear State Equation	25
2.5 Linear State Equation	26

Chapter 3 Speed Sensorless Vector Control Systems

3.1 Proposed System A	28
3.1.1 Block Diagram of System A	28
3.1.2 Description of System	32
3.1.3 Steady – state Analysis	35
3.1.4 Linear Model	39
3.2 Proposed System B	44
3.2.1 Block Diagram of System B	44
3.2.2 Description of System	46

3.2.3	Steady – state Analysis	47
3.2.4	Linear Model	48
3.3	Gain Selection of Controller	51
3.3.1	Current Controller	51
3.3.2	Speed Controller	53
Chapter 4	Simulation and Experimental Results	
4.1	Experimental System	55
4.1.1	Microcomputer Control System	55
4.1.2	Parameters of System	59
4.1.3	Experimental IM – DCM System	62
4.2	System Stability	66
4.3	Simulation Results	75
4.4	Experimental Results	84
Chapter 5	Conclusion	96
References	99

Chapter 1

Introduction

1.1 Background

The induction motors (IM) are very common and easy to find, because it is low in price and robust. Those are used in industrial applications such as electric train, pump, fan, machine tools, grinders, conveyors and home utilizations. Conventionally, till the last of the twentieth century, the induction motors are operated at a single speed, which is determined by the frequency of main voltage and the number of poles. Typically, they were operated from fixed-frequency sources 50 Hz or 60 Hz in most cases.

To control the IM speed, a variable-frequency source is required, and such kind source did not readily exist. Thus, applications necessitating variable speed were serviced by direct-current motors (DCM). So, controlling the speed of IM is more difficult than controlling the speed of DCM, because the relationship between the motor current and the resulting torque is not linear for IM.

The availability of solid-state power switches, development of power electronics and microelectronics change this scheme hugely. Recently developed solid-state power device such as insulated gate bipolar transistors (IGBT), metal-oxide semiconductor field-effect transistors (MOSFET) are applied to many favorable switches with wide range power ratings and switching frequency that make them suitable candidates for variable-frequency generation. Now the power electronics are capable for supplying the variable voltage/current, or frequency drive to realize variable-speed

performance for IM. About the microelectronics, a digital signal processor (DSP) has been developed. By using C language, control algorithm is programmed and realized without adding hardware.

Recently, to reduce the pollution problem in urban area and the availability of fossil fuel, the electric car is getting attention; but because of the limited performance of the battery as an energy storage, it would take considerable time to use pure electric car commonly. Many of electric cars use interior permanent magnet synchronous motor (IPMSM) from the viewpoint of motor efficiency. However, it is interesting that the Tesla Company uses the IM for electric car.

According to the development of pulse width modulation (PWM) inverter, the constant volt per hertz (V/f) control is applied at first as variable-speed control method for IM. However, the constant V/f control cannot control torque instantaneously. On the other hand, the vector control (or field oriented control) can control torque instantaneously and control speed of IM quickly. In order to realize vector control, the information of rotor flux angle is indispensable. In order to estimate the rotor flux angle, the angular frequency is computed by adding the rotor speed to the slip angular frequency. The slip angular frequency is obtained from a current model of IM by assuming that the q – axis flux becomes zero. The rotor flux angle is obtained by integrating the angular frequency. Many researches for rotor resistance identification are reported to compute accurate the slip frequency [10], [16], [20], [21].

By using the rotor flux angle, the three phases currents are transformed to two-axis ($d - q$) currents. In general, the d – axis is selected as the direction of rotor flux vector. Therefore, the d – axis current is proportional to the magnitude of the rotor flux. The electromagnetic torque is proportional to the product of d – and q – axis currents. By controlling the d –

and q – axis currents quickly, the torque is produced instantaneously without transient. In general, this currents control are achieved by PI control through voltage control by PWM inverter. At steady – state the d and q variables become constant. The d and q currents correspond to the field current and the armature current of DCM respectively.

However, the use of such direct speed sensor induces additional electronics, extra wiring, extra space, frequent maintenance, careful mounting and default probability. The use of speed sensor has problems occurred, mainly in harsh environment. Moreover, the speed sensor is sensitive for electromagnetic noise in hostile environments and has a limited temperature range. To avoid mechanical sensor (speed and position) of IM, several methods called sensorless vector control is used. In order to simplify the hardware, the speed sensorless vector control is studied and applied in practical uses.

In order to improve the performance of induction motor control without speed sensor, many model reference adaptive system (MRAS) based methods are studied. Representative speed estimation is MRAS based method proposed by Schauder [1]. Figure 1.1 shows the two independent simulators are constructed to estimate the component of the rotor flux vector. Hence, voltage model does not involve the quantity of rotor electrical-angular speed, this model is used as a reference model, and current model which does involve rotor electrical-angular speed is used as an adjustable model. The errors between the states of the two models are used to derive a proper adaptation mechanism that generates the estimation of rotor electrical-angular speed for the adjustable model. The terminal currents and voltages are measured and transformed to $\alpha - \beta$ variables. However, the vector control system using MRAS speed estimate is composed independently. Therefore, the system becomes complex. The speed estimation using flux simulator is

used for flux observer-based field-orientation (FOFO) controller [2]. The motor speed is estimated by comparing the output fluxes of two simulators. Its estimated speed is in good agreement with actual speed at high speed, but it has transient error in the lower speed.

The full-order observer is proposed in [3], [5], [22], [26]-[29]. Kubota estimates the $\alpha - \beta$ stator currents and $\alpha - \beta$ rotor fluxes in stationary reference frame [3], [5], [22]. The speed is estimated by using these variables. The vector rotator calculates the stator current command by using information from the flux angle from the observer. The influence of stator resistance variation on the speed estimation and the torque control at low speed region is minimized by identifying it.

The flux observer based sensorless system has an unstable region in the regenerating mode at low speeds. To remedy the problem, Hinkkanen proposed a modified speed-adaptation law [28]. Instead of using only the current estimation error perpendicular to the estimated flux, the parallel component is also exploited in the regenerating mode.

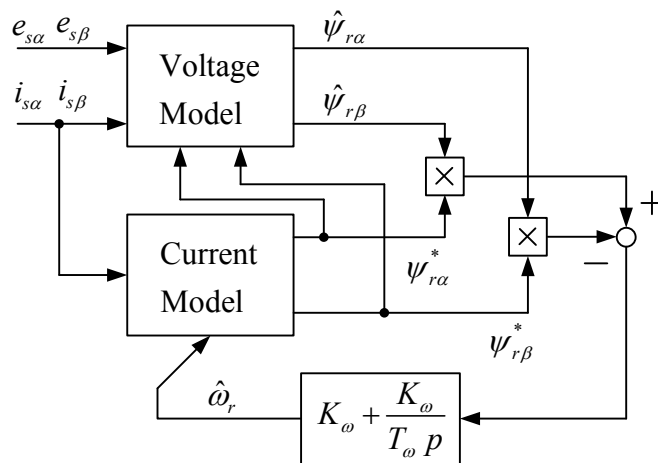


Fig. 1.1 Model reference adaptive system (MRAS) proposed by Schauder [1].

Design strategy of both observer gains and speed estimation gains for an adaptive full-order observer based sensorless system is necessary issue to assure the stability and the tracking performance. Suwankawin proposed a design of observer gains to achieve the stability over the whole operation especially in the low-speed region, including the regenerating operation [26]. The speed estimation gains are designed by considering the ramp response of the speed estimator. There is still an unstable region of experimental result in plugging region.

Tursini proposed an adaptive speed-sensorless field-oriented control of an induction motor, based on a sliding-mode observer [24]. Using the voltage equation, the observer computes the stator current and the rotor fluxes in $\alpha - \beta$ stationary reference frame. In the case of sliding-mode observer, it is considered that the observer gains are very large. The rotor speed estimation is obtained by using relation with a Lyapunov function. The system performance with different observer gains and the influence of the motor parameters deviations are shown. Sliding-mode full-order observer also are reported in [25], [30].

Tsuji proposed a speed estimation method by using q -axis flux [15], [39], [40]. This method is based on a reduce order flux observer and the adaptive control method. The q - axis rotor flux converges to zero for speed estimation. To solve the pure integral problem of flux computation using the voltage model, a flux-observer modified by a current model is applied. The method is constructed by using synchronously rotating reference frame which is on the flux of current model. The fluxes from the current model becomes simple by defining $d - q$ axis, and all fluxes quantities of current model and voltage model are in DC form. By using DC form, the system stability is easily analyzed. Fig.1.2 shows the system proposed by Tsuji. The q - axis

rotor flux is used to estimate the rotor speed by using PI controller. The flux is an output of flux-observer.

Another reduced-order observer-based sensorless method are discussed by Harnefors [31], [32]. By using the flux electromotive forces (EMF) of the voltage model and current model, the reduce-order observer for the rotor flux is considered. The rotor speed is estimated by the EMF and rotor flux. The reduced-order observer is simpler than the full-order observer.

Manipulated design of the observer can improve the stability of the sensorless system even at low speed regenerating operation. However, the configurations of these systems are relatively complicated. It is because the MRAS based methods need state observer and many PI controllers ($d - q$ currents, speed and speed estimation). On the other hand, some simplified speed sensorless vector controls are proposed.

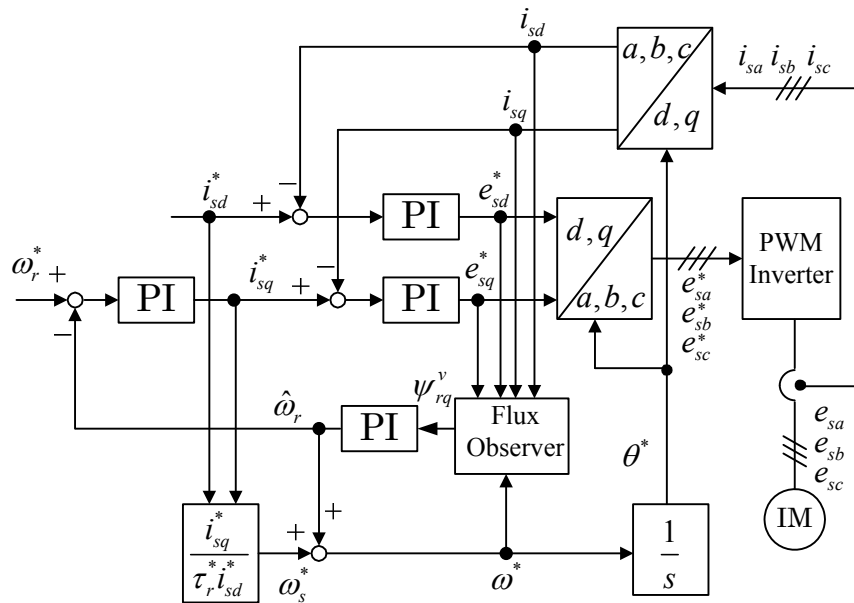


Fig. 1.2 Flux observer proposed by Tsuji [39].

Simplifying the system configuration by removing the current regulators is proposed [33], and the stability is improved by adding a flux-stabilizing controller using derivative of magnetic current [34]. However, these papers have no information about the stability of regenerating mode. A sensorless method using the induced d – axis and q – axis voltage obtained by a voltage model has been proposed [35], and a similar method is applied to railway vehicle traction [36]. However, the stable region is not clear in these papers. Furthermore, a primary flux control method are proposed in [17], [37] and the stability is improved at regenerating mode [38]. Simple method of stator – flux orientation is proposed in [23]. Some survey papers for IM sensorless control systems are reported in [4], [9], [18]. Parameter estimation of stator and rotor resistances are also important problem for the sensorless systems [6], [11].

In this thesis, a new simplified speed-sensorless vector control method of IM based on q – axis rotor flux is proposed [41] – [44]. A flux vector is obtained from voltage model, in which the derivative term is neglected. A flux angle of a current model must be aligned with the flux angle of voltage model. Since the output voltage of d – axis PI current controller is used for the flux angle estimation and speed control (q –axis voltage control), the system is simplified and stabilized at regenerating mode [41]. In conventional simplified methods, this scheme is not reported. A linear model of the proposed system in the state space equation is obtained to study the system stability by showing root loci. By virtue of the stability analysis, we can design the parameters of controller. The nonlinear simulation and experimental results of the proposed system show stable transient responses in both motoring and regenerating modes [43]. In order to improve the system stability at plugging region, a PI speed controller is studied instead of original I (integral) controller [42]. Furthermore, a simplified sensorless system that

uses a PI q - axis current controller and estimates the rotor speed is studied and compared [44].

1.2 Contents of Chapters

This thesis is divided into five chapters with the arrangement:

In chapter 1, the background and the purpose of this research are explained and the contents of chapters are specified.

Chapter 2 describes a space vector representation of induction motor. A three-phase mathematical model of induction motor is transformed to a $d - q$ model by using two-axis theory. This chapter introduces a non-linear model and a linear model of induction motor. The linear model of induction motor is derived by considering small perturbations at a steady state operating point.

In chapter 3, new simplified speed-sensorless vector control methods of IM based on rotor flux linkage are proposed . The two simplified sensorless systems are called as system A and system B. The main difference is the presence (in system A) or the absence (in system B) of $q -$ axis PI current controller. In system A, the angular frequency of rotor flux is estimated to bring q -axis flux to zero by using PI controller. The $q -$ axis flux is obtained by the output of $d -$ axis PI current controller with a non-interference control. The rotor speed is computed by subtracting a slip speed from the angular frequency. Flux angle is obtained by integrating the angular frequency. When $q -$ axis flux is larger (smaller) than zero and rotor flux is leading (lagging) than $d -$ axis, the controller must increase (decrease) the value of flux frequency. In system B, the computation of $q -$ axis flux is as same as the system A. The angular frequency of rotor flux is computed by adding the $q -$ axis flux to the speed command. The $q -$ axis flux is also used to control the rotor speed, by adjusting the $q -$ axis voltage. Non-linear models are derived

in both proposed systems A and B. From these non-linear models, linear models of the systems are derived in state space equations. The selection of PI current and speed controllers gains are outlined.

Chapter 4 demonstrates systems stability by showing the root loci obtained by the linear models, the transient responses of simulation results and the stable regions. The performance of both systems A and B are compared by using linear models and non-linear models. Transient responses of linear and non-linear models are computed and compared. Since both responses are almost same around a steady state operating point, the validity of the linear models are confirmed. By using the proposed methods, not only the motoring operation but also the low speed regenerating operation can be stabilized. Quick torque and speed responses of nonlinear models are obtained in both systems A and B. A digital signal processor based PWM inverter fed IM system is equipped and tested. It is confirmed that the experimental results are very close to those of simulation. Therefore, the effectiveness of the proposed methods are also demonstrated experimentally. It is considered that the system B is superior to the system A because its simple structure.

Chapter 5 is the conclusions presented in this thesis.

Chapter 2

Models of Induction Motor

2.1 Space Vector Representation of Induction Motor

For convenience of proposed systems analysis, the models of IM are outlined. In order to analyze the IM, it must be embodied in three-phase mathematical model. From three-phase model, the IM is simplified into two-phase by using the two-axis transformation [12], [13], [14].

To show windings configuration and to calculate inductances, the cross-section of simplified three-phase IM with two-poles is shown in Fig.2.1. The winding configurations are assumed the same to each phases of both the stator and the rotor. The winding of three-phase IM is separated by 120 electrical degrees with respect to each other as shown by the coils $a-a^*$, $b-b^*$ and $c-c^*$.

Fig.2.2 shows a circuit model of the three-phase IM with two-poles. An equivalent three-phase winding is used in case of short-circuited squirrel-cage rotor. The stator and rotor windings are wye connected. The a_s , b_s and c_s mean the axes of stator a , b and c phase winding respectively. The angle θ_r is an angular displacement of a -phase rotor winding axis from the axis a_s . By using the rotational angular velocity ω_r , the angle θ_r is expressed as

$$\theta_r = \int_0^t \omega_r dt + \theta_r(0) \dots\dots\dots (2.1)$$

The stator winding of IM is fundamentally the same as for a synchronous motor. In the below equations, the subscript s denotes variables and parameters associated with the stator circuits, and the subscript r denotes variables and parameters associated with the rotor circuits.

In Fig.2.2 (b), the leakage inductance at stator and rotor windings are l_s and l_r respectively. The mutual inductances M_{sr} has the relation with self-inductances L_{ss} and L_{rr} as follows:

$$L_{ss} L_{rr} = M_{sr}^2 \quad \dots\dots\dots (2.2)$$

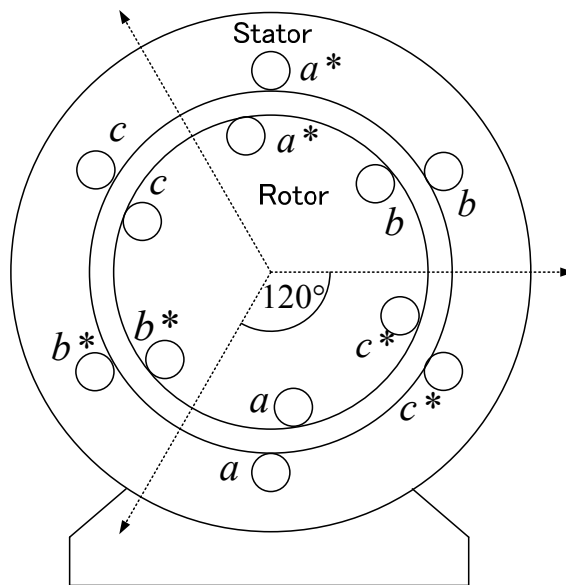
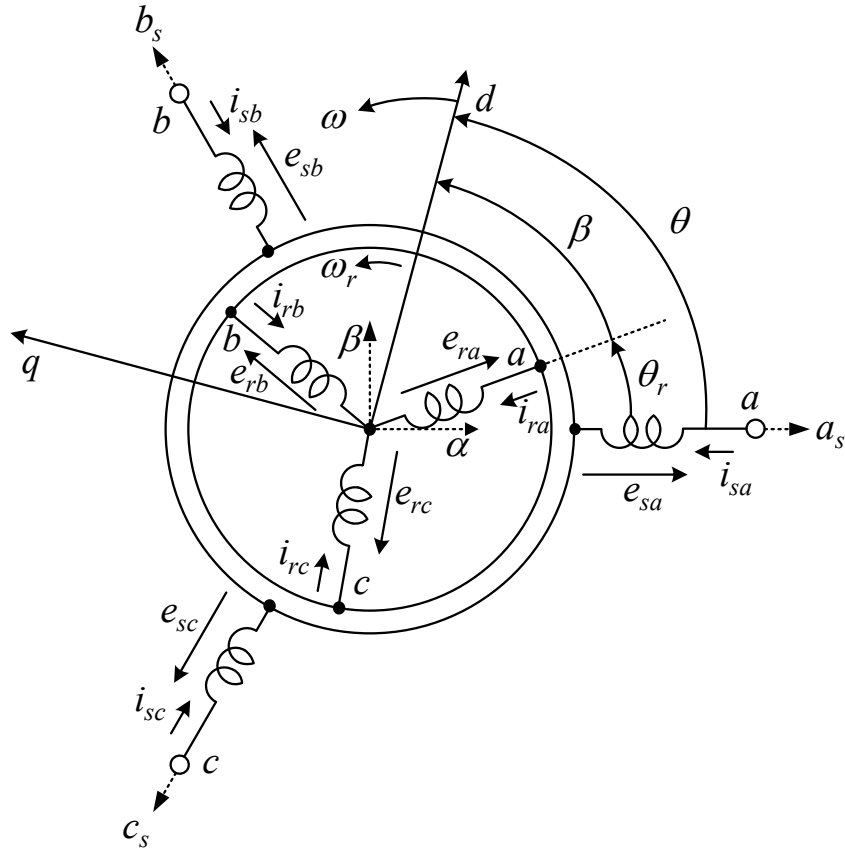
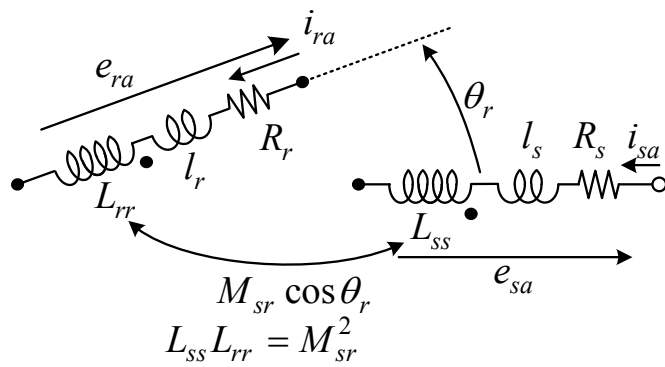


Fig. 2.1 Three-phase stator and rotor windings of IM.



(a) Definitions of axes.



(b) Definition of circuit parameters.

Fig.2.2 Circuit model of three-phase IM with $d - q$ axis.

The mutual inductance between stator and rotor changes when the rotor moves by the angle θ_r . The rotor a -phase current i_{ra} generates flux in the stator a -phase winding as shown in Fig2.3. If $\theta_r = 0$, all flux by i_{ra} passes L_{ss} and the mutual inductance is M_{sr} . As the cosine component of the flux by i_{ra} passes L_{ss} , the mutual inductance becomes $M_{sr} \cos \theta_r$. The flux linkages in three-phase windings of the stator and the rotor are defined as $\psi_{sa}, \psi_{sb}, \psi_{sc}$ and $\psi_{ra}, \psi_{rb}, \psi_{rc}$ respectively. By considering the cosine component of the angle of the winding, we can obtain the flux linkages of $\psi_{sa}, \psi_{sb}, \psi_{sc}, \psi_{ra}, \psi_{rb}, \psi_{rc}$ as follows:

$$\begin{aligned}
 \begin{bmatrix} \psi_{sa} \\ \psi_{sb} \\ \psi_{sc} \end{bmatrix} &= \begin{bmatrix} l_s + L_{ss} & -L_{ss}/2 & -L_{ss}/2 \\ -L_{ss}/2 & l_s + L_{ss} & -L_{ss}/2 \\ -L_{ss}/2 & -L_{ss}/2 & l_s + L_{ss} \end{bmatrix} \begin{bmatrix} i_{sa} \\ i_{sb} \\ i_{sc} \end{bmatrix} \\
 &+ M_{sr} \begin{bmatrix} \cos \theta_r & \cos \left(\theta_r + \frac{2}{3} \pi \right) & \cos \left(\theta_r - \frac{2}{3} \pi \right) \\ \cos \left(\theta_r - \frac{2}{3} \pi \right) & \cos \theta_r & \cos \left(\theta_r + \frac{2}{3} \pi \right) \\ \cos \left(\theta_r + \frac{2}{3} \pi \right) & \cos \left(\theta_r - \frac{2}{3} \pi \right) & \cos \theta_r \end{bmatrix} \begin{bmatrix} i_{ra} \\ i_{rb} \\ i_{rc} \end{bmatrix} \dots \quad (2.3)
 \end{aligned}$$

$$\begin{bmatrix} \psi_{ra} \\ \psi_{rb} \\ \psi_{rc} \end{bmatrix} = \begin{bmatrix} l_r + L_{rr} & -L_{rr}/2 & -L_{rr}/2 \\ -L_{rr}/2 & l_r + L_{rr} & -L_{rr}/2 \\ -L_{rr}/2 & -L_{rr}/2 & l_r + L_{rr} \end{bmatrix} \begin{bmatrix} i_{ra} \\ i_{rb} \\ i_{rc} \end{bmatrix} \\
+ M_{sr} \begin{bmatrix} \cos \theta_r & \cos \left(\theta_r - \frac{2}{3} \pi \right) & \cos \left(\theta_r + \frac{2}{3} \pi \right) \\ \cos \left(\theta_r + \frac{2}{3} \pi \right) & \cos \theta_r & \cos \left(\theta_r - \frac{2}{3} \pi \right) \\ \cos \left(\theta_r - \frac{2}{3} \pi \right) & \cos \left(\theta_r + \frac{2}{3} \pi \right) & \cos \theta_r \end{bmatrix} \begin{bmatrix} i_{sa} \\ i_{sb} \\ i_{sc} \end{bmatrix} \dots \quad (2.4)$$

By using the flux linkages, the following voltage equations are obtained for stator and rotor windings.

$$\begin{bmatrix} e_{sa} \\ e_{sb} \\ e_{sc} \end{bmatrix} = R_s \begin{bmatrix} i_{sa} \\ i_{sb} \\ i_{sc} \end{bmatrix} + p \begin{bmatrix} \psi_{sa} \\ \psi_{sb} \\ \psi_{sc} \end{bmatrix} \dots \dots \dots \quad (2.5)$$

$$\begin{bmatrix} e_{ra} \\ e_{rb} \\ e_{rc} \end{bmatrix} = R_r \begin{bmatrix} i_{ra} \\ i_{rb} \\ i_{rc} \end{bmatrix} + p \begin{bmatrix} \psi_{ra} \\ \psi_{rb} \\ \psi_{rc} \end{bmatrix} \dots \dots \dots \quad (2.6)$$

where, p means d/dt , R_s and R_r is stator resistance and rotor resistance respectively.

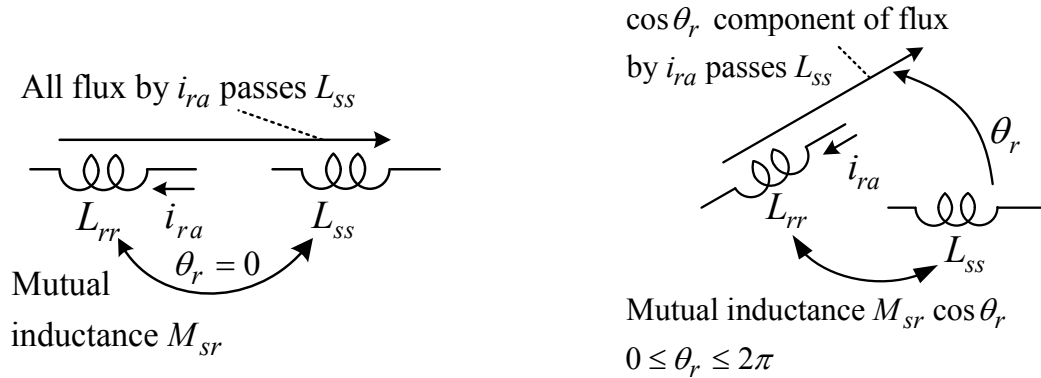


Fig.2.3 Mutual inductance of windings.

In stationary reference frame, by considering cosine components of the angle that is formed between the winding axis and $\alpha - \beta$ axis as shown in Fig.2.4, the $\alpha - \beta$ components $f_{s\alpha}$ and $f_{s\beta}$ for the stator side are obtained. The f means voltage, current and flux linkage. The space vector is defined as

$$\dot{f}_s = f_{s\alpha} + j f_{s\beta} \quad \dots\dots\dots (2.7)$$

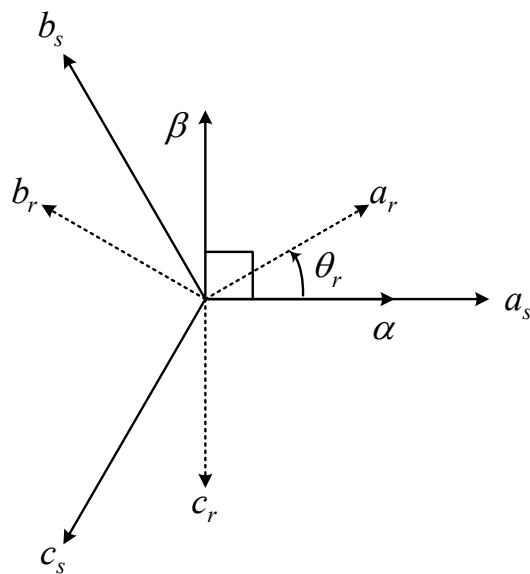


Fig.2.4 $\alpha - \beta$ stationary reference frame.

then,

$$\dot{f}_s = \sqrt{\frac{2}{3}} \left(f_{sa} + e^{j\frac{2}{3}\pi} f_{sb} + e^{-j\frac{2}{3}\pi} f_{sc} \right) \quad \dots\dots\dots (2.8)$$

For the rotor side, the following equations are defined:

$$\begin{bmatrix} f_{r\alpha} \\ f_{r\beta} \end{bmatrix} = \sqrt{\frac{2}{3}} \begin{bmatrix} \cos \theta_r & \cos(\theta_r + \frac{2}{3}\pi) & \cos(\theta_r - \frac{2}{3}\pi) \\ \sin \theta_r & \sin(\theta_r + \frac{2}{3}\pi) & \sin(\theta_r - \frac{2}{3}\pi) \end{bmatrix} \begin{bmatrix} f_{ra} \\ f_{rb} \\ f_{rc} \end{bmatrix} \quad \dots\dots\dots (2.9)$$

By using $f_{r\alpha}$ and $f_{r\beta}$, the space vector is defined as

$$\dot{f}_r = f_{r\alpha} + j f_{r\beta} \quad \dots\dots\dots (2.10)$$

then,

$$\dot{f}_r = \sqrt{\frac{2}{3}} e^{j\theta_r} \left(f_{ra} + e^{j\frac{2}{3}\pi} f_{rb} + e^{-j\frac{2}{3}\pi} f_{rc} \right) \quad \dots\dots\dots (2.11)$$

The space vector of stator voltage is expressed as

$$\dot{e}_s = \sqrt{\frac{2}{3}} (e_{sa} + e^{j\frac{2}{3}\pi} e_{sb} + e^{-j\frac{2}{3}\pi} e_{sc}) \quad \dots\dots\dots (2.12)$$

From (2.5), we have

$$\dot{e}_s = R_s \dot{i}_s + p \dot{\psi}_s \quad \dots\dots\dots (2.13)$$

The stator flux linkage is computed from (2.3) as

$$\begin{aligned} \dot{\psi}_s &= \sqrt{\frac{2}{3}} (\psi_{sa} + e^{j\frac{2}{3}\pi} \psi_{sb} + e^{-j\frac{2}{3}\pi} \psi_{sc}) \\ &= (l_s + L_{ss}) \dot{i}_s - \frac{L_{ss}}{2} \sqrt{\frac{2}{3}} \left\{ (i_{sb} + i_{sc}) + e^{j\frac{2}{3}\pi} (i_{sa} + i_{sc}) + e^{-j\frac{2}{3}\pi} (i_{sa} + i_{sb}) \right\} \\ &\quad + \sqrt{\frac{2}{3}} M_{sr} \cos \theta_r \left(i_{ra} + e^{j\frac{2}{3}\pi} i_{rb} + e^{-j\frac{2}{3}\pi} i_{rc} \right) \\ &\quad + \sqrt{\frac{2}{3}} M_{sr} \cos \left(\theta_r + \frac{2}{3} \pi \right) \left(i_{rb} + e^{j\frac{2}{3}\pi} i_{rc} + e^{-j\frac{2}{3}\pi} i_{ra} \right) \\ &\quad + \sqrt{\frac{2}{3}} M_{sr} \cos \left(\theta_r - \frac{2}{3} \pi \right) \left(i_{rc} + e^{j\frac{2}{3}\pi} i_{ra} + e^{-j\frac{2}{3}\pi} i_{rb} \right) \end{aligned}$$

By using $i_{sa} + i_{sb} = -i_{sc}$, $i_{sb} + i_{sc} = -i_{sa}$ and $i_{sc} + i_{sa} = -i_{sb}$, we have

$$\begin{aligned}
 \dot{\psi}_s &= \left(l_s + \frac{3}{2} L_{ss} \right) \dot{i}_s \\
 &+ M_{sr} \left\{ \dot{i}_r e^{-j\theta_r} \cos \theta_r + \dot{i}_r e^{-j\theta_r} e^{-j\frac{2}{3}\pi} \cos \left(\theta_r + \frac{2}{3}\pi \right) + \dot{i}_r e^{-j\theta_r} e^{j\frac{2}{3}\pi} \cos \left(\theta_r - \frac{2}{3}\pi \right) \right\} \\
 &= \left(l_s + \frac{3}{2} L_{ss} \right) \dot{i}_s + M_{sr} \dot{i}_r e^{-j\theta_r} \cdot \frac{3}{2} e^{j\theta_r} \\
 &= \left(l_s + \frac{3}{2} L_{ss} \right) \dot{i}_s + \frac{3}{2} M_{sr} \dot{i}_r \quad \dots\dots\dots (2.14)
 \end{aligned}$$

By setting $L_s = \frac{3}{2} L_{ss} + l_s$ and $M = \frac{3}{2} M_{sr}$, (2.14) can be written as:

$$\dot{\psi}_s = L_s \dot{i}_s + M \dot{i}_r \quad \dots\dots\dots (2.15)$$

Substituting (2.15) into (2.13), we have

$$\dot{e}_s = (R_s + pL_s) \dot{i}_s + pM \dot{i}_r \quad \dots\dots\dots (2.16)$$

The space vector of rotor is expressed as follows:

$$\dot{e}_r = \sqrt{\frac{2}{3}} e^{j\theta_r} \left(e_{ra} + e^{j\frac{2}{3}\pi} e_{rb} + e^{-j\frac{2}{3}\pi} e_{rc} \right) \quad \dots\dots\dots (2.17)$$

From (2.6), we have

$$\dot{e}_r = R_r \dot{i}_r + \sqrt{\frac{2}{3}} e^{j\theta_r} p \left(\psi_{ra} + e^{j\frac{2}{3}\pi} \psi_{rb} + e^{-j\frac{2}{3}\pi} \psi_{rc} \right) \quad \dots\dots\dots (2.18)$$

hence,

$$\dot{e}_r = R_r \dot{i}_r + e^{j\theta_r} p \left(\dot{\psi}_r e^{-j\theta_r} \right) \quad \dots\dots\dots (2.19)$$

The space vector of the rotor flux linkage is computed from (2.4) as

$$\begin{aligned}
\psi_r &= \sqrt{\frac{2}{3}} e^{j\theta_r} \left(\psi_{ra} + e^{j\frac{2}{3}\pi} \psi_{rb} + e^{-j\frac{2}{3}\pi} \psi_{rc} \right) \\
&= \left(l_r + \frac{3}{2} L_{rr} \right) i_r + \sqrt{\frac{2}{3}} e^{j\theta_r} M_{sr} \left\{ \cos \theta_r \left(i_{sa} + e^{j\frac{2}{3}\pi} i_{sb} + e^{-j\frac{2}{3}\pi} i_{sc} \right) \right. \\
&\quad \left. + \cos \left(\theta_r - \frac{2}{3} \pi \right) \left(i_{sb} + e^{j\frac{2}{3}\pi} i_{sc} + e^{-j\frac{2}{3}\pi} i_{sa} \right) \right. \\
&\quad \left. + \cos \left(\theta_r + \frac{2}{3} \pi \right) \left(i_{sc} + e^{j\frac{2}{3}\pi} i_{sa} + e^{-j\frac{2}{3}\pi} i_{sb} \right) \right\} \dots\dots\dots (2.20)
\end{aligned}$$

therefore,

$$\psi_r = \left(l_r + \frac{3}{2} L_{rr} \right) i_r + \frac{3}{2} M_{sr} i_s \dots\dots\dots (2.21)$$

By setting $L_r = \frac{3}{2} L_{rr} + l_r$, the rotor flux linkage is expressed as

$$\psi_r = L_r i_r + M i_s \dots\dots\dots (2.22)$$

From (2.19), we have

$$\dot{e}_r = R_r \dot{i}_r + (p - j\omega_r) L_r \dot{i}_r + (p - j\omega_r) M \dot{i}_s \dots\dots\dots (2.23)$$

The space vector equation of IM from equations (2.16) and (2.23) is expressed as

$$\begin{bmatrix} \dot{e}_s \\ \dot{e}_r \end{bmatrix} = \begin{bmatrix} R_s + L_s p & Mp \\ (p - j\omega_r) M & R_r + (p - j\omega_r) L_r \end{bmatrix} \begin{bmatrix} \dot{i}_s \\ \dot{i}_r \end{bmatrix} \dots\dots\dots (2.24)$$

The voltages \dot{e}_s and \dot{e}_r in (2.24) are divided into real and imaginary parts to have $\alpha - \beta$ stationary reference model as

$$\begin{bmatrix} e_{s\alpha} \\ e_{s\beta} \\ e_{r\alpha} \\ e_{r\beta} \end{bmatrix} = \begin{bmatrix} R_s + L_s p & 0 & Mp & 0 \\ 0 & R_s + L_s p & 0 & Mp \\ Mp & \omega_r M & R_r + L_r p & \omega_r L_r \\ -\omega_r M & Mp & -\omega_r L_r & R_r + L_r p \end{bmatrix} \begin{bmatrix} i_{s\alpha} \\ i_{s\beta} \\ i_{r\alpha} \\ i_{r\beta} \end{bmatrix} \dots\dots\dots (2.25)$$

2.2 $d - q$ Model

We consider a rotating $d - q$ axis shown in Fig.2.5. Where, θ is the angle between $\alpha - \beta$ axis and $d - q$ axis. The $d - q$ axis rotates at an arbitrary angular velocity ω . Then, θ can be expressed by the following equation:

$$\theta = \int_0^t \omega dt + \theta(0) \dots\dots\dots (2.26)$$

The $\alpha - \beta$ stationary reference frame quantities are transformed into rotating reference frame quantities using $d - q$ transformation as follows:

$$\dot{f}_{sdq} = e^{-j\theta} (f_{s\alpha} + j f_{s\beta}) = e^{-j\theta} \dot{f}_s \dots\dots\dots (2.27)$$

$$\dot{f}_{rdq} = e^{-j\theta} \dot{f}_r \dots\dots\dots (2.28)$$

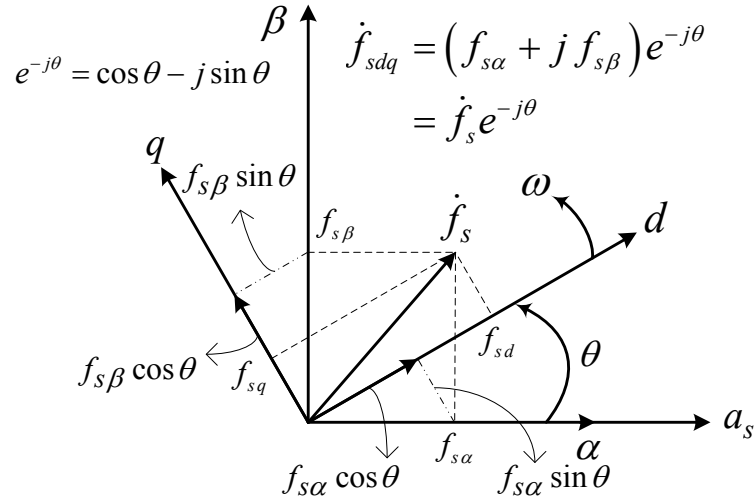


Fig.2.5 Reference frame transformation from $\alpha - \beta$ to $d - q$.

Hence, the transformation of reference frame from $\alpha - \beta$ to $d - q$ axis can be expressed as

$$\begin{bmatrix} f_{sd} \\ f_{sq} \end{bmatrix} = \begin{bmatrix} \cos \theta & \sin \theta \\ -\sin \theta & \cos \theta \end{bmatrix} \begin{bmatrix} f_{s\alpha} \\ f_{s\beta} \end{bmatrix} \quad \dots\dots\dots (2.29)$$

From (2.16) and (2.27), we have

$$\begin{aligned} \dot{i}_{sdq} &= e^{-j\theta} \dot{i}_s \\ &= e^{-j\theta} ((R_s + pL_s) i_s + pM i_r) \\ &= R_s \dot{i}_{sdq} + e^{-j\theta} L_s p (e^{j\theta} i_{sdq}) + e^{-j\theta} M p (e^{j\theta} i_{rdq}) \\ &= R_s \dot{i}_{sdq} + L_s p \dot{i}_{sdq} + j\omega L_s i_{sdq} + M p \dot{i}_{rdq} + j\omega M p i_{rdq} \quad \dots\dots\dots (2.30) \end{aligned}$$

From (2.23) and (2.28), we have

$$\begin{aligned}
\dot{e}_{rdq} &= e^{-j\theta} \dot{e}_r \\
&= e^{-j\theta} \left((p - j\omega_r) M \dot{i}_s + (R_r + (p - j\omega_r) L_r) \dot{i}_r \right) \\
&= e^{-j\theta} R_r \left(e^{j\theta} \dot{i}_{rdq} \right) + e^{-j\theta} M p \left(e^{j\theta} \dot{i}_{sdq} \right) - e^{-j\theta} j \omega_r M \left(e^{j\theta} \dot{i}_{sdq} \right) \\
&\quad + e^{-j\theta} L_r p \left(e^{j\theta} \dot{i}_{rdq} \right) - e^{-j\theta} j \omega_r L_r \left(e^{j\theta} \dot{i}_{rdq} \right) \\
&= R_r \dot{i}_{rdq} + M p \dot{i}_{sdq} + j \omega M \dot{i}_{sdq} - j \omega_r M \dot{i}_{sdq} \\
&\quad + L_r p \dot{i}_{rdq} + j \omega L_r \dot{i}_{rdq} - j \omega_r L_r \dot{i}_{rdq} \quad \dots\dots\dots (2.31)
\end{aligned}$$

The voltage equations of (2.30) and (2.31) can be written in matrix form as

$$\begin{bmatrix} \dot{e}_{sdq} \\ \dot{e}_{rdq} \end{bmatrix} = \begin{bmatrix} R_s + L_s p + j \omega L_s & M p + j \omega M \\ M p + j (\omega - \omega_r) M & R_r + L_r p + j (\omega - \omega_r) L_r \end{bmatrix} \begin{bmatrix} \dot{i}_{sdq} \\ \dot{i}_{rdq} \end{bmatrix} \quad \dots\dots (2.32)$$

Hence, \dot{e}_{sdq} and \dot{e}_{rdq} can be divided into real and imaginary parts as follows:

$$\begin{bmatrix} e_{sd} \\ e_{sq} \\ e_{rd} \\ e_{rq} \end{bmatrix} = \begin{bmatrix} R_s + L_s p & -\omega L_s & M p & -\omega M \\ \omega L_s & R_s + L_s p & \omega M & M p \\ M p & -(\omega - \omega_r) M & R_r + L_r p & -(\omega - \omega_r) L_r \\ (\omega - \omega_r) M & M p & (\omega - \omega_r) L_r & R_r + L_r p \end{bmatrix} \begin{bmatrix} i_{sd} \\ i_{sq} \\ i_{rd} \\ i_{rq} \end{bmatrix} \quad \dots\dots\dots (2.33)$$

The relation between \dot{f}_{sdq} and three-phase variables can be expressed as

$$\dot{f}_{sdq} = e^{-j\theta} \sqrt{\frac{2}{3}} \left(f_{sa} + e^{j\frac{2}{3}\pi} f_{sb} + e^{-j\frac{2}{3}\pi} f_{sc} \right) \quad \dots\dots\dots (2.34)$$

Therefore, we have

$$\begin{bmatrix} f_{sd} \\ f_{sq} \end{bmatrix} = \sqrt{\frac{2}{3}} \begin{bmatrix} \cos \theta & \cos\left(\theta - \frac{2}{3}\pi\right) & \cos\left(\theta + \frac{2}{3}\pi\right) \\ -\sin \theta & -\sin\left(\theta - \frac{2}{3}\pi\right) & -\sin\left(\theta + \frac{2}{3}\pi\right) \end{bmatrix} \begin{bmatrix} f_{sa} \\ f_{sb} \\ f_{sc} \end{bmatrix} \dots\dots\dots (2.35)$$

The relation between \dot{f}_{rdq} and three-phase variables can be expressed as

$$\dot{f}_{rdq} = e^{-j\theta} \sqrt{\frac{2}{3}} e^{j\theta_r} \left(f_{ra} + e^{j\frac{2}{3}\pi} f_{rb} + e^{-j\frac{2}{3}\pi} f_{rc} \right) \dots\dots\dots (2.36)$$

Therefore, we have

$$\begin{bmatrix} f_{rd} \\ f_{rq} \end{bmatrix} = \sqrt{\frac{2}{3}} \begin{bmatrix} \cos \beta & \cos\left(\beta - \frac{2}{3}\pi\right) & \cos\left(\beta + \frac{2}{3}\pi\right) \\ -\sin \beta & -\sin\left(\beta - \frac{2}{3}\pi\right) & -\sin\left(\beta + \frac{2}{3}\pi\right) \end{bmatrix} \begin{bmatrix} f_{ra} \\ f_{rb} \\ f_{rc} \end{bmatrix} \dots\dots\dots (2.37)$$

From (2.14) and (2.21), the flux linkages are expressed as

$$\begin{bmatrix} \psi_{sd} \\ \psi_{sq} \\ \psi_{rd} \\ \psi_{rq} \end{bmatrix} = \begin{bmatrix} L_s & 0 & M & 0 \\ 0 & L_s & 0 & M \\ M & 0 & L_r & 0 \\ 0 & M & 0 & L_r \end{bmatrix} \begin{bmatrix} i_{sd} \\ i_{sq} \\ i_{rd} \\ i_{rq} \end{bmatrix} \dots\dots\dots (2.38)$$

Since the rotor is squirrel-cage short-circuited type and the voltage equations are derived from (2.33) and (2.38) by using rotor flux linkage as follows:

$$\begin{bmatrix} e_{sd} \\ e_{sq} \\ 0 \\ 0 \end{bmatrix} = \begin{bmatrix} R_s + \sigma L_s p & -\omega \sigma L_s & \frac{M}{L_r} p & -\frac{\omega M}{L_r} \\ \omega \sigma L_s & R_s + \sigma L_s p & \frac{\omega M}{L_r} & \frac{M}{L_r} p \\ -\frac{M}{\tau_r} & 0 & \frac{1}{\tau_r} + p & -(\omega - \omega_r) \\ 0 & -\frac{M}{\tau_r} & (\omega - \omega_r) & \frac{1}{\tau_r} + p \end{bmatrix} \begin{bmatrix} i_{sd} \\ i_{sq} \\ \psi_{rd} \\ \psi_{rq} \end{bmatrix} \dots \quad (2.39)$$

where,

$$\sigma = 1 - \frac{M^2}{L_s L_r} \text{ and } \tau_r = \frac{L_r}{R_r} \text{ (rotor open circuit time constant).}$$

2.3 Electromagnetic Torque

To determine the torque developed in IM, we can calculate the input power as follows:

$$\begin{aligned} P_{in} &= e_{sa} i_{sa} + e_{sb} i_{sb} + e_{sc} i_{sc} + e_{ra} i_{ra} + e_{rb} i_{rb} + e_{rc} i_{rc} \\ &= \begin{bmatrix} e_{sa} & e_{sb} & e_{sc} \end{bmatrix} \begin{bmatrix} i_{sa} \\ i_{sb} \\ i_{sc} \end{bmatrix} + \begin{bmatrix} e_{ra} & e_{rb} & e_{rc} \end{bmatrix} \begin{bmatrix} i_{ra} \\ i_{rb} \\ i_{rc} \end{bmatrix} \\ &= (C_s^T \mathbf{e}_s)^T C_s^T \mathbf{i}_s + (C_r^T \mathbf{e}_r)^T C_r^T \mathbf{i}_r \\ &= \mathbf{e}_s^T C_s C_s^T \mathbf{i}_s + \mathbf{e}_r^T C_r C_r^T \mathbf{i}_r \\ &= \mathbf{e}_s^T \mathbf{i}_s + \mathbf{e}_r^T \mathbf{i}_r \dots \dots \dots \quad (2.40) \end{aligned}$$

where,

$$C_s = \sqrt{\frac{2}{3}} \begin{bmatrix} 1 & -\frac{1}{2} & -\frac{1}{2} \\ 0 & \frac{\sqrt{3}}{2} & -\frac{\sqrt{3}}{2} \end{bmatrix}, C_r = \sqrt{\frac{2}{3}} \begin{bmatrix} \cos\theta_r & \cos\left(\theta_r + \frac{2\pi}{2}\right) & \cos\left(\theta_r - \frac{2\pi}{2}\right) \\ \sin\theta_r & \sin\left(\theta_r + \frac{2\pi}{2}\right) & \sin\left(\theta_r - \frac{2\pi}{2}\right) \end{bmatrix}$$

$$\mathbf{e}_s = \begin{bmatrix} e_{s\alpha} \\ e_{s\beta} \end{bmatrix}, \mathbf{i}_s = \begin{bmatrix} i_{s\alpha} \\ i_{s\beta} \end{bmatrix}, \mathbf{e}_r = \begin{bmatrix} e_{r\alpha} \\ e_{r\beta} \end{bmatrix}, \mathbf{i}_r = \begin{bmatrix} i_{r\alpha} \\ i_{r\beta} \end{bmatrix}$$

Therefore,

$$P_{in} = e_{s\alpha}i_{s\alpha} + e_{s\beta}i_{s\beta} + e_{r\alpha}i_{r\alpha} + e_{r\beta}i_{r\beta} \quad \dots\dots\dots (2.41)$$

By using space vector, P_{in} is expressed as

$$\begin{aligned} P_{in} &= \text{Re}(\dot{e}_s i_s^* + \dot{e}_r i_r^*) \\ &= \text{Re}\left\{ i_s^* (R_s \dot{i}_s + L_s p \dot{i}_s + M p \dot{i}_r) + i_r^* (M p \dot{i}_s - j\omega_r M \dot{i}_s \right. \\ &\quad \left. + R_r \dot{i}_r + L_r p \dot{i}_r - j\omega_r L_r \dot{i}_r) \right\} \\ &= R_s |i_s|^2 + R_r |i_r|^2 + \frac{1}{2} L_s p |i_s|^2 + \frac{1}{2} L_r p |i_r|^2 \\ &\quad + \frac{1}{2} M p (i_s^* i_r + i_s i_r^*) + \text{Re}(-j\omega_r M i_s i_r^*) \quad \dots\dots\dots (2.42) \end{aligned}$$

The each term of (2.42) is considered as

$R_s |i_s|^2$: primary copper loss

$R_r |i_r|^2$: secondary copper loss

$\frac{1}{2} L_s p |i_s|^2 + \frac{1}{2} L_r p |i_r|^2$: reactive power of self-inductance

$\frac{1}{2} M p (i_s^* i_r + i_s i_r^*)$: reactive power of mutual inductance

$\text{Re}(-j \omega_r M \dot{i}_s \dot{i}_r^*)$: mechanical power

Hence, the electromagnetic torque τ_e is given by

$$\begin{aligned} \tau_e &= \frac{\text{Re}\{-j \omega_r M (\dot{i}_s \dot{i}_r^*)\}}{\frac{2}{P} \omega_r} \\ &= \frac{P}{2} M \text{Im}(i_s i_r^*) \end{aligned} \quad \dots\dots\dots (2.43)$$

where, P : number of poles.

Therefore,

$$\tau_e = \frac{P}{2} M (i_{sq} i_{rd} - i_{sd} i_{rq}) = \frac{P}{2} \frac{M}{L_r} (i_{sq} \psi_{rd} - i_{sd} \psi_{rq}) \quad \dots\dots\dots (2.44)$$

2.4 Non – linear State Equation

In order to compute the transient responses, we derive a non-linear state equation from (2.39). The non-linear state equation is expressed as

$$p i_{sd} = \frac{e_{sd}}{\sigma L_s} - \left(\frac{R_s}{\sigma L_s} + \frac{M^2}{\sigma L_s L_r \tau_r} \right) i_{sd} + \omega i_{sq} + \frac{M \psi_{rd}}{\sigma L_s L_r \tau_r} + \frac{\omega_r M \psi_{rq}}{\sigma L_s L_r} \quad (2.45)$$

$$p i_{sq} = \frac{e_{sq}}{\sigma L_s} - \omega i_{sd} - \left(\frac{R_s}{\sigma L_s} + \frac{M^2}{L_r \tau_r \sigma L_s} \right) i_{sq} - \frac{\omega_r M \psi_{rd}}{L_r \sigma L_s} + \frac{M \psi_{rq}}{L_r \tau_r \sigma L_s} \quad (2.46)$$

$$p \psi_{rd} = \frac{M}{\tau_r} i_{sd} - \frac{1}{\tau_r} \psi_{rd} + (\omega - \omega_r) \psi_{rq} \quad \dots\dots\dots (2.47)$$

$$p \psi_{rq} = \frac{M}{\tau_r} i_{sq} - (\omega - \omega_r) \psi_{rd} - \frac{1}{\tau_r} \psi_{rq} \quad \dots\dots\dots (2.48)$$

The mechanical equation of motion is expressed as

$$p\omega_r = \frac{P}{2J}(\tau_e - T_L) = \frac{M P^2}{4J L_r}(i_{sq} \psi_{rd} - i_{sd} \psi_{rq}) - \frac{P}{2J} T_L \quad \dots\dots\dots (2.49)$$

where, J : inertia of the rotor plus load, T_L : load torque.

The above equations are described by a non-linear state equation

$$p \mathbf{x}_s = \mathbf{f}(\mathbf{x}_s, \mathbf{u}_s, T_L) \quad \dots\dots\dots (2.50)$$

where, \mathbf{x}_s is state vector and \mathbf{u}_s is input vector of IM.

$$\mathbf{x}_s = [i_{sd}, i_{sq}, \psi_{rd}, \psi_{rq}, \omega_r]^T \quad \dots\dots\dots (2.51)$$

$$\mathbf{u}_s = [e_{sd}, e_{sq}, \omega]^T \quad \dots\dots\dots (2.52)$$

2.5 Linear State Equation

An essential problem connected to the modeling of the induction machine is the non-linearity of the equations that describe its operation. This non-linearity is caused by the voltage equations and the electromagnetic torque relation as well, due to the products between the state variables. When a control system is designed, it is very convenient to linearize the machine equations [7], [8].

The stability analysis of non-linear system is difficult in general. So, we derive a linear model of IM by considering small perturbation at a steady state operating point which is obtained by setting $p = 0$. The linear model of IM is derived as follows from (2.50):

$$p\Delta \mathbf{x}_s = \mathbf{A}_s \Delta \mathbf{x}_s + \mathbf{B}_s \Delta \mathbf{u}_s + \mathbf{B}_L \Delta T_L \quad \dots\dots\dots (2.53)$$

where,

$$\Delta \mathbf{x}_s = \left[\Delta i_{sd}, \Delta i_{sq}, \Delta \psi_{rd}, \Delta \psi_{rq}, \Delta \omega_r \right]^T$$

$$\Delta \mathbf{u}_s = \left[\Delta e_{sd}, \Delta e_{sq}, \Delta \omega \right]^T$$

$$A_s = \begin{bmatrix} -a_1 & \omega & \frac{M}{\sigma L_s L_r \tau_r} & \frac{M \omega_r}{\sigma L_s L_r} & \frac{M \psi_{rq}}{\sigma L_s L_r} \\ -\omega & -a_1 & -\frac{M \omega_r}{\sigma L_s L_r} & \frac{M}{\sigma L_s L_r \tau_r} & -\frac{M \psi_{rd}}{\sigma L_s L_r} \\ \frac{M}{\tau_r} & 0 & -\frac{1}{\tau_r} & (\omega - \omega_r) & -\psi_{rq} \\ 0 & \frac{M}{\tau_r} & -(\omega - \omega_r) & -\frac{1}{\tau_r} & \psi_{rd} \\ -a_2 \psi_{rq} & a_2 \psi_{rd} & a_2 i_{sq} & -a_2 i_{sd} & 0 \end{bmatrix} \dots\dots\dots (2.54)$$

$$a_1 = \frac{R_s}{\sigma L_s} + \frac{M^2}{\sigma L_s L_r \tau_r}, \quad a_2 = \frac{MP^2}{4JL_r}$$

$$B_s = \begin{bmatrix} \frac{1}{\sigma L_s} & 0 & i_{sq} \\ 0 & \frac{1}{\sigma L_s} & -i_{sd} \\ 0 & 0 & \psi_{rq} \\ 0 & 0 & -\psi_{rd} \\ 0 & 0 & 0 \end{bmatrix}, B_L = \begin{bmatrix} 0 \\ 0 \\ 0 \\ 0 \\ -\frac{P}{2J} \end{bmatrix} \dots\dots\dots (2.55)$$

Chapter 3

Speed Sensorless Vector Control Systems

3.1 Proposed System A

A speed sensorless vector control system in which the rotor speed of IM is estimated explicitly is proposed and analyzed to investigate the system stability. We call the sensorless system “system A”.

3.1.1 Block Diagram of System A

In order to simplify the controller and to stabilize the system at low speed regenerating operations, the speed sensorless vector control system A is proposed as shown in Fig.3.1. As described in (2.39), the $d-q$ rotating reference frame equations of IM are modified as

Voltage model:

$$e_{sd}^* = (R_s^* + \sigma L_s p) i_{sd}^* - \omega^* \sigma L_s i_{sq} + \frac{M}{L_r} p \psi_{rd}^v - \frac{M}{L_r} \omega^* \psi_{rq}^v \quad \dots\dots\dots (3.1)$$

$$e_{sq}^* = \omega^* \sigma L_s i_{sd}^* + (R_s^* + \sigma L_s p) i_{sq} + \frac{M}{L_r} \omega^* \psi_{rd}^v + \frac{M}{L_r} p \psi_{rq}^v \quad \dots\dots\dots (3.2)$$

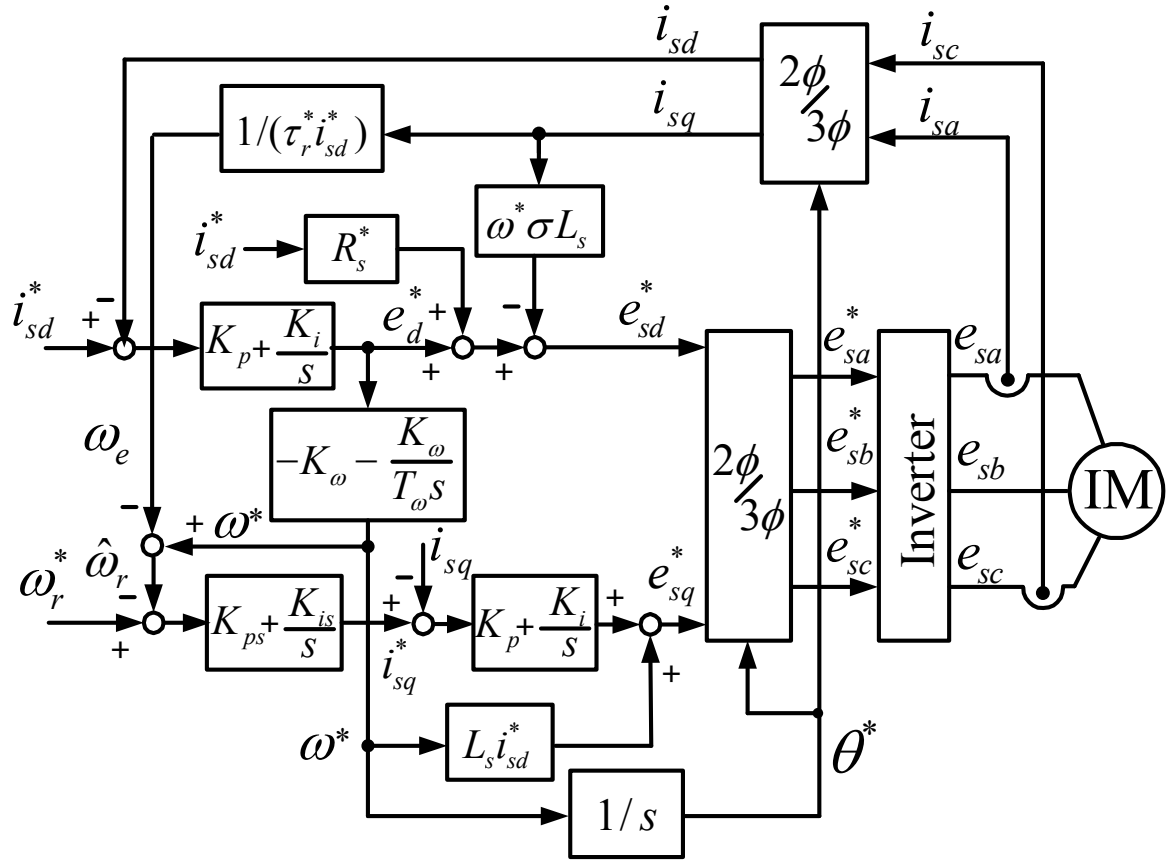


Fig.3.1 Block diagram of system A.

Current model

$$0 = -\frac{M}{\tau_r} i_{sd}^* + \left(\frac{1}{\tau_r} + p\right) \psi_{rd}^* - (\omega^* - \hat{\omega}_r) \psi_{rq}^* \quad \dots \quad (3.3)$$

$$0 = -\frac{M}{\tau_r} i_{sq}^* + (\omega^* - \hat{\omega}_r) \psi_{rd}^* + \left(\frac{1}{\tau_r} + p\right) \psi_{rq}^* \quad \dots \quad (3.4)$$

Where, $\tau_r^* = L_r / R_r^*$, $\hat{\omega}_r$: estimated rotor speed.

The synchronously rotating angular frequency ω^* of $d-q$ reference frame is defined to satisfy that the rotor flux of the current model ψ_{rq}^* is zero.

Therefore,

$$\psi_{rq}^* = 0 \quad \dots \quad (3.5)$$

This means that the $d - q$ axis is selected to synchronize the direction of the current model rotor flux. By assuming that the $d -$ axis current reference i_{sd}^* is constant, from (3.3) we have

$$\psi_{rd}^* = Mi_{sd}^* \quad \dots\dots\dots (3.6)$$

By substituting (3.5) and (3.6) into (3.4) we have

$$\omega^* - \hat{\omega}_r = \frac{i_{sq}}{\tau_r^* i_{sd}^*} \quad \dots\dots\dots (3.7)$$

Therefore, the estimated slip speed ω_e is defined as

$$\omega_e = \frac{i_{sq}}{\tau_r^* i_{sd}^*} \quad \dots\dots\dots (3.8)$$

The assumption of constant i_{sd}^* causes that the $d -$ axis flux becomes constant described in (3.6). Therefore, we make the following assumption:

$$p\psi_{rd}^v = 0 \quad \dots\dots\dots (3.9)$$

By using (3.9), from (3.1) we have

$$e_{sd}^* = R_s^* i_{sd}^* - \omega^* \sigma L_s i_{sq} - \frac{\omega^* M}{L_r} \psi_{rq}^v \quad \dots\dots\dots (3.10)$$

In (3.10), the induced voltage e_d^* is defined as

$$e_d^* = -\frac{\omega^* M}{L_r} \psi_{rq}^v \quad \dots\dots\dots (3.11)$$

In the proposed system, the induced voltage e_d^* is computed by using the output voltage of $d -$ axis PI current controller. We can estimate the phase of rotor flux θ^* by changing ω^* to satisfy

$$\psi_{rq}^v = 0 \quad \dots\dots\dots (3.12)$$

Fig.3.2 shows the rotor flux vector of current model $\dot{\psi}_r^*$ and that of voltage model $\dot{\psi}_r^v$. The $\dot{\psi}_r^*$ is on the d – axis. When $\psi_{rq}^v > 0$, we must increase ω^* and we must decrease ω^* when $\psi_{rq}^v < 0$ to satisfy (3.11).

Because the ψ_{rq}^v is proportional to e_d^* in (3.11), the angular speed ω^* is estimated by using PI control as

$$\omega^* = -\left(K_\omega + \frac{K_\omega}{T_\omega s}\right)e_d^* \quad \dots\dots\dots (3.13)$$

The sign of K_ω must be changed according to the sign of ω^* as

$sign(\omega^*)$ is 1 if $\omega^* > 0$ and -1 if $\omega^* < 0$.

$$K_\omega = sign(\omega^*)|K_\omega| \quad \dots\dots\dots (3.14)$$

The angle of the rotor flux is computed by integrating the angular speed as follows:

$$\theta^* = \frac{\omega^*}{s} \quad \dots\dots\dots (3.15)$$

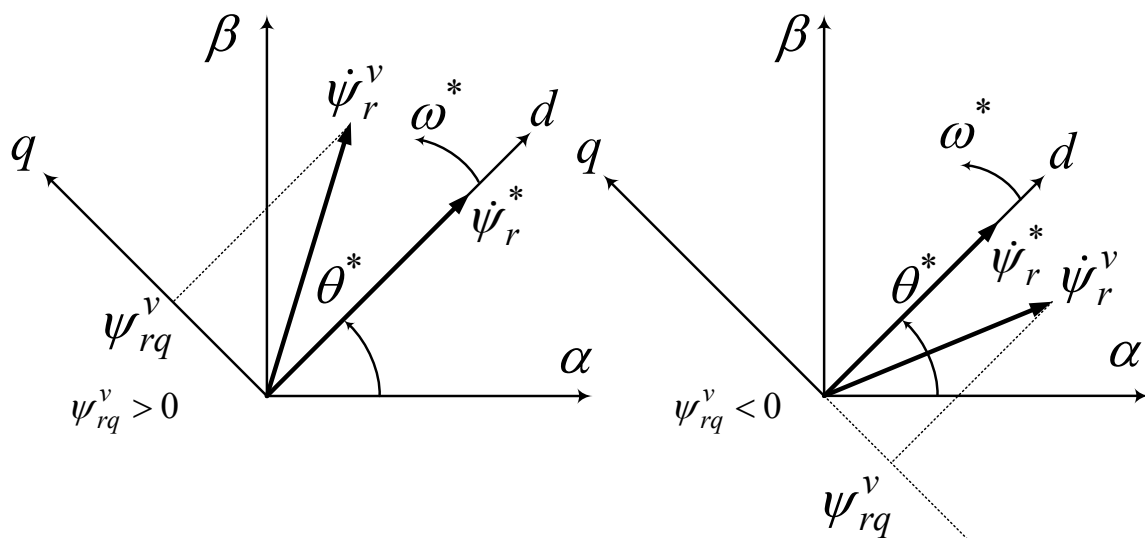


Fig.3.2 The rotor flux vectors and $d - q$ reference frame.

The rotor speed is estimated by using (3.7). The speed PI control and q – axis PI current control are composed like conventional system as shown in Fig.3.1.

By assuming $\psi_{rq}^v = 0$ and $\psi_{rd}^v = M i_{sd}^*$, we have following equation from (3.2):

$$\begin{aligned} e_{sq}^* &= \omega^* \sigma L_s i_{sd}^* + (R_s^* + \sigma L_s p) i_{sq} + \frac{M^2}{L_r} \omega^* i_{sd}^* \\ &= \omega^* L_s i_{sd}^* + (R_s^* + \sigma L_s p) i_{sq} \end{aligned} \quad \dots\dots\dots (3.16)$$

The $2\phi/3\phi$ transformation of Fig.3.1 is performed as

$$\begin{bmatrix} i_{sd} \\ i_{sq} \end{bmatrix} = \sqrt{\frac{2}{3}} \begin{bmatrix} \cos \theta^* & \cos\left(\theta^* - \frac{2}{3}\pi\right) & \cos\left(\theta^* + \frac{2}{3}\pi\right) \\ -\sin \theta^* & -\sin\left(\theta^* - \frac{2}{3}\pi\right) & -\sin\left(\theta^* + \frac{2}{3}\pi\right) \end{bmatrix} \begin{bmatrix} i_{sa} \\ i_{sb} \\ i_{sc} \end{bmatrix} \quad \dots\dots (3.17)$$

$$\begin{bmatrix} e_{sa}^* \\ e_{sb}^* \\ e_{sc}^* \end{bmatrix} = \sqrt{\frac{2}{3}} \begin{bmatrix} \cos \theta^* & -\sin \theta^* \\ \cos\left(\theta^* - \frac{2}{3}\pi\right) & -\sin\left(\theta^* - \frac{2}{3}\pi\right) \\ \cos\left(\theta^* + \frac{2}{3}\pi\right) & -\sin\left(\theta^* + \frac{2}{3}\pi\right) \end{bmatrix} \begin{bmatrix} e_{sd}^* \\ e_{sq}^* \end{bmatrix} \quad \dots\dots\dots (3.18)$$

3.1.2 Description of System

The following assumptions are set in analysis.

- (1) i_{sd}^* is constant.
- (2) Voltage control is performed ideally and the following equation is valid:

$$e_{sa}^* = e_{sa}, \quad e_{sb}^* = e_{sb}, \quad e_{sc}^* = e_{sc} \quad \dots\dots\dots (3.19)$$

In order to analyze an IM, the $d-q$ reference frame that rotates synchronously with the flux angle θ^* is taken as θ of (2.26). Thus, $\omega = \omega^*$.

Therefore, the $d-q$ transformation is expressed as

$$\begin{bmatrix} f_{sd} \\ f_{sq} \end{bmatrix} = \sqrt{\frac{2}{3}} \begin{bmatrix} \cos \theta^* & \cos\left(\theta^* - \frac{2}{3}\pi\right) & \cos\left(\theta^* + \frac{2}{3}\pi\right) \\ -\sin \theta^* & -\sin\left(\theta^* - \frac{2}{3}\pi\right) & -\sin\left(\theta^* + \frac{2}{3}\pi\right) \end{bmatrix} \begin{bmatrix} f_{sa} \\ f_{sb} \\ f_{sc} \end{bmatrix}. \quad (3.20)$$

From (3.18), (3.19) and (3.20) we have

$$e_{sd}^* = e_{sd}, \quad e_{sq}^* = e_{sq} \quad \dots\dots\dots (3.21)$$

The PI d – axis controller is expressed as

$$e_d^* = K_p (i_{sd}^* - i_{sd}) + e_{cd} \quad \dots\dots\dots (3.22)$$

where,

$$e_{cd} = \frac{K_i}{s} (i_{sd}^* - i_{sd}) \quad \dots\dots\dots (3.23)$$

Then the derivative of e_{cd} is expressed as

$$pe_{cd} = K_i (i_{sd}^* - i_{sd}) \quad \dots\dots\dots (3.24)$$

The PI angular speed estimator is expressed as

$$\omega^* = e_\omega - K_\omega e_d^* \quad \dots\dots\dots (3.25)$$

where,

$$e_\omega = -\frac{K_\omega}{T_\omega s} e_d^* \quad \dots\dots\dots (3.26)$$

Then, the derivative of e_ω is expressed as

$$pe_\omega = -\frac{K_\omega}{T_\omega} e_d^* \quad \dots\dots\dots (3.27)$$

By using (3.22), we have

$$pe_\omega = -\frac{K_\omega}{T_\omega} (K_p (i_{sd}^* - i_{sd}) + e_{cd}) \quad \dots\dots\dots (3.28)$$

From (3.22) and (3.25)

$$\omega^* = e_\omega - K_\omega K_p i_{sd}^* + K_\omega K_p i_{sd} - K_\omega e_{cd} \quad \dots\dots\dots (3.29)$$

The output variable of PI speed controller i_{sq}^* is expressed as

$$\begin{aligned} i_{sq}^* &= \left(K_{ps} + \frac{K_{is}}{s} \right) (\omega_r^* - \hat{\omega}_r) \\ &= K_{ps} \left(\omega_r^* - \omega^* + \frac{i_{sq}}{\tau_r^* i_{sd}^*} \right) + \omega_{cd} \quad \dots\dots\dots (3.30) \end{aligned}$$

where,

$$\omega_{cd} = \frac{K_{is}}{s} \left(\omega_r^* - \omega^* + \frac{i_{sq}}{\tau_r^* i_{sd}^*} \right) \quad \dots\dots\dots (3.31)$$

By using ω^* in (3.29), we have

$$p\omega_{cd} = K_{is} \left(\omega_r^* + K_\omega K_p i_{sd}^* - K_\omega K_p i_{sd} + K_\omega e_{cd} - e_\omega + \frac{i_{sq}}{\tau_r^* i_{sd}^*} \right) \quad \dots\dots (3.32)$$

The d – axis voltage is expressed as

$$e_{sd}^* = K_p (i_{sd}^* - i_{sd}) + e_{cd} - \omega^* \sigma L_s i_{sq} + R_s^* i_{sd}^* \quad \dots\dots\dots (3.33)$$

The q – axis voltage is expressed as

$$\begin{aligned} e_{sq}^* &= \left(K_p + \frac{K_i}{s} \right) (i_{sq}^* - i_{sq}) + \omega^* L_s i_{sd}^* \\ &= K_p (i_{sq}^* - i_{sq}) + e_{cq} + \omega^* L_s i_{sd}^* \quad \dots\dots\dots (3.34) \end{aligned}$$

where,

$$e_{cq} = \frac{K_i}{s} (i_{sq}^* - i_{sq}) \quad \dots\dots\dots (3.35)$$

Then, the derivative of e_{cq} is expressed as

$$pe_{cq} = K_i (i_{sq}^* - i_{sq}) \quad \dots\dots\dots (3.36)$$

3.1.3 Steady State Analysis

In this system, we can choose any value of speed command ω_r^* and magnetizing current command i_{sd}^* . Load torque T_L is an arbitrary input that depends on any load connected to motor. When we set the ω_r^* , i_{sd}^* , T_L , other all quantities can be determined. It has three degrees of freedom. In order to simplify the procedure of computation, the slip speed is given instead of the load torque.

Actually, angular frequency ω^* , rotor speed ω_r are constant in steady state condition, and then the differential equation of the system becomes linear. If the system is linear, it is similar to DC circuit. Then, we can set the differential operator $p = 0$ in steady state analysis because there is no change of state quantity.

The following equations is obtained by letting $p = 0$ in steady state condition:

$$i_{sd}^* = i_{sd}, i_{sq}^* = i_{sq}, e_d^* = 0, e_{cd} = 0, \omega_r^* = \hat{\omega}_r \quad \dots\dots\dots (3.37)$$

From (2.39), the induction motor is expressed as

$$e_{sd}^* = R_s i_{sd} - \omega^* \sigma L_s i_{sq} - \frac{\omega^* M}{L_r} \psi_{rq} \quad \dots\dots\dots (3.38)$$

$$e_{sq}^* = \omega^* \sigma L_s i_{sd} + R_s i_{sq} + \frac{\omega^* M}{L_r} \psi_{rd} \quad \dots\dots\dots (3.39)$$

$$0 = -\frac{M}{\tau_r} i_{sd} + \frac{1}{\tau_r} \psi_{rd} - (\omega^* - \omega_r) \psi_{rq} \quad \dots\dots\dots (3.40)$$

$$0 = -\frac{M}{\tau_r} i_{sq} + (\omega^* - \omega_r) \psi_{rd} + \frac{1}{\tau_r} \psi_{rq} \quad \dots\dots\dots (3.41)$$

$$\tau_e = T_L \quad \dots\dots\dots (3.42)$$

From (3.33) and (3.37), we have

$$e_{sd}^* = R_s^* i_{sd}^* - \omega^* \sigma L_s i_{sq} \quad \dots\dots\dots (3.43)$$

If we assume $R_s = R_s^*$, from (3.38) and (3.43), we have

$$\psi_{rq} = 0 \quad \dots\dots\dots (3.44)$$

From (3.40) and (3.44)

$$\psi_{rd} = M i_{sd} \quad \dots\dots\dots (3.45)$$

From (3.41) and (3.44),

$$\omega^* - \omega_r = \frac{M i_{sq}}{\tau_r \psi_{rd}} = \frac{i_{sq}}{\tau_r i_{sd}^*} \quad \dots\dots\dots (3.46)$$

By assuming $R_r = R_r^*$ and using (3.7), we have

$$\omega_r = \hat{\omega}_r \quad \dots\dots\dots (3.47)$$

Therefore,

$$\omega_r = \omega_r^* \quad \dots\dots\dots (3.48)$$

By comparing (3.34) and (3.39), we have

$$e_{cq} = R_s i_{sq} \quad \dots\dots\dots (3.49)$$

A steady-state solution is calculated in the following procedures by setting $N_r^* [\text{min}^{-1}]$, $N_{sl} [\text{min}^{-1}]$, and i_{sd}^* as given values.

[1] Electrical angular speed command ω_r^* is calculated by

$$\omega_r^* = \frac{P}{2} 2\pi \frac{N_r^*}{60} \quad \dots\dots\dots (3.50)$$

[2] Similarly, electrical slip angular frequency ω_{sl} is calculated by

$$\omega_{sl} = \omega_r^* - \omega_r = \frac{P}{2} 2\pi \frac{N_{sl}}{60} \quad \dots\dots\dots (3.51)$$

[3] $\psi_{rq} = 0$ is calculated by referred to(3.12)

$$[4] \psi_{rd} = M i_{sd}$$

[5] i_{sq} is calculated by

$$i_{sq} = \frac{\omega_{sl} \tau_r}{M} \psi_{rd} \quad \dots\dots\dots (3.52)$$

[6] Slip speed ω_e is equal to ω_{sl} and rotor speed ω_r is equal to ω_r^* .

[7] ω^* is calculated by

$$\omega^* = \omega_r + \omega_{sl} \quad \dots\dots\dots (3.53)$$

$$[8] e_{sd}^* = R_s i_{sd} - \omega^* \sigma L_s i_{sq}$$

$$[9] e_{sq}^* = \omega^* L_s i_{sd} + R_s i_{sq}$$

$$[10] e_{cq} = R_s i_{sq}$$

$$[11] \omega_{cd} = i_{sq}^*$$

$$[12] e_\omega = \omega^*$$

$$[13] \tau_e = \frac{P M^2}{2 L_r} i_{sd} i_{sq}$$

The non-linear state equation of induction motor in the rotating reference frame that rotates synchronously with θ^* is obtained from (2.45) to (2.49). In these equations, e_{sd} , e_{sq} and ω must be replaced with e_{sd}^* , e_{sq}^* and ω^* respectively by using (3.21).

3.1.4 Linear Model

From (2.53) the linear model of IM of Fig.3.1 is expressed by

$$p\Delta \mathbf{x}_s = \mathbf{A}_s \Delta \mathbf{x}_s + \mathbf{B}_s \Delta \mathbf{u}_s + \mathbf{B}_L \Delta T_L \quad \dots\dots\dots (3.54)$$

where,

$$\Delta \mathbf{x}_s = [\Delta i_{sd}, \Delta i_{sq}, \Delta \psi_{rd}, \Delta \psi_{rq}, \Delta \omega_r]^T$$

$$\Delta \mathbf{u}_s = [\Delta e_{sd}^*, \Delta e_{sq}^*, \Delta \omega^*]^T$$

In these equations, Δe_{sd} , Δe_{sq} , $\Delta \omega$ and ω were replaced with Δe_{sd}^* , Δe_{sq}^* , $\Delta \omega^*$ and ω^* respectively.

By considering small perturbation at a steady state operating point, the following equations are obtained from equation (3.24), (3.28), (3.32) and (3.36).

$$p\Delta e_{cd} = -K_i \Delta i_{sd} \quad \dots\dots\dots (3.55)$$

$$p\Delta e_{\omega} = \frac{K_{\omega}}{T_{\omega}} K_p \Delta i_{sd} - \frac{K_{\omega}}{T_{\omega}} \Delta e_{cd} \quad \dots\dots\dots (3.56)$$

$$p\Delta \omega_{cd} = K_{is} \left(\Delta \omega_r^* - K_{\omega} K_p \Delta i_{sd} + K_{\omega} \Delta e_{cd} - \Delta e_{\omega} + \frac{\Delta i_{sq}}{\tau_r^* i_{sd}^*} \right) \quad \dots\dots (3.57)$$

$$p\Delta e_{cq} = K_i \Delta i_{sq}^* - K_i \Delta i_{sq} \quad \dots\dots\dots (3.58)$$

By using (3.30), (3.58) becomes

$$p\Delta e_{cq} = -K_i K_{ps} K_{\omega} K_p \Delta i_{sd} + K_i \left(\frac{K_{ps}}{\tau_r^* i_{sd}^*} - 1 \right) \Delta i_{sq} \\ + K_i K_{ps} K_{\omega} \Delta e_{cd} - K_i K_{ps} \Delta e_{\omega} + K_i \Delta \omega_{cd} + K_i K_{ps} \Delta \omega_r^* \quad \dots\dots (3.59)$$

These equations can be expressed in a matrix form as follows:

$$\begin{aligned}
 p \begin{bmatrix} \Delta e_{cd} \\ \Delta e_{\omega} \\ \Delta \omega_{cd} \\ \Delta e_{cq} \end{bmatrix} &= \begin{bmatrix} -K_i & 0 & 0 & 0 & 0 \\ \frac{K_{\omega}}{T_{\omega}} K_p & 0 & 0 & 0 & 0 \\ -K_{is} K_{\omega} K_p & \frac{K_{is}}{\tau_r i_{sd}^{**}} & 0 & 0 & 0 \\ -K_i K_{ps} K_{\omega} K_p & K_i \left(\frac{K_{ps}}{\tau_r i_{sd}^{**}} - 1 \right) & 0 & 0 & 0 \end{bmatrix} \begin{bmatrix} \Delta i_{sd} \\ \Delta i_{sq} \\ \Delta \psi_{rd} \\ \Delta \psi_{rq} \\ \Delta \omega_r \end{bmatrix} \\
 &+ \begin{bmatrix} 0 & 0 & 0 & 0 \\ -\frac{K_{\omega}}{T_{\omega}} & 0 & 0 & 0 \\ K_{is} K_{\omega} & -K_{is} & 0 & 0 \\ K_i K_{ps} K_{\omega} & -K_i K_{ps} & K_i & 0 \end{bmatrix} \begin{bmatrix} \Delta e_{cd} \\ \Delta e_{\omega} \\ \Delta \omega_{cd} \\ \Delta e_{cq} \end{bmatrix} + \begin{bmatrix} 0 \\ 0 \\ K_{is} \\ K_i K_{ps} \end{bmatrix} \begin{bmatrix} \Delta \omega_r^* \end{bmatrix}
 \end{aligned}$$

Simply is expressed as

$$p \Delta \mathbf{z} = \mathbf{A}_x \Delta \mathbf{x} + \mathbf{A}_z \Delta \mathbf{z} + \mathbf{B}_r \Delta \mathbf{r} \quad \dots \quad (3.60)$$

where,

$$\Delta \mathbf{z} = \left[\Delta e_{cd} \ \Delta e_{\omega} \ \Delta \omega_{cd} \ \Delta e_{cq} \right]^T, \quad \Delta \mathbf{r} = \left[\Delta \omega_r^* \right]$$

From the equations (3.29), (3.33) and (3.34) we have

$$\Delta \omega^* = K_{\omega} K_p \Delta i_{sd} - K_{\omega} \Delta e_{cd} + \Delta e_{\omega} \quad \dots \quad (3.61)$$

$$\begin{aligned}
 \Delta e_{sd}^* &= -K_p \Delta i_{sd} + \Delta e_{cd} - \omega^* \sigma L_s \Delta i_{sq} - \Delta \omega^* \sigma L_s i_{sq} \\
 &= -K_p \left(K_{\omega} \sigma L_s i_{sq} + 1 \right) \Delta i_{sd} - \omega^* \sigma L_s \Delta i_{sq} \\
 &\quad + \left(K_{\omega} \sigma L_s i_{sq} + 1 \right) \Delta e_{cd} - \sigma L_s i_{sq} \Delta e_{\omega} \quad \dots \quad (3.62)
 \end{aligned}$$

$$\begin{aligned}
\Delta e_{sq}^* &= K_p \Delta i_{sq}^* - K_p \Delta i_{sq} + \Delta e_{cq} + L_s i_{sd}^* \Delta \omega^* \\
&= K_p K_{ps} \Delta \omega_r^* + K_p \Delta \omega_{cd} + \left(\frac{K_{ps}}{\tau_r^* i_{sd}^*} - 1 \right) K_p \Delta i_{sq} \\
&\quad + \Delta e_{cq} + \left(L_s i_{sd}^* - K_p K_{ps} \right) K_\omega K_p \Delta i_{sd} \\
&\quad + \left(K_p K_{ps} - L_s i_{sd}^* \right) K_\omega \Delta e_{cd} + \left(L_s i_{sd}^* - K_p K_{ps} \right) \Delta e_\omega \quad \dots \dots \dots (3.63)
\end{aligned}$$

We can write a matrix form of $\Delta \mathbf{u}_s$ as follows:

$$\Delta \mathbf{u}_s = F_x \Delta \mathbf{x}_s + F_z \Delta \mathbf{z} + F_r \Delta \mathbf{r} \quad \dots \dots \dots (3.64)$$

$$\begin{aligned}
\begin{bmatrix} \Delta e_{sd}^* \\ \Delta e_{sq}^* \\ \Delta \omega^* \end{bmatrix} &= \begin{bmatrix} -K_p (K_\omega \sigma L_s i_{sq} + 1) & -\omega^* \sigma L_s & 0 & 0 & 0 \\ K_p K_\omega (L_s i_{sd}^* - K_p K_{ps}) & K_p \left(\frac{K_{ps}}{\tau_r^* i_{sd}^*} - 1 \right) & 0 & 0 & 0 \\ K_p K_\omega & 0 & 0 & 0 & 0 \end{bmatrix} \begin{bmatrix} \Delta i_{sd} \\ \Delta i_{sq} \\ \Delta \psi_{rd} \\ \Delta \psi_{rq} \\ \Delta \omega_r \end{bmatrix} \\
&+ \begin{bmatrix} K_\omega \sigma L_s i_{sq} + 1 & -\sigma L_s i_{sq} & 0 & 0 \\ K_\omega (K_p K_{ps} - L_s i_{sd}^*) & L_s i_{sd}^* - K_p K_{ps} & K_p & 1 \\ -K_\omega & 1 & 0 & 0 \end{bmatrix} \begin{bmatrix} \Delta e_{cd} \\ \Delta e_\omega \\ \Delta \omega_{cd} \\ \Delta e_{cq} \end{bmatrix} + \begin{bmatrix} 0 \\ K_p K_{ps} \\ 0 \end{bmatrix} \begin{bmatrix} \Delta \omega_r^* \end{bmatrix}
\end{aligned}$$

From equation (3.54), (3.61) and (3.64) the linear model of proposed system A can be derived as follows:

$$p \begin{bmatrix} \Delta \mathbf{x}_s \\ \Delta \mathbf{z} \end{bmatrix} = \begin{bmatrix} \mathbf{A}_s + \mathbf{B}_s \mathbf{F}_x & \mathbf{B}_s \mathbf{F}_z \\ \mathbf{A}_x & \mathbf{A}_z \end{bmatrix} \begin{bmatrix} \Delta \mathbf{x}_s \\ \Delta \mathbf{z} \end{bmatrix} + \begin{bmatrix} \mathbf{B}_s \mathbf{F}_r \\ \mathbf{B}_r \end{bmatrix} \begin{bmatrix} \Delta \mathbf{r} \end{bmatrix} + \begin{bmatrix} \mathbf{B}_L \\ \mathbf{0} \end{bmatrix} \begin{bmatrix} \Delta T_L \end{bmatrix} \dots \dots (3.65)$$

Simply we can express as

$$p \Delta \mathbf{x} = \mathbf{A} \Delta \mathbf{x}_s + \mathbf{B} \Delta \mathbf{r} + \mathbf{B}_L \Delta T_L \quad \dots \dots \dots (3.66)$$

Where,

$$A = \begin{bmatrix} -a_1 - \frac{K_p}{\sigma L_s} & 0 & \frac{1}{\tau_r} \frac{M}{\sigma L_s L_r} \\ -\omega^* + K_p K_\omega \left(\frac{L_s i_{sd}^* - K_p K_{ps}}{\sigma L_s} - i_{sd} \right) & -a_1 + \frac{K_p}{\sigma L_s} \left(\frac{K_{ps}}{\tau_r^* i_{sd}^*} - 1 \right) & -\frac{M \omega_r}{\sigma L_s L_r} \\ \frac{1}{\tau_r} M + K_p K_\omega \psi_{rq} & 0 & -\frac{1}{\tau_r} \\ -K_p K_\omega \psi_{rd} & \frac{1}{\tau_r} M & \omega_r - \omega^* \\ -a_2 \psi_{rq} & a_2 \psi_{rd} & a_2 i_{sq} \\ -K_i & 0 & 0 \\ \frac{K_\omega K_p}{T_\omega} & 0 & 0 \\ -K_{is} K_\omega K_p & \frac{K_{is}}{\tau_r^* i_{sd}^*} & 0 \\ K_i K_{ps} K_\omega K_p & K_i \left(\frac{K_{ps}}{\tau_r^* i_{sd}^*} - 1 \right) & 0 \end{bmatrix} *$$

$$* \begin{bmatrix} \frac{M \omega_r}{\sigma L_s L_r} & \frac{M \psi_{rq}}{\sigma L_s L_r} & \frac{1}{\sigma L_s} & 0 & 0 & 0 \\ \frac{1}{\tau_r} \frac{M}{\sigma L_s L_r} & -\frac{M \psi_{rd}}{\sigma L_s L_r} & K_\omega \left(\frac{K_p K_{ps} - L_s i_{sd}^*}{\sigma L_s} + i_{sd} \right) & \frac{L_s i_{sd}^* - K_p K_{ps}}{\sigma L_s} - i_{sd} & \frac{K_p}{\sigma L_s} & \frac{1}{\sigma L_s} \\ \omega^* - \omega_r & -\psi_{rq} & -K_\omega \psi_{rq} & \psi_{rq} & 0 & 0 \\ -\frac{1}{\tau_r} & \psi_{rd} & K_\omega \psi_{rd} & -\psi_{rd} & 0 & 0 \\ -a_2 i_{sd} & 0 & 0 & 0 & 0 & 0 \\ 0 & 0 & 0 & 0 & 0 & 0 \\ 0 & 0 & -\frac{K_\omega}{T_\omega} & 0 & 0 & 0 \\ 0 & 0 & K_{is} K_\omega & -K_{is} & 0 & 0 \\ 0 & 0 & K_i K_{ps} K_\omega & -K_i K_{ps} & K_i & 0 \end{bmatrix}$$

$$\mathbf{B} = \begin{bmatrix} 0 & 0 \\ \frac{K_p K_{ps}}{\sigma L_s} & 0 \\ 0 & 0 \\ 0 & 0 \\ 0 & -\frac{P}{2J} \\ 0 & 0 \\ 0 & 0 \\ K_{is} & 0 \\ K_i K_{ps} & 0 \end{bmatrix}, \quad \mathbf{B}_L = \begin{bmatrix} 0 \\ 0 \\ 0 \\ 0 \\ \frac{P}{2J} \\ 0 \\ 0 \\ 0 \\ 0 \end{bmatrix}$$

The output equation is expressed as

$$\Delta y = C \Delta x \quad \dots\dots\dots (3.67)$$

Where,

$$C = [0 \ 0 \ 0 \ 0 \ 1 \ 0 \ 0 \ 0 \ 0]$$

3.2 Proposed System B

In the proposed system B, q -axis current controller is removed. Therefore, the system B is simpler than the system A.

3.2.1 Block Diagram of System B

Figure 3.3 shows the block diagram of proposed system B. The output voltage e_d^* of d -axis PI current controller is used in both the flux angle estimation and the speed control (q -axis voltage control).

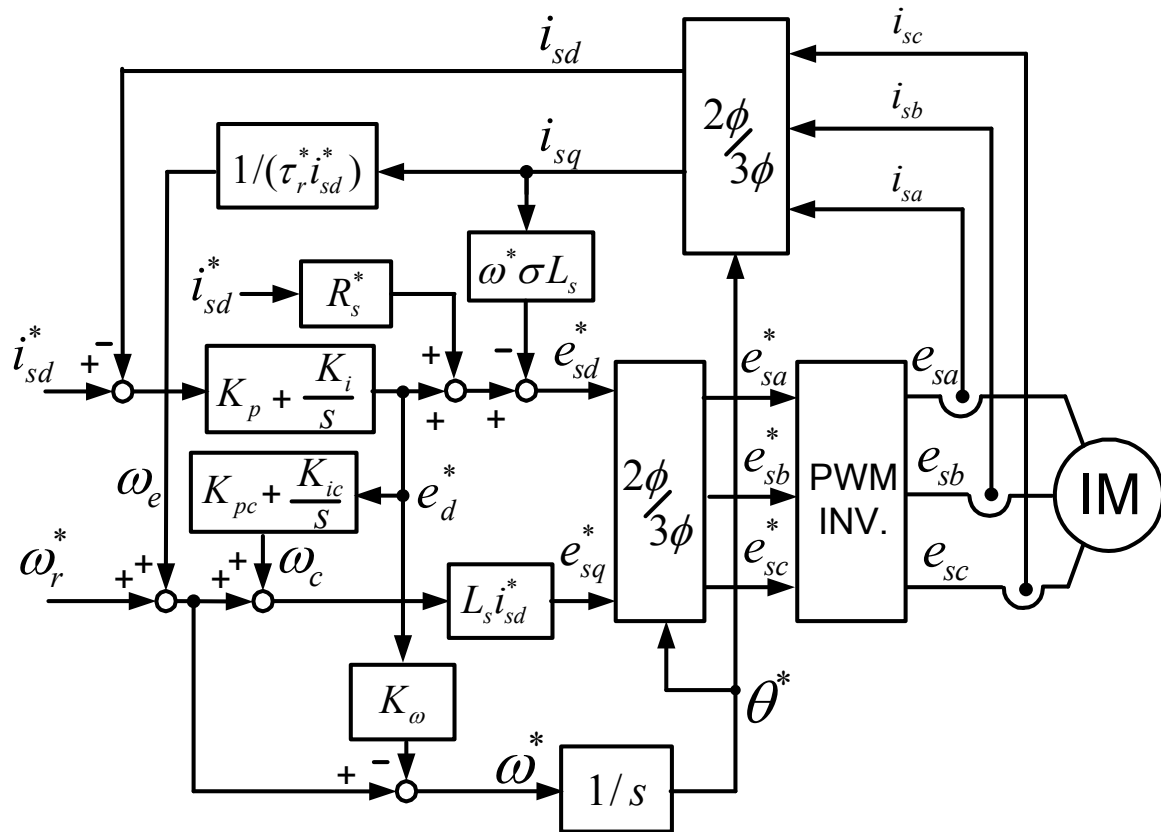


Fig.3.3. Block diagram of system B.

The e_d^* is proportional to ψ_{rq}^v as described in (3.11). By using e_d^* , the angular frequency ω^* is modified as follows:

$$\omega^* = \omega_r^* + \omega_e - K_\omega e_d^* \quad \dots\dots\dots (3.68)$$

The term $\omega_r^* + \omega_e$ is considered as feed-forward value of the angular frequency. The gain K_ω sign must be changed according to ω^* as

$$K_\omega = \text{sign}(\omega^*) |K_\omega| \quad \dots\dots\dots (3.69)$$

The estimated rotor speed $\hat{\omega}_r$ is defined as

$$\hat{\omega}_r = \omega^* - \omega_e \quad \dots\dots\dots (3.70)$$

where,

$$\omega_e = \frac{i_{sq}}{\tau_r i_{sd}^*}$$

From (3.68) and (3.70), we have

$$K_\omega e_d^* = \omega_r^* - \hat{\omega}_r \quad \dots\dots\dots (3.71)$$

Therefore, the speed control can be accomplished by using $K_\omega e_d^*$. Since the torque current i_{sq} is controlled by the q – axis voltage e_{sq}^* , we compute the e_{sq}^* as

$$e_{sq}^* = L_s i_{sd}^* (\omega_r^* + \omega_e + \omega_c) \quad \dots\dots\dots (3.72)$$

where,

$$\omega_c = \left(K_{pc} + \frac{K_{ic}}{s} \right) e_d^* \quad \dots\dots\dots (3.73)$$

Other equations of Fig.3.3 are the same as those of Fig. 3.1.

3.2.2 Description of System

The proposed system B shown in Fig.3.3 is described. The d – axis PI current controller is described by (3.22) – (3.24). The output of PI speed controller ω_c is computed by

$$\omega_c = K_\omega K_{pc} e_d^* + \omega_{ci} \quad \dots\dots\dots (3.74)$$

where,

$$\omega_{ci} = \frac{K_\omega K_{ic}}{s} e_d^* \quad \dots\dots\dots (3.75)$$

The derivative of ω_{ci} is expressed as

$$p\omega_{ci} = K_\omega K_{ic} e_d^* \quad \dots\dots\dots (3.76)$$

The angular frequency is expressed as

$$\omega^* = \omega_r^* + \frac{i_{sq}}{\tau_r^* i_{sd}^*} - K_\omega \left(K_p (i_{sd}^* - i_{sd}) + e_{cd} \right) \quad \dots\dots\dots (3.77)$$

The variable e_{cd} is defined in (3.23).

The d – axis voltage is calculated by (3.33). The q – axis voltage is written as

$$e_{sq}^* = L_s i_{sd}^* \left(\omega_r^* + \frac{i_{sq}}{\tau_r^* i_{sd}^*} + K_\omega K_{pc} \left(K_p (i_{sd}^* - i_{sd}) + e_{cd} \right) + \omega_{ci} \right) \quad \dots\dots\dots (3.78)$$

In order to analyze the IM of Fig.3.3, the d – q axis that rotates synchronously with the flux angle θ^* is defined. If the ideal voltage control of (3.19) is assumed, the actual d – q voltage are equal to those references as described in (3.21). Therefore, the equation of IM is described by (2.39). By replacing the variables e_{sd} , e_{sq} , and ω with e_{sd}^* , e_{sq}^* , and ω^* respectively.

3.2.3 Steady State Analysis

At steady state condition, the derivative operator p is set to zero. By the integral controllers of d – axis current and speed, we have

$$i_{sd} = i_{sd}^* \quad \dots\dots\dots (3.79)$$

$$e_d^* = 0 \quad \dots\dots\dots (3.80)$$

Therefore, $e_{cd} = 0$ from (3.22).

The actual IM equations at steady state are described in (3.38) – (3.42). By assuming $R_s = R_s^*$, the q – axis flux ψ_{rq} becomes zero as the same of system A. Therefore, (3.46) is valid in this case too. From (3.80), we have

$$\omega^* = \omega_r^* + \frac{i_{sq}}{\tau_r i_{sd}^*} \quad \dots\dots\dots (3.81)$$

By assuming $R_r = R_r^*$, the following equation is obtained from (3.46) and (3.81):

$$\omega_r^* = \omega_r$$

From (3.78) and (3.81), we have

$$e_{sq}^* = \omega^* L_s i_{sd}^* + \omega_{ci} L_s i_{sd}^* \quad \dots\dots\dots (3.82)$$

By comparing (3.39), (3.45) and (3.82)

$$\omega_{ci} = \frac{R_s i_{sq}}{L_s i_{sd}^*} \quad \dots\dots\dots (3.83)$$

Steady-state values are calculated by giving N_r^* , N_{sl} and i_{sd}^* as known values, similar to the case of system A.

3.2.4 Linear Model

The linear state equation of the IM is described by (3.54). From (3.55), (3.76), (3.77) for a small signal perturbation, the following equations are obtained:

$$p\Delta e_{cd} = -K_i i_{sd}$$

$$p\Delta \omega_{ci} = K_\omega K_{ic} (\Delta e_{cd} - K_p \Delta i_{sd})$$

$$\Delta \omega^* = \Delta \omega_r^* + \frac{\Delta i_{sq}}{\tau_r^* i_{sd}^*} + K_\omega (K_p \Delta i_{sd} - \Delta e_{cd})$$

The d – axis voltage e_{sd}^* in (3.33) is linearized as

$$\begin{aligned} \Delta e_{sd}^* &= -K_p \Delta i_{sd} + \Delta e_{cd} - \omega^* \sigma L_s \Delta i_{sq} - \Delta \omega^* \sigma L_s i_{sq} \\ &= -(\sigma L_s i_{sq} K_\omega + 1) K_p \Delta i_{sd} - \left(\omega^* + \frac{i_{sq}}{\tau_r^* i_{sd}^*} \right) \sigma L_s \Delta i_{sq} \\ &\quad + (K_\omega \sigma L_s i_{sq} + 1) \Delta e_{cd} - \sigma L_s i_{sq} \Delta \omega_r^* \dots \dots \dots (3.84) \end{aligned}$$

The q – axis voltage e_{sq}^* in (3.78) is linearized as

$$\Delta e_{sq}^* = L_s i_{sd}^* \left(\Delta \omega_r^* + \frac{\Delta i_{sq}}{\tau_r^* i_{sd}^*} + K_\omega K_{pc} (\Delta e_{cd} - K_p \Delta i_{sd}) + \Delta \omega_{ci} \right) \dots \dots \dots (3.85)$$

The state equation of the controller is expressed as

$$p\Delta\mathbf{z} = \mathbf{A}_x\Delta\mathbf{x}_s + \mathbf{A}_z\Delta\mathbf{z} + \mathbf{B}_r\Delta\mathbf{r} \quad \dots\dots\dots (3.86)$$

$$p \begin{bmatrix} \Delta e_{cd} \\ \Delta \omega_{ci} \end{bmatrix} = \begin{bmatrix} -K_i & 0 & 0 & 0 & 0 \\ -K_\omega K_{ic} K_p & 0 & 0 & 0 & 0 \end{bmatrix} \begin{bmatrix} \Delta i_{sd} \\ \Delta i_{sq} \\ \Delta \psi_{rd} \\ \Delta \psi_{rq} \\ \Delta \omega_r \end{bmatrix} + \begin{bmatrix} 0 & 0 \\ K_\omega K_{ic} & 0 \end{bmatrix} \begin{bmatrix} \Delta e_{cd} \\ \Delta \omega_{ci} \end{bmatrix}$$

$$\Delta\mathbf{u}_s = \mathbf{F}_x \Delta\mathbf{x}_s + \mathbf{F}_z \Delta\mathbf{z} + \mathbf{F}_r \Delta\mathbf{r} \quad \dots\dots\dots (3.87)$$

$$\begin{bmatrix} \Delta e_{sd}^* \\ \Delta e_{sq}^* \\ \Delta \omega^* \end{bmatrix} = \begin{bmatrix} -(K_\omega \sigma L_s i_{sq} + 1) K_p & -\left(\omega^* - \frac{i_{sq}}{\tau_r i_{sd}^*}\right) \sigma L_s & 0 & 0 & 0 \\ -L_s i_{sd}^* K_\omega K_{pc} K_p & \frac{L_s}{\tau_r} & 0 & 0 & 0 \\ K_\omega K_p & \frac{1}{\tau_r i_{sd}^*} & 0 & 0 & 0 \end{bmatrix} \begin{bmatrix} \Delta i_{sd} \\ \Delta i_{sq} \\ \Delta \psi_{rd} \\ \Delta \psi_{rq} \\ \Delta \omega_r \end{bmatrix} \\ + \begin{bmatrix} 1 + K_\omega \sigma L_s i_{sq} & 0 \\ L_s i_{sd}^* K_\omega K_{pc} & L_s i_{sd}^* \\ -K_\omega & 0 \end{bmatrix} \begin{bmatrix} \Delta e_{cd} \\ \Delta \omega_{ci} \end{bmatrix} + \begin{bmatrix} -\sigma L_s i_{sq} \\ L_s i_{sd}^* \\ 1 \end{bmatrix} \begin{bmatrix} \Delta \omega_r^* \end{bmatrix}$$

The linear model of whole system is obtained as follows:

$$p \begin{bmatrix} \Delta\mathbf{x}_s \\ \Delta\mathbf{z} \end{bmatrix} = \begin{bmatrix} \mathbf{A}_s + \mathbf{B}_s \mathbf{F}_x & \mathbf{B}_s \mathbf{F}_z \\ \mathbf{A}_x & \mathbf{A}_z \end{bmatrix} \begin{bmatrix} \Delta\mathbf{x}_s \\ \Delta\mathbf{z} \end{bmatrix} + \begin{bmatrix} \mathbf{B}_s \mathbf{F}_r \\ \mathbf{B}_r \end{bmatrix} \Delta\mathbf{r} + \begin{bmatrix} \mathbf{B}_L \\ 0 \end{bmatrix} \Delta T_L$$

Simply,

$$p\Delta\mathbf{x} = \mathbf{A} \Delta\mathbf{x} + \mathbf{B}_r \Delta\mathbf{r} + \mathbf{B}_L \Delta T_L \quad \dots\dots\dots (3.88)$$

where,

$$\begin{aligned}
 A = & \begin{bmatrix}
 -a_1 - \frac{K_p}{\sigma L_s} & 0 \\
 -\omega^* + i_{sd} K_\omega K_p \left(-\frac{K_{pc}}{\sigma} - 1 \right) & -a_1 + \frac{1}{\sigma \tau_r} - \frac{i_{sd}}{\tau_r i_{sd}^*} \\
 \frac{M}{\tau_r} + K_\omega K_p \psi_{rq} & \frac{\psi_{rq}}{\tau_r i_{sd}^*} & * \\
 -K_\omega K_p \psi_{rd} & \frac{M}{\tau_r} - \frac{\psi_{rd}}{\tau_r i_{sd}^*} \\
 -a_2 \psi_{rq} & a_2 \psi_{rd} \\
 -K_i & 0 \\
 -K_\omega K_{ic} K_p & 0
 \end{bmatrix} \\
 & \begin{bmatrix}
 \frac{M}{\sigma L_s L_r \tau_r} & \frac{M \omega_r}{\sigma L_s L_r} & \frac{M \psi_{rq}}{\sigma L_s L_r} & \frac{1}{\sigma L_s} & 0 \\
 -\frac{M \omega_r}{\sigma L_s L_r} & \frac{M}{\sigma L_s L_r \tau_r} & -\frac{M \psi_{rd}}{\sigma L_s L_r} & \frac{i_{sd}^* K_\omega K_{pc}}{\sigma} + K_\omega i_{sd} & \frac{i_{sd}^*}{\sigma} \\
 * & -\frac{1}{\tau_r} & (\omega^* - \omega_r) & -\psi_{rq} & -\psi_{rq} K_\omega & 0 \\
 -(\omega^* - \omega_r) & -\frac{1}{\tau_r} & \psi_{rd} & \psi_{rd} K_\omega & 0 \\
 a_2 i_{sq} & -a_2 i_{sd} & 0 & 0 & 0 \\
 0 & 0 & 0 & 0 & 0 \\
 0 & 0 & 0 & K_\omega K_{ic} & 0
 \end{bmatrix}
 \end{aligned}$$

$$\mathbf{B} = \begin{bmatrix} 0 \\ \frac{i_{sd}^* - i_{sd}}{\sigma} \\ \psi_{rq} \\ -\psi_{rd} \\ 0 \\ 0 \\ 0 \end{bmatrix}, \quad \mathbf{B}_L = \begin{bmatrix} 0 \\ 0 \\ 0 \\ 0 \\ -\frac{P}{2J} \\ 0 \\ 0 \end{bmatrix}$$

The output equation is expressed as

$$\Delta y = C \Delta x \quad \dots\dots\dots (3.89)$$

where,

$$C = [0 \ 0 \ 0 \ 0 \ 1 \ 0 \ 0]$$

3.3 Gain Selection of Controller

3.3.1 Current Controller

Figure 3.4 shows a block diagram of the PI current control system of IM. The IM is modeled as a series circuit of the resistance R_{sr} and leakage inductance σL_s . The disturbance means a counter electromotive force. The resistance R_{sr} is expressed as

$$R_{sr} = R_s + \left(\frac{M}{L_r}\right)^2 R_r \quad \dots\dots\dots (3.90)$$

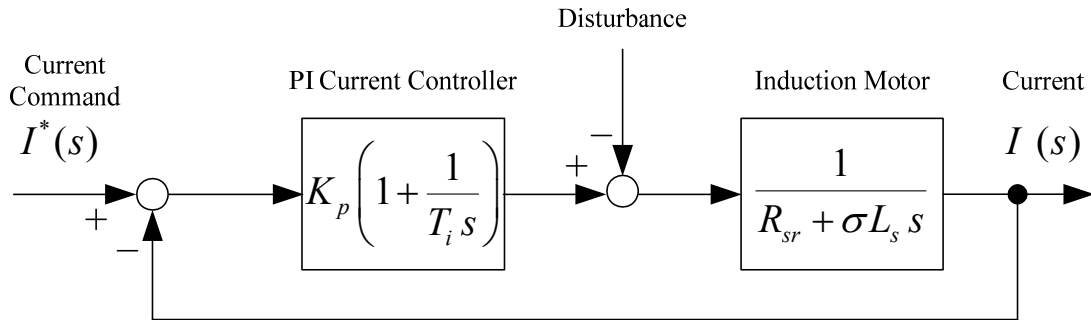


Fig.3.4 Block diagram of the current control system.

Assuming that there are no disturbances, the closed-loop transfer function of the current control becomes the following equations:

$$\frac{I}{I^*} = \frac{K_p (T_i s + 1)}{(\sigma L_s s + R_{sr}) T_i s + K_p (T_i s + 1)}$$

The T_i is usually designed as [45]

$$T_i = \frac{\sigma L_s}{R_{sr}} \dots\dots\dots (3.91)$$

The current transfer function becomes as

$$\frac{I}{I^*} = \frac{K_p}{\sigma L_s s + K_p} = \frac{1}{T_{eq} s + 1} \dots\dots\dots (3.92)$$

where,

$$T_{eq} = \frac{\sigma L_s}{K_p}$$

Cut-off frequency ω_c of this transfer function is expressed by the following equation:

$$\omega_c = \frac{K_p}{R_{sr} T_i} = \frac{1}{T_{eq}} \dots\dots\dots (3.93)$$

By setting the cut-off frequency ω_c , the proportional gain K_p is determined by (3.93).

3.3.2 Speed Controller

The block diagram of speed control system is shown in Fig.3.5. When the vector control is ideal, the torque can be controlled as

$$\tau_e = \frac{PM^2}{2L_r} i_{sd}^* i_{sq} = K_T i_{sq} \quad \dots\dots\dots (3.94)$$

The loop transfer function G_0 of Fig. 3.5 is

$$G_0 = \left(K_{ps} + \frac{K_{is}}{s} \right) \frac{1}{1 + T_{eq}s} \frac{PK_T}{2Js} \quad \dots\dots\dots (3.95)$$

The Bode diagram of (3.95) is shown in Fig.3.6. The angular frequency ω_{pi} is expressed as

$$\omega_{pi} = K_{is} / K_{ps} \quad \dots\dots\dots (3.96)$$

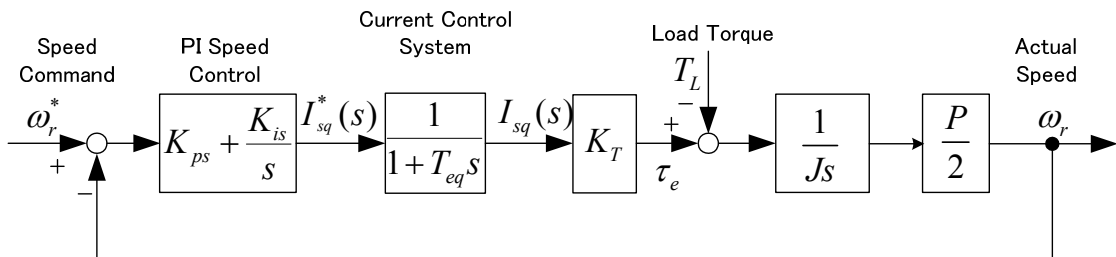


Fig.3.5 Block diagram of the speed control system.

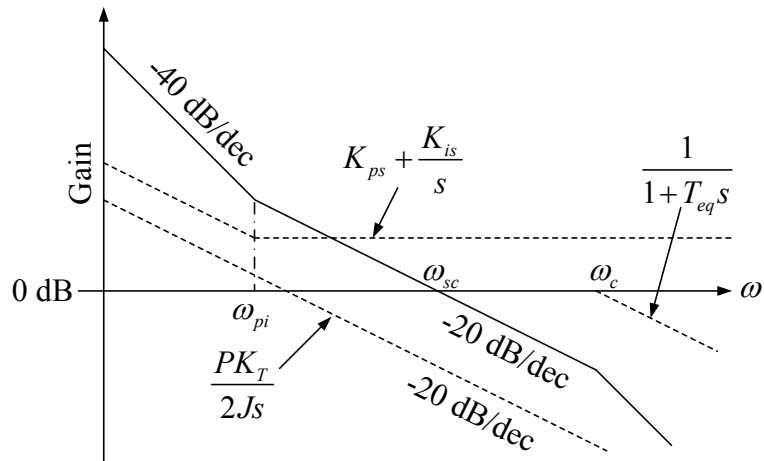


Fig.3.6 Bode diagram of loop transfer function G_0 .

In order to have sufficient phase margin, the following equation should be satisfied [45]:

$$\omega_{pi} \leq \omega_{sc} / 5 \quad \dots\dots\dots (3.97)$$

Under the condition (3.97), the crossover frequency ω_{sc} is obtained as

$$\omega_{sc} = \frac{PK_T K_{ps}}{2J} \quad \dots\dots\dots (3.98)$$

If we set the ω_{pi} and ω_{sc} , the gains K_{ps} and K_{is} is determined by (3.98) and (3.96).

Chapter 4

Simulation and Experimental Results

4.1 Experimental System

4.1.1 Microcomputer control system

The IM control system by using a digital signal processor (DSP) is shown in Fig.4.1. The power circuit is composed by rectifier, smoothing capacitor, and IGBT inverter. A DC machine is used as a load through a torque sensor for the induction machine. Torque sensor is used for detecting the torsion of the shaft. The motor currents and DC link voltage are detected to the DSP through an analog to digital (A/D) converter.

PWM gate signal generator is connected to IGBT inverter. These signals are carried by an optical fiber cable and are not affected by noise. Resistor is connected to the braking circuit and the regenerative energy is consumed as heat. When the IM operates as a generator, IGBT brake circuit is turned on. The dangerous voltage rise can damage the rectifier circuit diode and the smoothing capacitor, because its energy is not returned to the power supply.

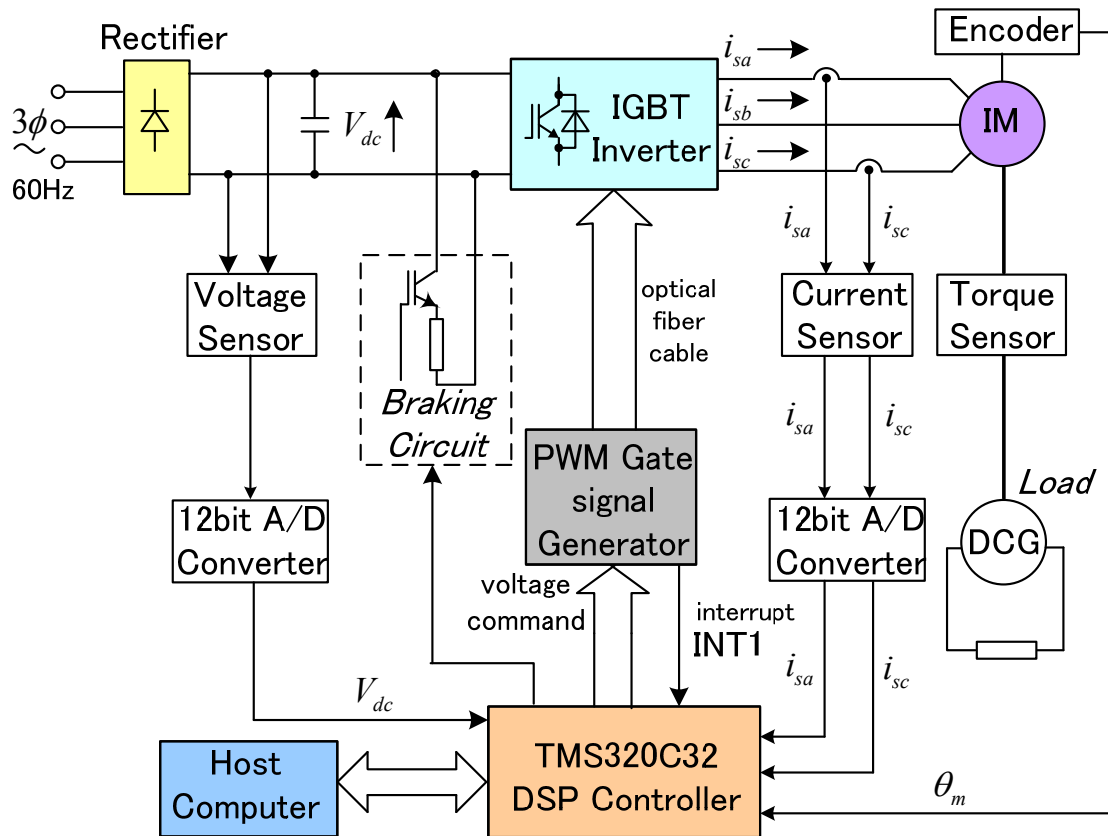


Fig.4.1 Experimental system.

The interrupt signal INT1 of the DSP is sent from the PWM gate signal generator to synchronize the period of PWM. The host computer has a segment that can be connected to the DSP, so it can transfer control program, or display information on the screen from DSP. The PWM inverter and DSP control circuit is made by My Way Co., Ltd. Block diagram of DSP 320C32 is shown in Fig.4.2.

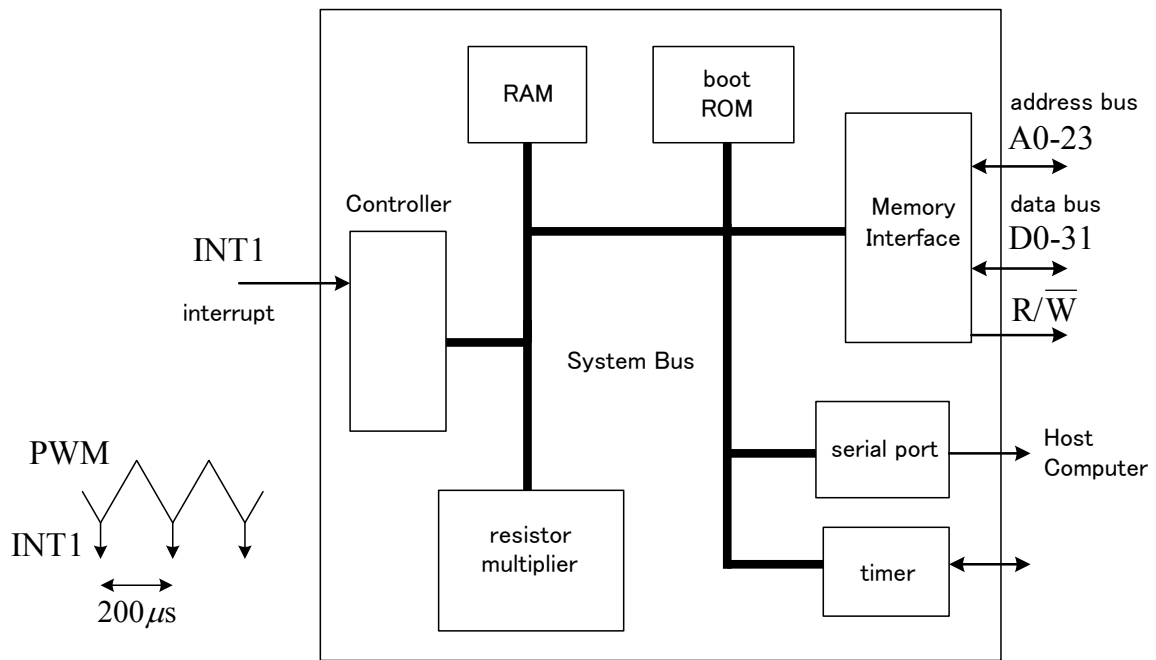


Fig.4.2 Block diagram of DSP TMS320C32.

The experimental program of the DSP is written by using C language. The developed program is divided into the main routine, INT1 interrupt routine and the timer0 interrupt routine. Fig.4.3 shows the flow chart of the sensorless vector control B.

First, the main program starts. After the permission of interrupt, the INT1 and Timer0 interrupts can be accepted to DSP and the main program enters into infinite loop to communicate with the host computer. For example, the waveform data is sent to the host computer such as speed and current, when INT1 signal enters the DSP from the gate signal generator, the main program is stopped. Timer0 interrupt program is accepted to DSP after the INT1 program ended. The INT1 has dominant priority. The main program priority is the lowest, and it is executed when two interrupt programs are ended. The INT1 program runs every $200\mu s$.

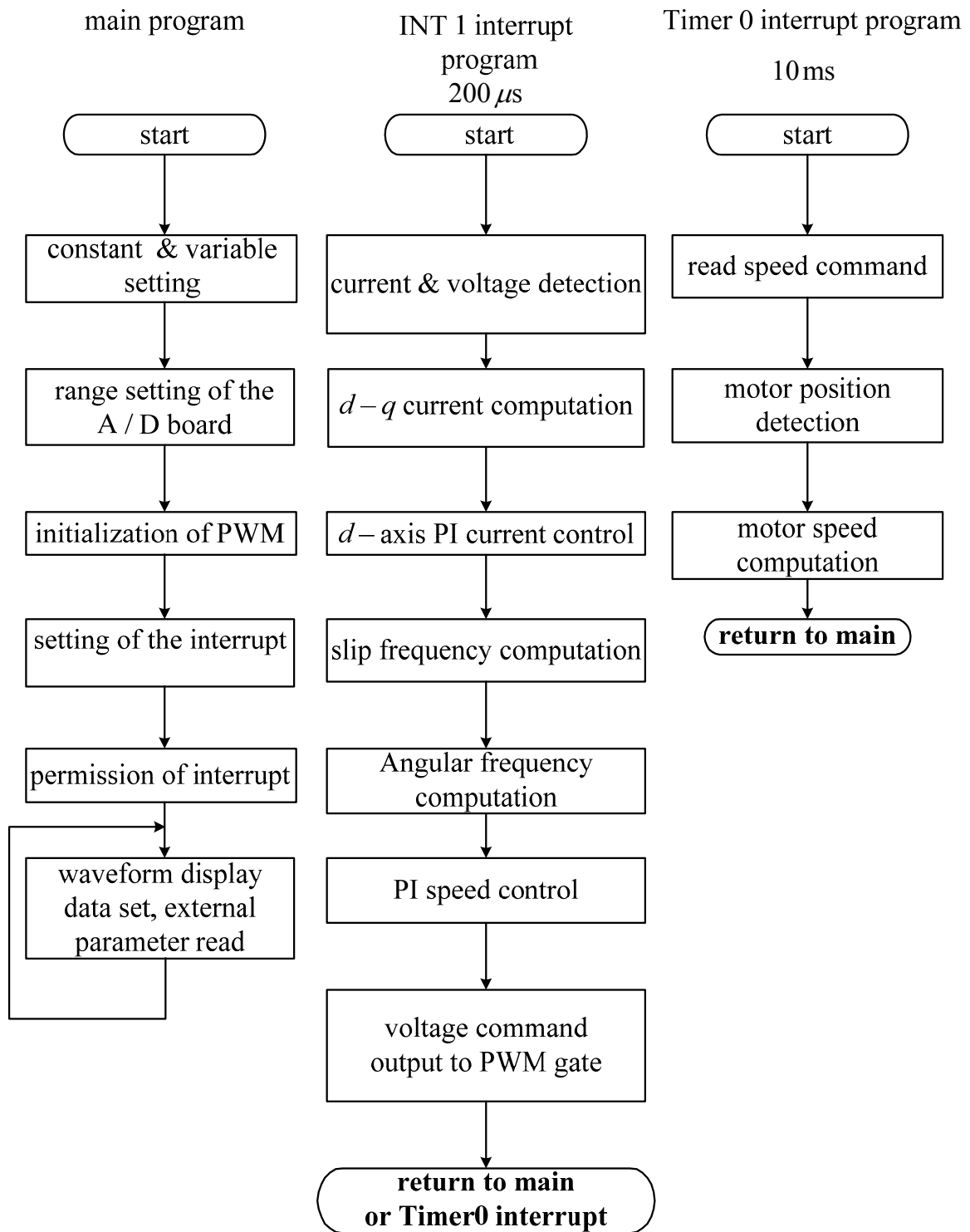


Fig.4.3 Flow chart of sensorless vector control B program.

The experimental programs are changed to machine language by using C compiler and sent to RAM of DSP. This process is called “downloading”. Process and communication program commands are made by My Way Co. Ltd. It is necessary for both the DSP and the PC.

4.1.2 Parameters of System

The IM specifications used in the experimental system are shown in Table 4.1.

The leakage inductance σL_s is computed as

$$\sigma L_s = \left(1 - \frac{M^2}{L_s L_r}\right) L_s = \left(1 - \frac{0.11^2}{0.115^2}\right) \times 0.115 = 0.00978 \text{ H}$$

Resistance of stator and rotor of (3.90) is computed as

$$R_{sr} = R_s + \left(\frac{M}{L_r}\right)^2 R_r = 1.54 + \left(\frac{0.11}{0.115}\right)^2 \times 0.787 = 2.26 \Omega$$

Integration time T_i is computed from (3.91) as

$$T_i = \frac{\sigma L_s}{R_{sr}} = \frac{0.00978}{2.26} = 0.00433$$

By choosing that the cut-off frequency of (3.93) is 1500 rad/s, the current PI gains are computed as follows:

$$K_p = R_{sr} T_i \omega_c = \sigma L_s \omega_c = 0.00978 \times 1500 = 14.7$$

$$K_i = \frac{K_p}{T_i} = \frac{14.7}{0.00433} = 3395$$

Table 4.1 Parameters of the three-phase IM.

Number of poles P [poles]	4
Rated Output [kW]	1.5
Rated Torque [N-m]	8.43
Speed [min^{-1}]	1700
Rated Line Voltage [V]	200
Rated Current [A]	6.4
Excitation Current i_{sd}^* [A]	4.2
Moment Inertia J [$\text{kg}\cdot\text{m}^2$]	0.0126
Primary Resistance Nominal Value R_s [Ω]	1.54
Secondary Resistance Nominal Value R_r [Ω]	0.787
Iron Loss Resistance R_m [Ω]	391
Primary Self-inductance L_s [H]	0.115
Secondary Self-Inductance L_r [H]	0.115
Mutual Inductance M [H]	0.11
Motor Manufacturer	Mitsubishi Electric Corporation

For the design of PI speed control system, torque constant is computed as

$$K_T = \frac{PM^2}{2L_r} i_{sd}^* = \frac{4 \times 0.11^2}{2 \times 0.115} \times 4.2 = 0.8838$$

The PI speed proportional gain (3.98) is computed by

$$K_{ps} = \frac{2J\omega_{sc}}{PK_T} = \frac{2 \times 0.0126 \times \omega_{sc}}{4 \times 0.8838} = 0.00713 \times \omega_{sc}$$

When the cut-off frequency of PI speed control system ω_{sc} is set to 20, then

$$K_{ps} = 0.0713 \times 20 = 0.1426$$

The angular frequency ω_{pi} of PI speed controller is set to 4 rad/s.

The integral gain K_{is} of PI speed controller is computed as

$$K_{is} = \omega_{pi} K_{ps} = 4 \times 0.1426 = 0.5704$$

The integration time T_{is} of PI speed controller is computed as

$$T_{is} = \frac{K_{ps}}{K_{is}} = \frac{0.1426}{0.5704} = 0.25$$

Table 4.2 shows the control parameters of system A.

Table 4.2 Control Parameters of System A.

Current PI Proportional Gain K_p	14.7
Current PI Integral Gain K_i	3395
Current PI Integration Time T_i	0.00433
Current PI Cut-off Frequency ω_c	1500
Speed PI Proportional Gain K_{ps}	0.1426
Speed PI Integral Gain K_{is}	0.5704
Speed PI Integration Time T_{is}	0.25
Speed PI Cut-off Frequency ω_{sc}	20.0
PI Proportional Gain $ K_{p\omega} $	(K_ω) 20.0
PI Integral Gain $ K_{i\omega} $	(K_ω /T_ω) 20.0

In system B, the PI current control gain and integration time are the same with system A, and other gains are derived from the analysis of system stability. Control parameters of system B are shown in Table 4.3.

Table 4.3 Control Parameters of System B.

Current PI Proportional Gain K_p	14.7
Current PI Integral Gain K_i	3395
Current PI Integration Time T_i	0.00433
Current PI Cut-off Frequency ω_c	1500
PI Proportional Gain K_{pc}	1.0
PI Integral Gain K_{ic}	20.0
Gain $ K_\omega $	5.0

4.1.3 Experimental IM – DCM System

Figure 4.4 shows the experimental DCM circuit for the forward rotation of IM. In the motoring operation of IM, the direction of rotation, the rotating magnetic field direction and the produced torque T_e are in the same direction. The load torque T_L has equal magnitude to the T_e in the opposite direction at the steady state operation.

If the terminals X and Y are directly connected, the current flows through the bulb in the direction of I_a in motoring operation. The armature current I_a becomes maximum when all the light bulbs which are connected parallels are switched on. The DCM voltage generated is proportional to the velocity. Therefore, this voltage becomes smaller during low-speed operation; the armature current I_a does not increased even if all the light bulbs are turned on. To solve this problem, we use a diode bridge which is connected

between the terminals X and Y. This polarity can be changed depending on whether the DCM operation as motoring or regenerating. By increasing the voltage of the variable transformer connected to the diode bridge, DC voltage of the diode bridge and armature current I_a are increased.

The load torque T_L delivered by DCM is proportional to I_a . In this way, it is possible to perform experiment with different load torque. The maximum torque in this experiment is 8.0 N-m. The speed of IM does not change even by changing the load torque T_L .

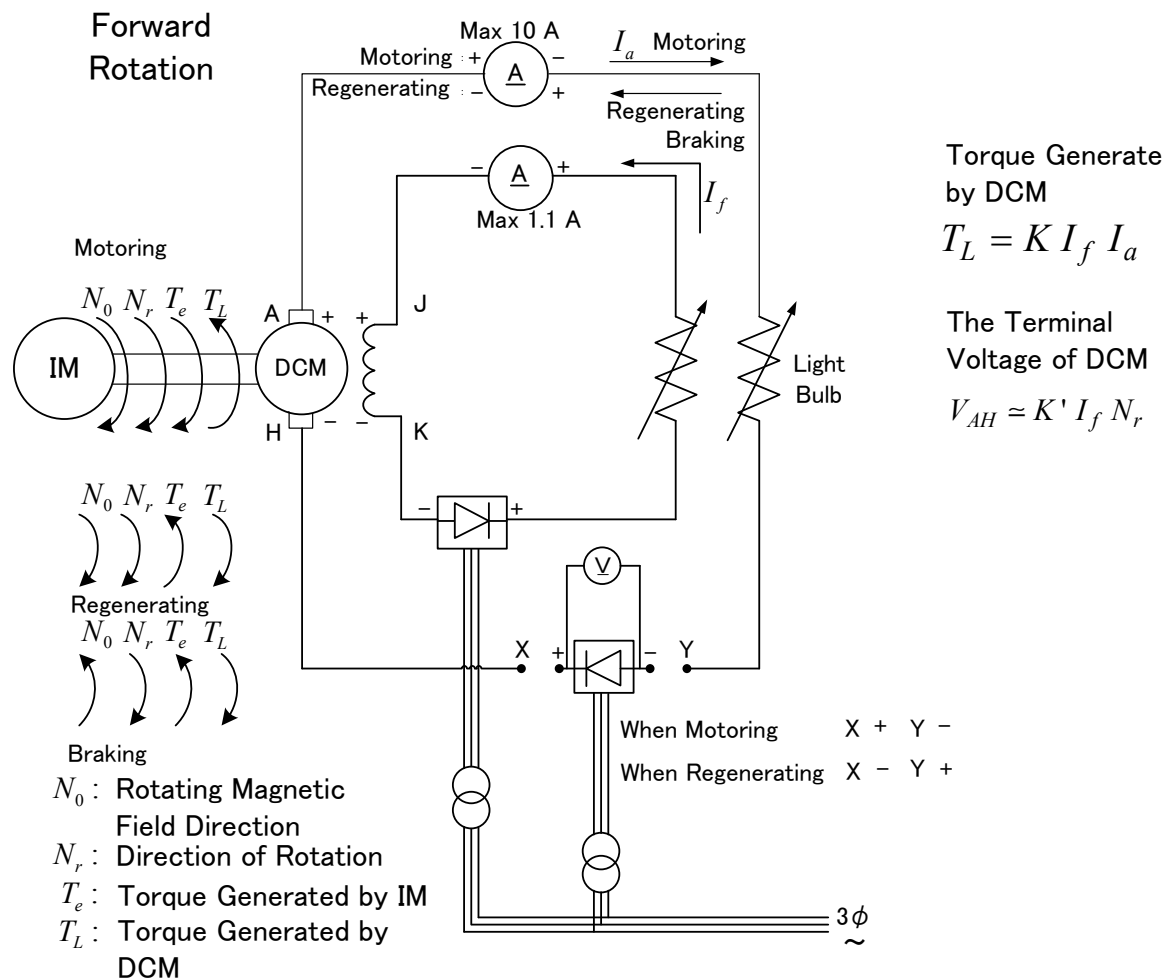


Fig. 4.4 Experimental DCM circuit for motoring and regenerating operations of IM.

By considering the climbing slopes, the IM is under resistance from the gravity, that is the load torque as shown in Fig.4.5. This situation is called motoring operation. When the motor rotates higher than the synchronous speed, it generates a braking force. This condition is called regenerating operation. In this process, the mechanical energy is converted to electrical energy (so-called operation as an induction generator). There is also another circumstance, when the direction of synchronous speed is opposite to the rotor rotation. This situation is called plugging. In this case, the direction of motor rotation follows the load torque and the direction of the torque produced by the motor follows the synchronous speed.

In regenerating operation and forward rotation, the DCM must be operated as a motor. For this reason, in the diode bridge, X and Y are connected to (-) and (+) respectively. The armature current I_a becomes opposite in regenerating operation, the load torque T_L generated by DCM is also reversed. However, the speed of IM is does not change if the speed command of IM control system is constant. Therefore, torque current i_{sq} and T_e change automatically to keep the constant velocity until T_e is equal to T_L the same value in the opposite direction. As a result, the direction of T_e is reversed with respect to the rotation direction N_r . Mechanical energy goes into the IM; and it is operated as a generator. During this time, DCM provides mechanical energy. This energy is used by the resistance of IM and inverter, but a lot of energy is used to charge the DC capacitor. Then, the capacitor voltage increases rapidly. The energy is not sent to the three-phase power supply side because of the diode bridge, but there is a brake circuit in order to keep a constant capacitor voltage by turning on and off the dynamic brake (DB) switch. Fig.4.6 shows the experimental IM connected to the DC motor as a load and a torque detector in between.

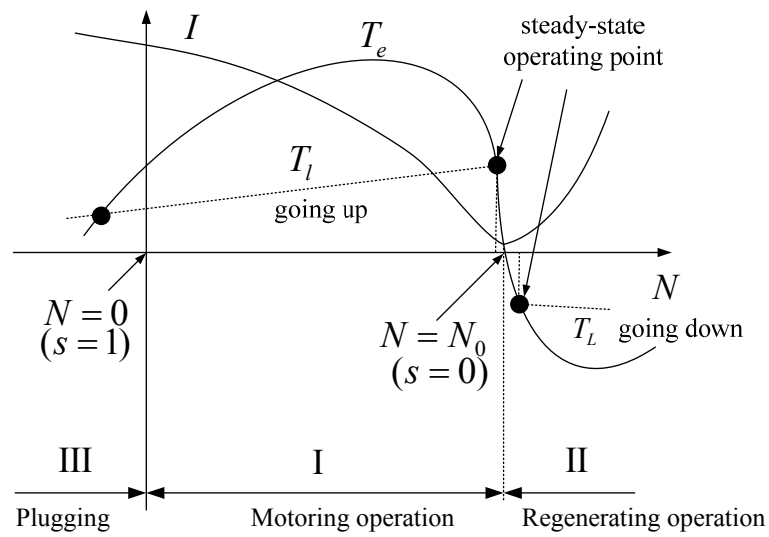
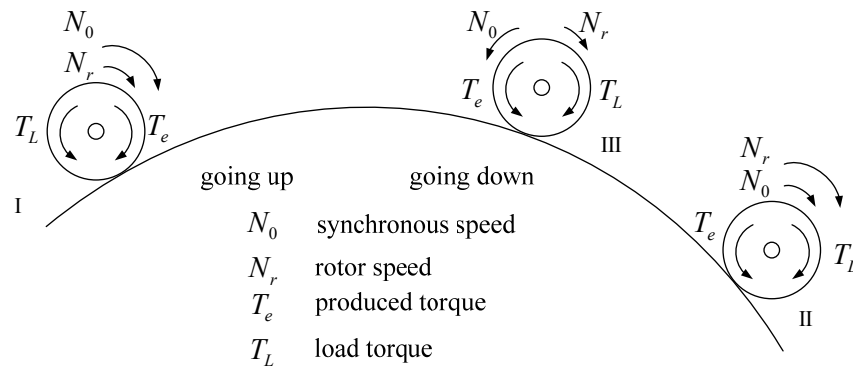


Fig.4.5 Operating regions of IM.

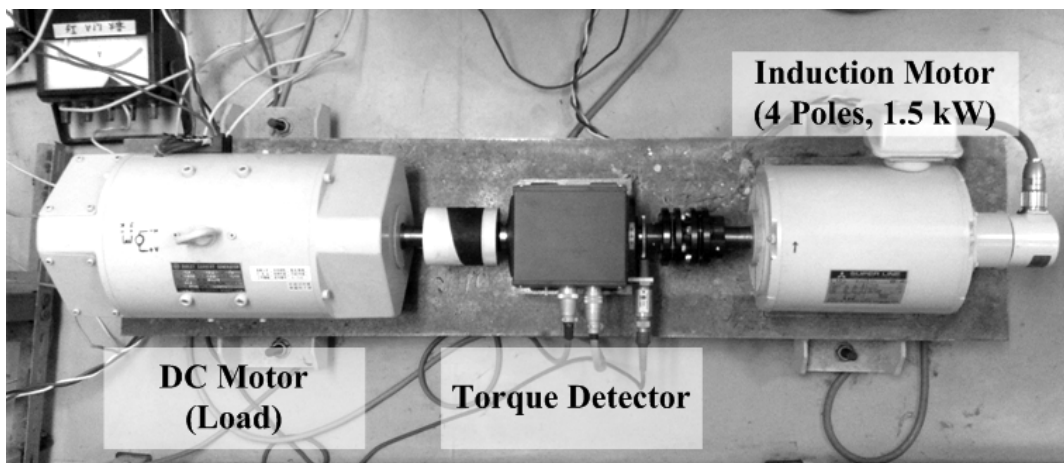


Fig.4.6 IM with DCM as a load and a torque detector in between.

4.2 System Stability

Figure 4.7 shows the root trajectories that are computed by the linear model of proposed system B. The speed command N_r^* is 700 min^{-1} , and slip speed N_{sl} are changed from -80 min^{-1} to 80 min^{-1} as parameter of load. The different integral gain K_{ic} such as 100.0, 50.0, 33.3, 25.0 and 20.0 are selected. If the integral gain K_{ic} is very large, the system becomes unstable. However, if K_{ic} is selected smaller than 100.0, the system is stable at both motoring and regenerating operation.

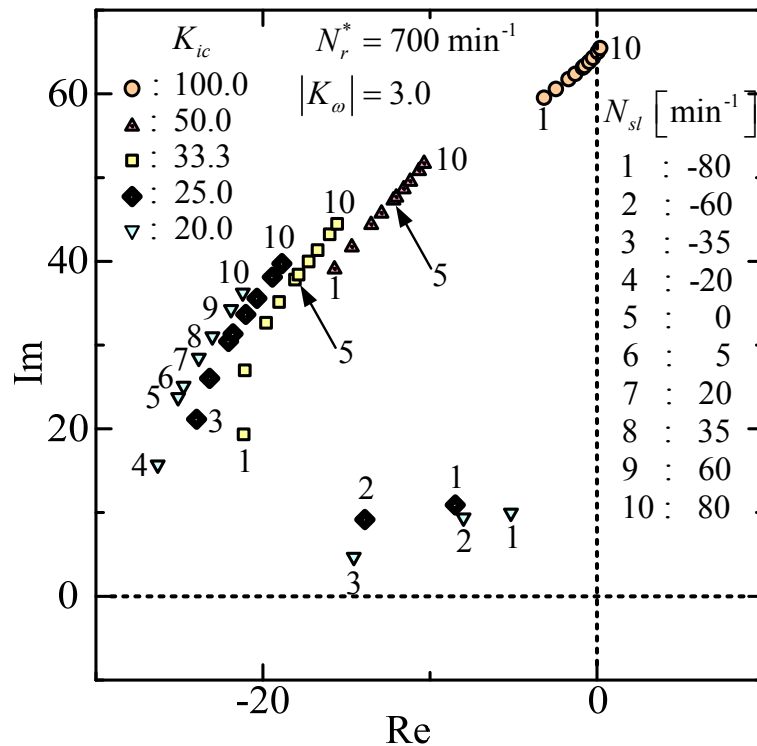


Fig.4.7 Root trajectories with parameters of slip speed N_{sl} and integral gain K_{ic} (system B).

Figure 4.8 shows the root trajectories when the gain $|K_\omega|$ and the integral gain K_{ic} are changed. The speed command N_r^* is 700 min^{-1} , and slip speed N_{sl} is 35.0 min^{-1} . It is observed that the system becomes stable by choosing larger value of $|K_\omega|$ and smaller value of K_{ic} .

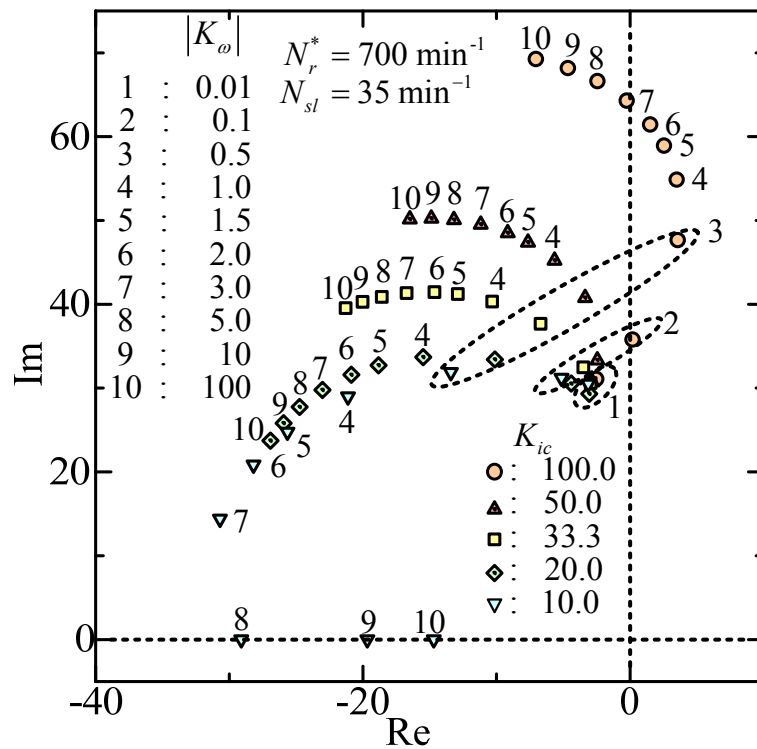


Fig.4.8 Root trajectories with parameters of integral gain K_{ic} and gain $|K_\omega|$ (system B).

To see the movement of roots by changing the gain $|K_\omega|$ and the slip speed N_{sl} is shown in Fig.4.9. The gain $|K_\omega|$ is changed to 0.1, 1.0, 3.0, and 10.0 and the slip speed N_{sl} is changed from -80 min^{-1} to 80 min^{-1} . When $|K_\omega|$ is larger than 3.0, the system becomes stable at motoring and regenerating operation. When $|K_\omega|$ is small the system is unstable at high load in both motoring and regenerating operations.

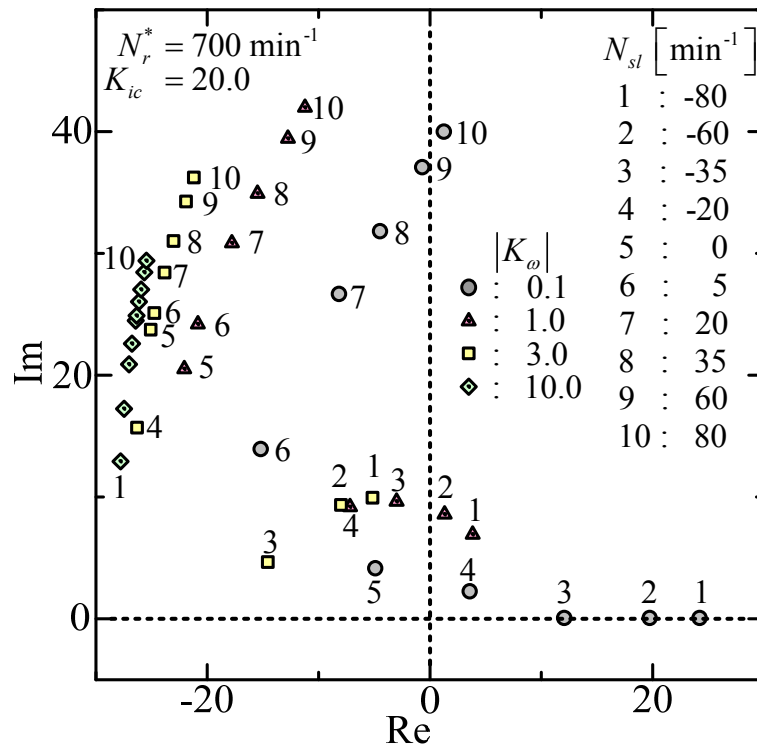


Fig.4.9 Root trajectories with parameters slip speed N_{sl} and gain $|K_\omega|$ (system B).

In Fig.4.10, the root loci is shown when $N_r^* = 1500 \text{ min}^{-1}$, $K_{ic} = 20.0$, $|K_\omega| = 3.0$, for the change of slip speed N_{sl} from -80 min^{-1} to 80 min^{-1} . The system is stable in all operating points. By comparing Fig.4.9 and Fig.4.10 the system works more stable at higher speed in motoring operations, because the real part of the root is smaller.

Figures 4.11 and 4.12 show the root trajectories computed by the linear models of the systems A and B in the case of $N_r^* = 50 \text{ min}^{-1}$ and $N_r^* = 100 \text{ min}^{-1}$ respectively. The slip speed is changed from -80 min^{-1} to 80 min^{-1} as parameter of load by the increment 4 min^{-1} . The system is stable at low speed regenerating operation. However, the system is unstable at plugging region as shown in Fig.4.11 (a) and (b) by the poles on real axis in both systems.

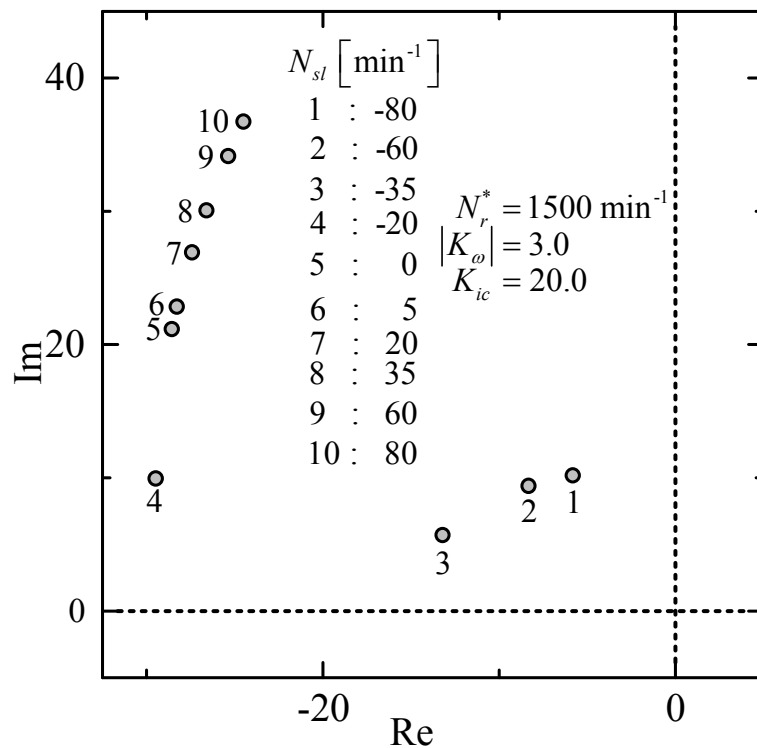
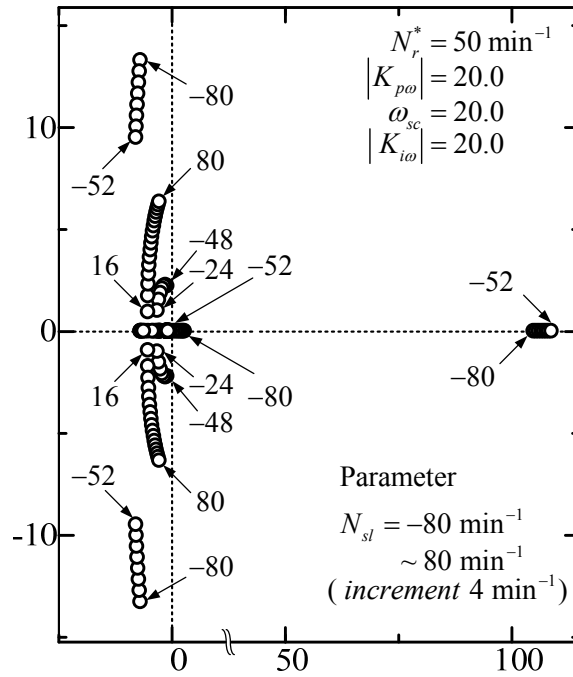
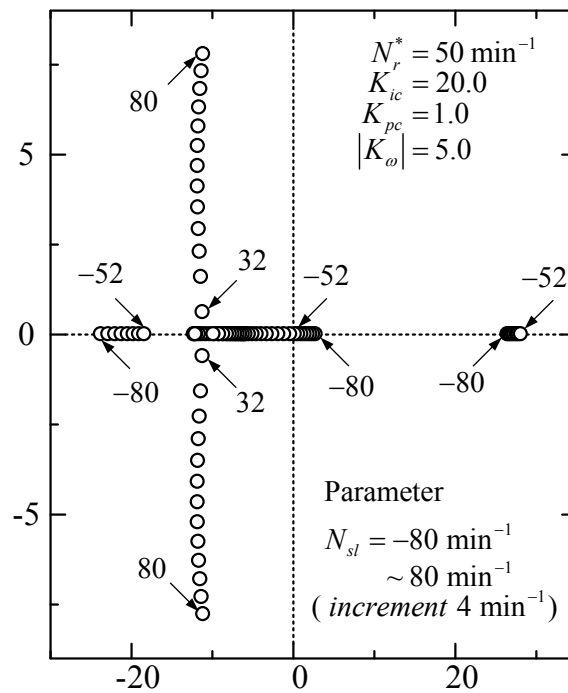


Fig.4.10 Root trajectory at 1500 min^{-1} (system B).

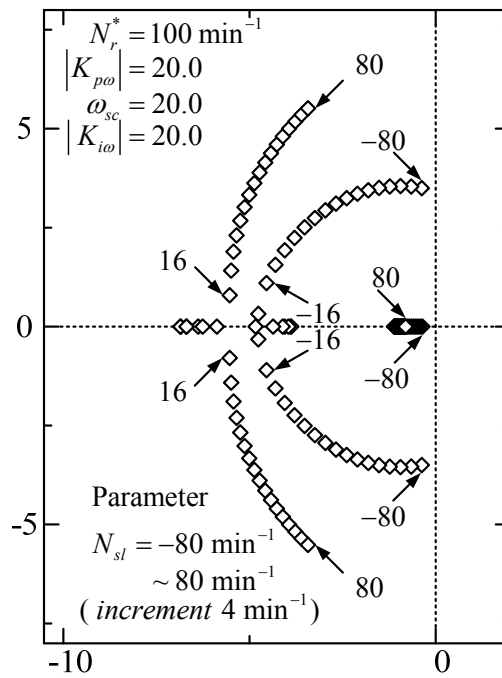


(a) System A

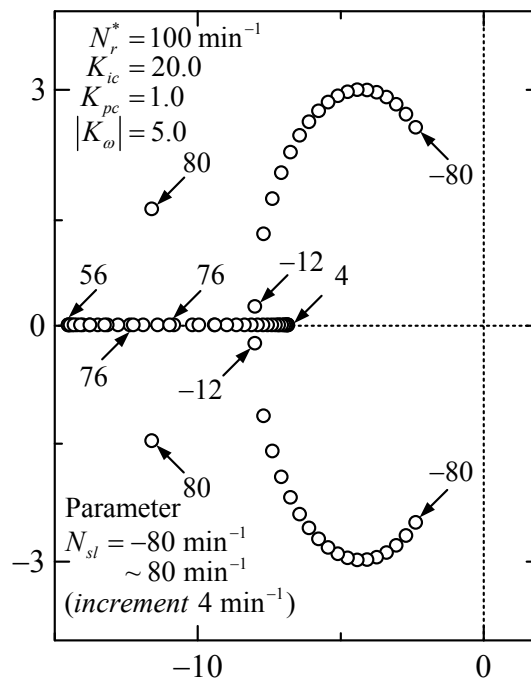


(b) System B

Fig.4.11 Root trajectories with parameter N_{sl} at speed $N_r^* = 50 \text{ min}^{-1}$ (systems A and B).



(a) System A



(b) System B

Fig.4.12 Root trajectories with parameter N_{sl} at speed $N_r^* = 100 \text{ min}^{-1}$ (systems A and B).

Figure 4.13 shows the unstable operating region of system A with parameters; $|K_{p\omega}| = 20.0$, $|K_{i\omega}| = 20.0$, and $\omega_{sc} = 20.0$. The ω_{sc} is cut-off angular frequency of the speed control. These gains are selected to have wide stable operating points.

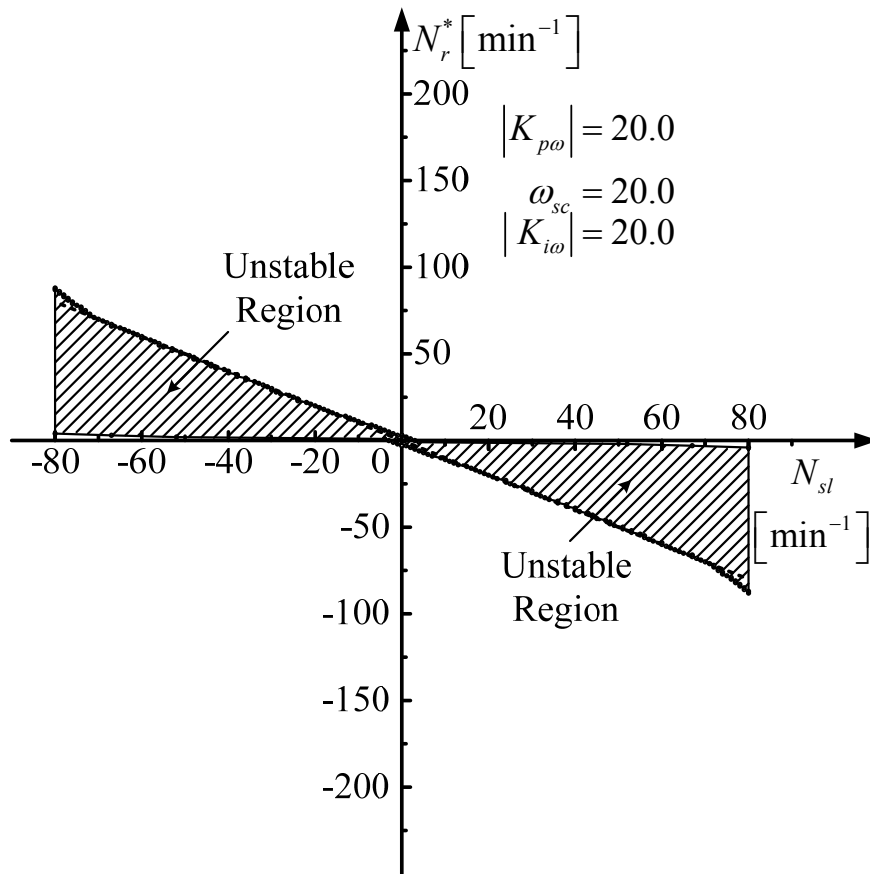


Fig.4.13 Unstable region of system A.

In Fig.4.14 shows the unstable operating region when speed command and slip speed are changed with parameters $|K_\omega|=5.0$, $K_{ic}=20.0$, and $K_{pc}=0.0$ for system B. By comparing the results of Fig.4.13 and 4.14, it is observed that the unstable plugging region is almost same.

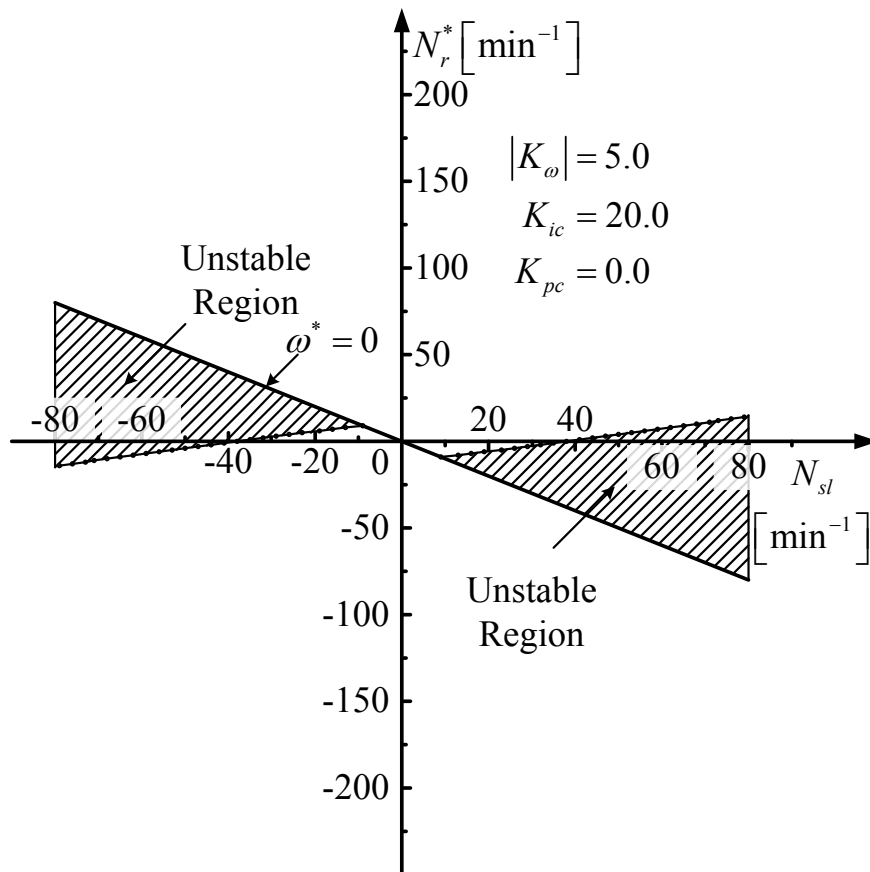


Fig.4.14 Unstable region with parameter $K_{pc} = 0.0$ for system B.

The increasing gain value of speed control proportional gain K_{pc} can improve the stability region at low speed of motoring and plugging operation as shown in Fig. 4.15.

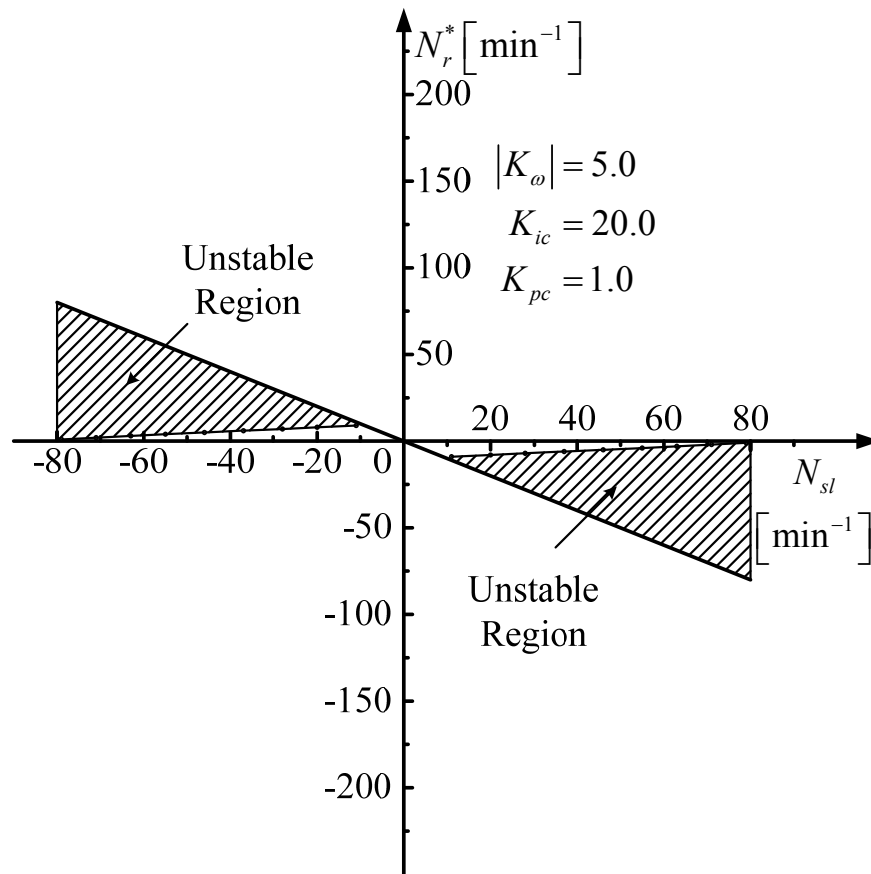


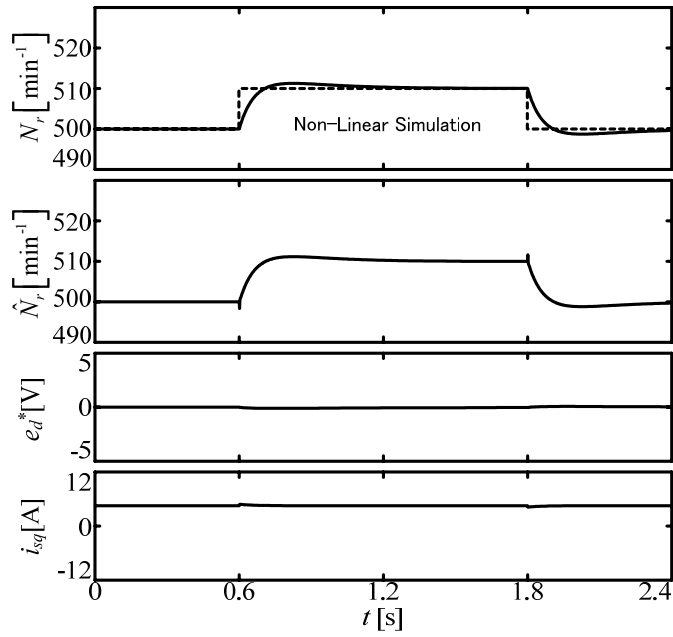
Fig.4.15 Unstable region with parameter $K_{pc} = 1.0$ of system B.

4.3 Simulation Results

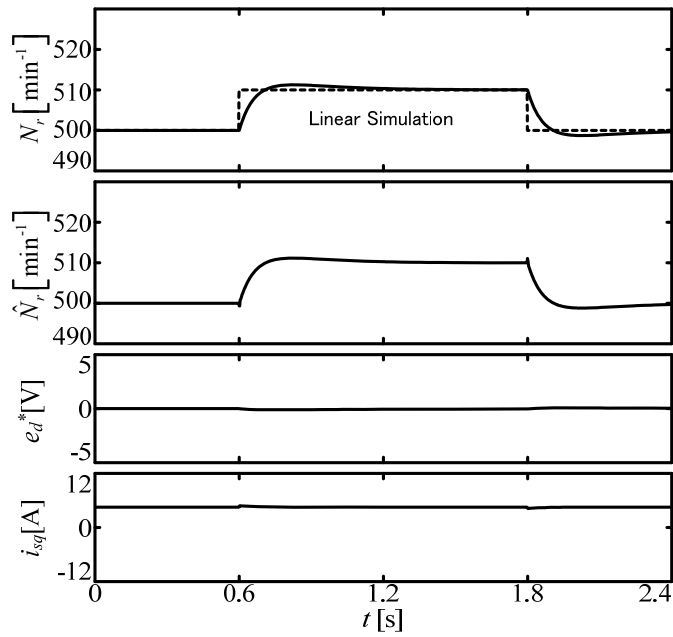
Figure 4.16 shows the simulation results of non-linear and linear models of system A. The simulation results of linear and non-linear are almost same. Therefore, the modeling of the system is appropriate. The parameters used in this simulations are $|K_{p\omega}|=20.0$, $|K_{i\omega}|= 20.0$ and $\omega_{sc} = 20.0$ for system A. In the case of system B, the result is shown in Fig. 4.17. For system B, the parameters are: $|K_{\omega}|=5.0$, $K_{ic} = 20.0$, and $K_{pc} = 1$. The load torque $T_L = 4.0$ N-m is selected.

In Figs.4.18, 4.20 and 4.22, the transient responses of system A and B are shown for the step change of speed command at motoring operation. These figures are correspondent to low-speed, medium-speed and high-speed operations. On the other hand, the transient responses at regenerating operations are shown in Figs 4.19, 4.21 and 4.23 for low-speed, medium-speed and high-speed operations respectively.

In system A, the estimated speed $\hat{\omega}_r$ is shown to compare with rotor speed, while in system B flux frequency ω^* is shown. Both systems A and B are stable in both regenerating and motoring operations.

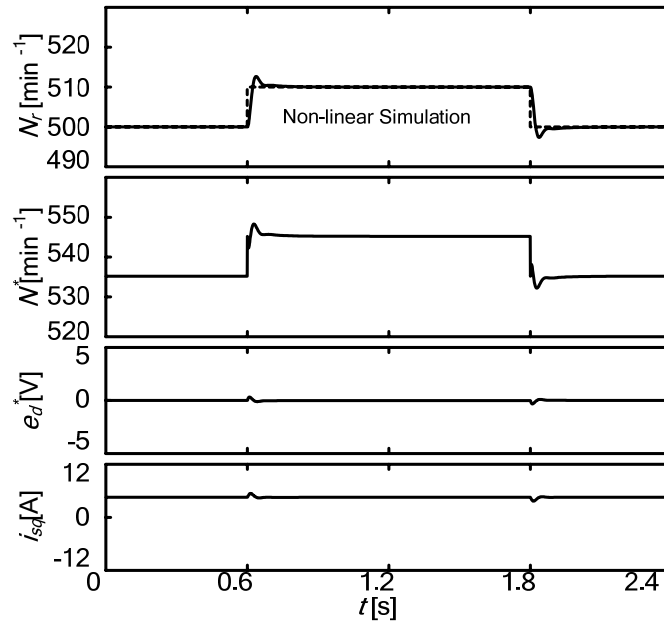


(a) Non-linear simulation

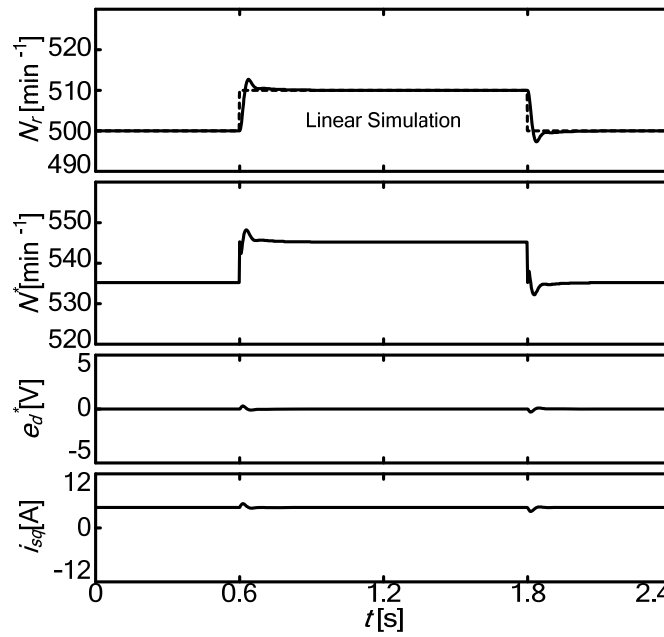


(b) Linear simulation

Fig.4.16 Transient responses in motoring operation of system A.

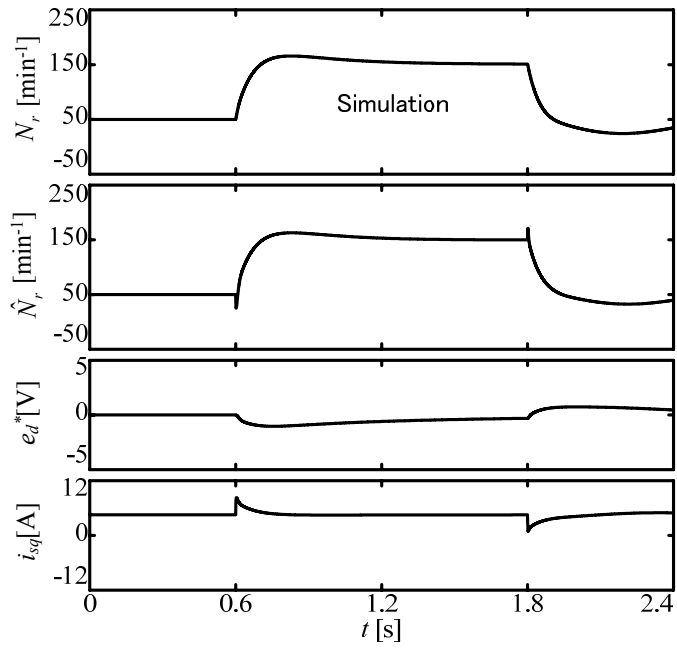


(a) Non-linear simulation

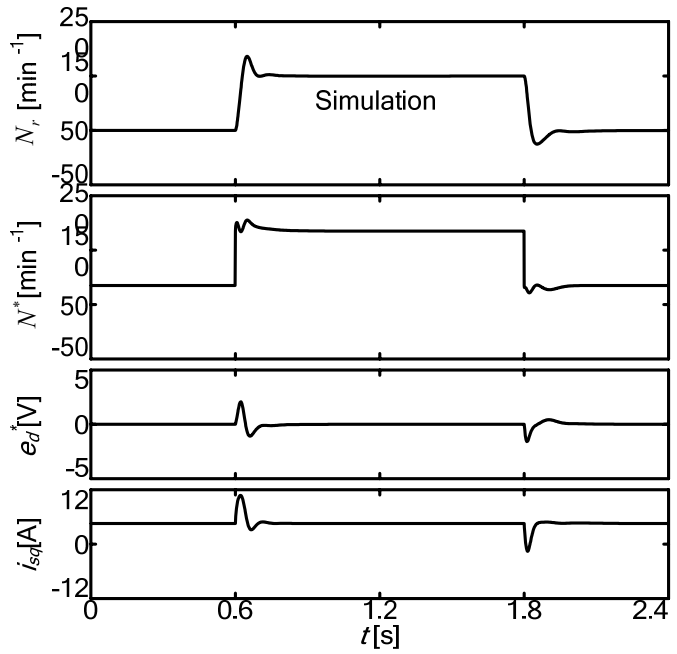


(b) Linear simulation

Fig.4.17 Transient responses in motoring operation of system B.

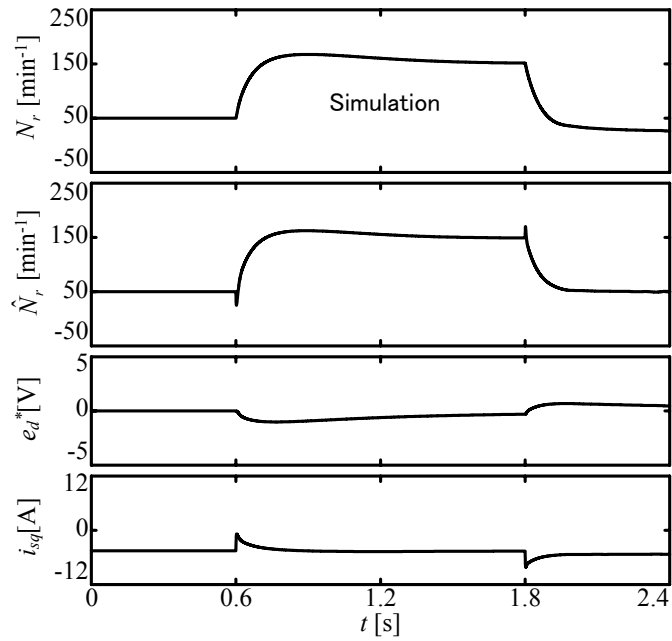


(a) System A

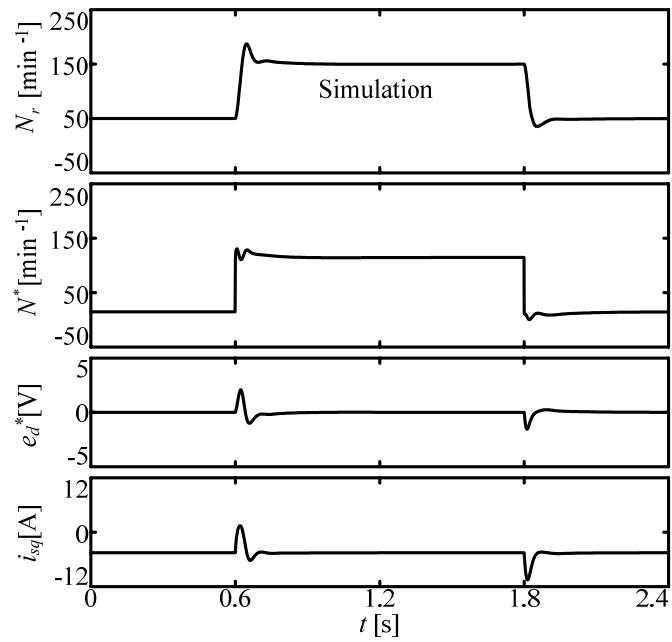


(b) System B

Fig.4.18 Transient response for the step change $50 \text{ min}^{-1} \rightarrow 150 \text{ min}^{-1} \rightarrow 50 \text{ min}^{-1}$ and $T_L = 4.0 \text{ N}\cdot\text{m}$ with selected parameters.

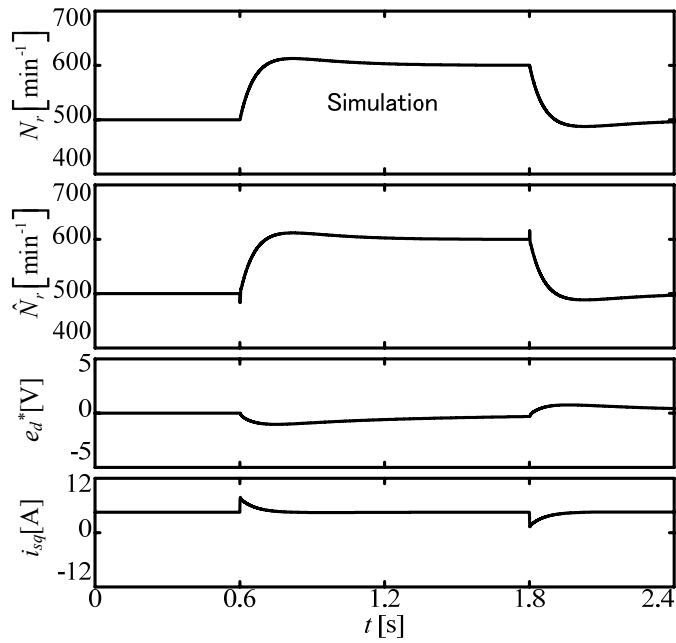


(a) System A

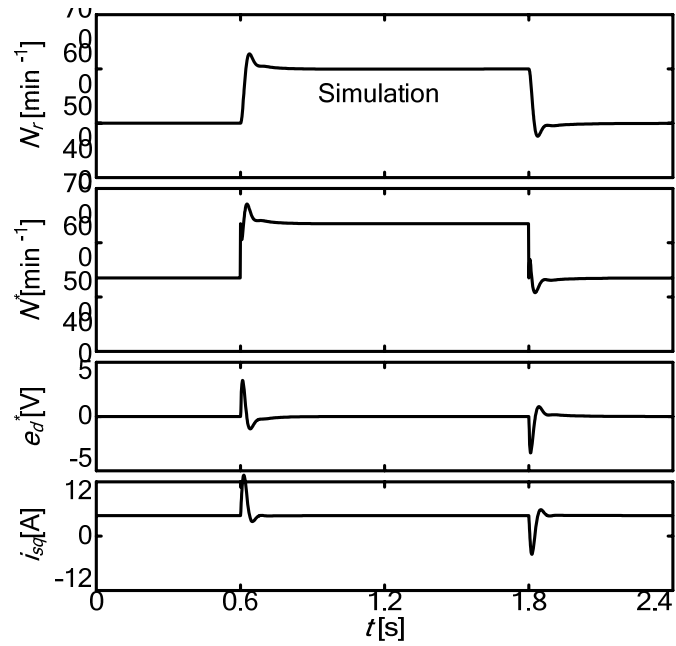


(b) System B

Fig.4.19 Transient response for the step change $50 \text{ min}^{-1} \rightarrow 150 \text{ min}^{-1} \rightarrow 50 \text{ min}^{-1}$ and $T_L = -4.0 \text{ N}\cdot\text{m}$ with selected parameters.

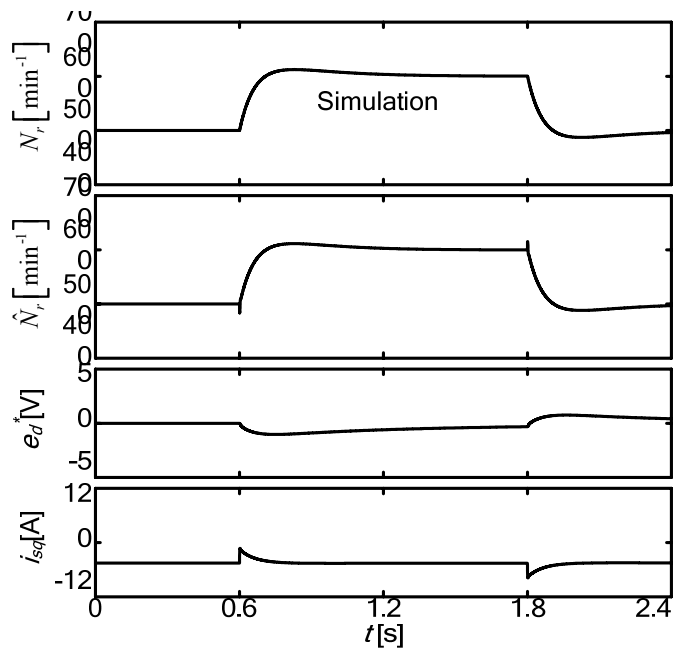


(a) System A

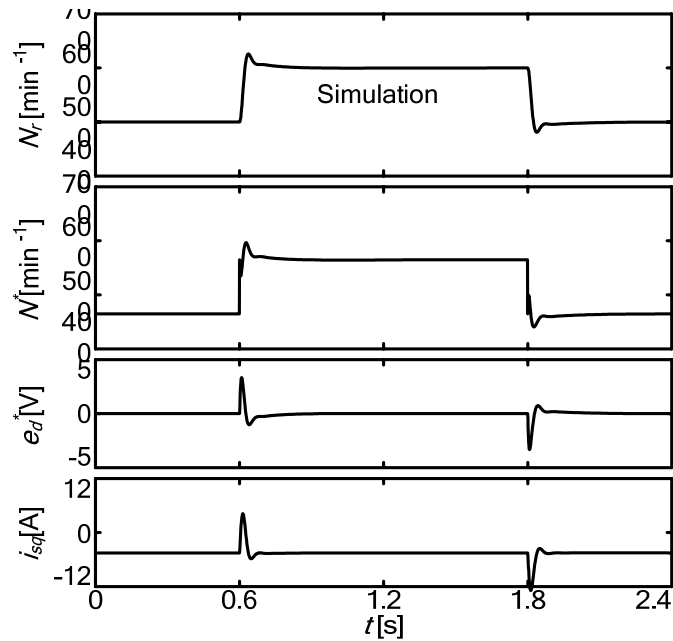


(b) System B

Fig.4.20 Transient response for the step change $500 \text{ min}^{-1} \rightarrow 600 \text{ min}^{-1} \rightarrow 500 \text{ min}^{-1}$ and $T_L = 4.0 \text{ N}\cdot\text{m}$ with selected parameters.

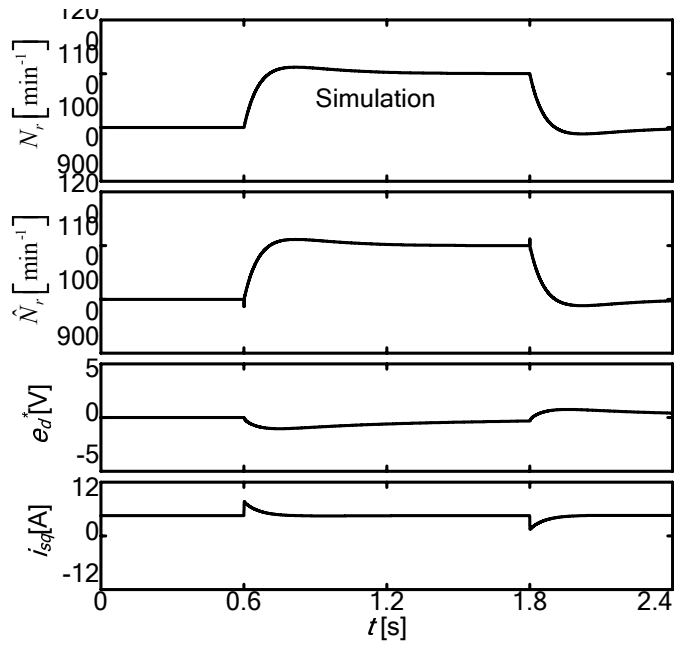


(a) System A

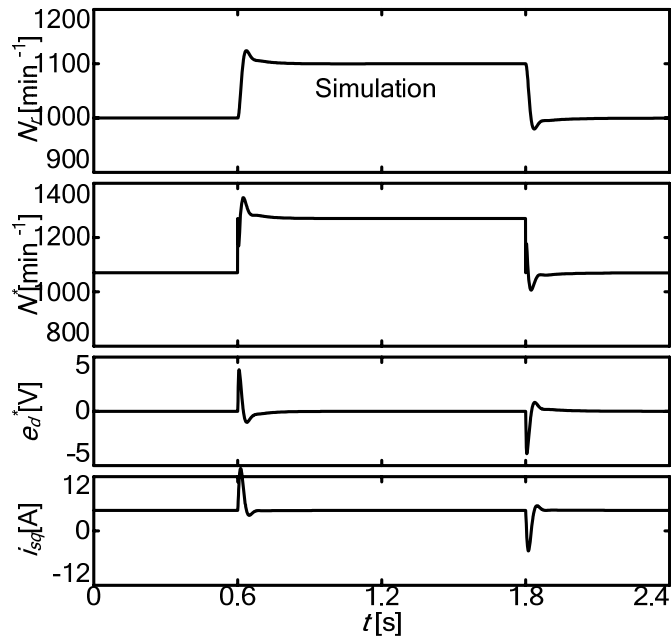


(b) System B

Fig.4.21 Transient response for the step change $500 \text{ min}^{-1} \rightarrow 600 \text{ min}^{-1} \rightarrow 500 \text{ min}^{-1}$ and $T_L = -4.0 \text{ N-m}$ with selected parameters.

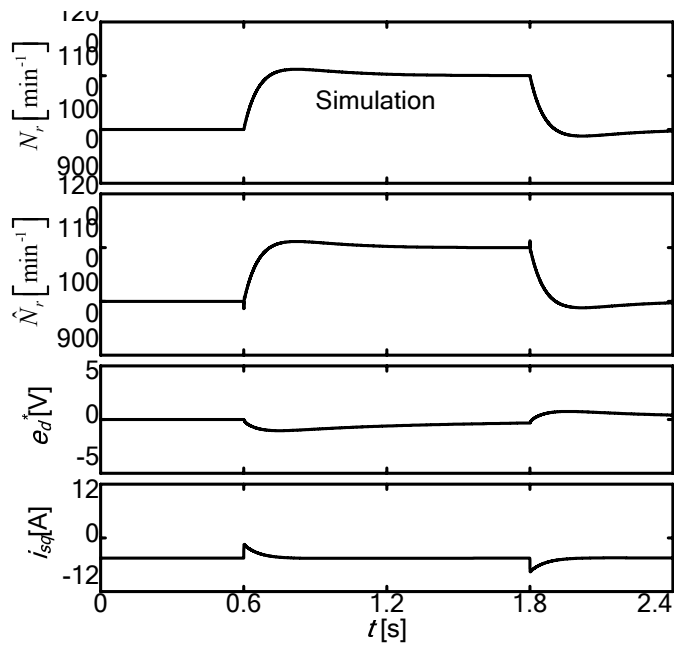


(a) System A

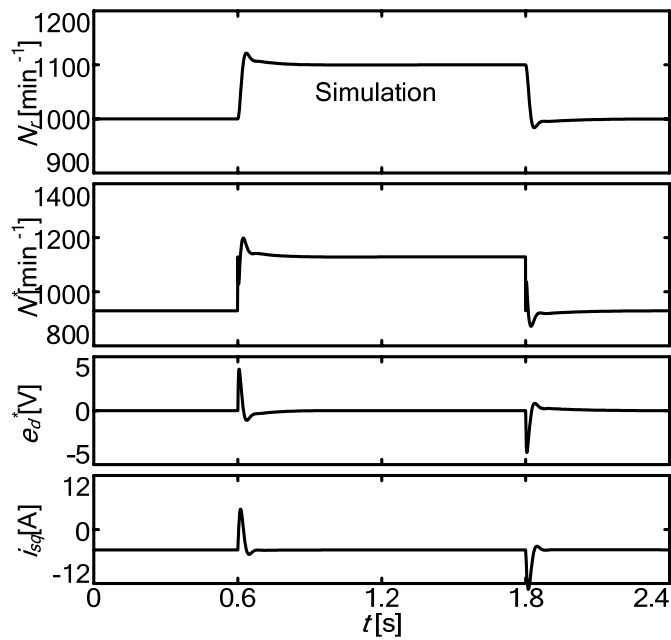


(b) System B

Fig.4.22 Transient response for the step change $1000 \text{ min}^{-1} \rightarrow 1100 \text{ min}^{-1} \rightarrow 1000 \text{ min}^{-1}$ and $T_L = 4.0 \text{ N}\cdot\text{m}$ with selected parameters.



(a) System A

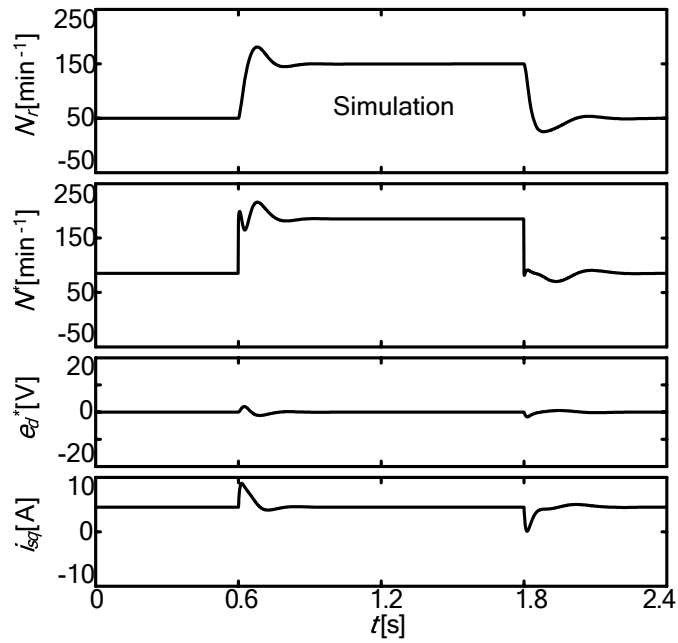


(b) System B

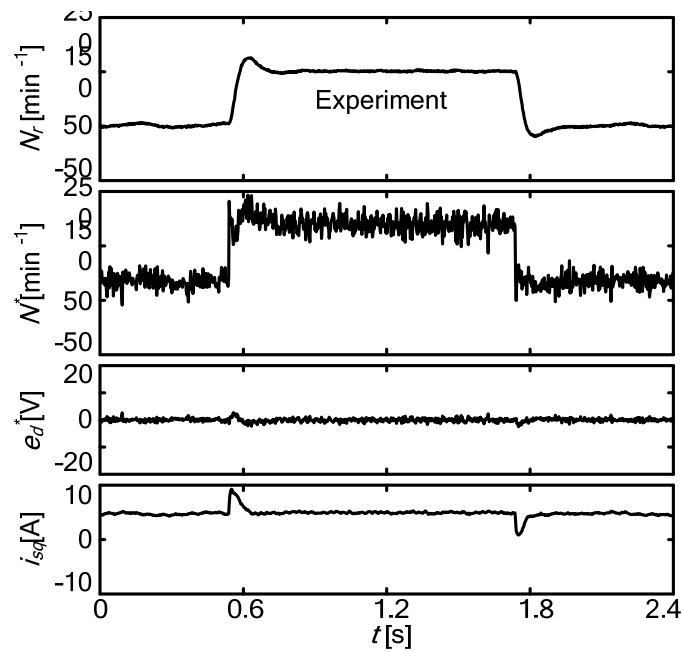
Fig.4.23 Transient response for the step change $1000 \text{ min}^{-1} \rightarrow 1100 \text{ min}^{-1} \rightarrow 1000 \text{ min}^{-1}$ and $T_L = -4.0 \text{ N-m}$ with selected parameters.

4.4 Experimental Results

All experimental results are shown in the case of system B. Figures 4.24, 4.25 and 4.26 shows the simulation and the experimental results for low, medium and high speed respectively. N_r is actual motor speed (ω_r) and N^* is synchronous speed (ω^*). The control parameters are set as $|K_\omega|=5.0$, $K_{ic}=20.0$ and $K_{pc}=0.0$. The load torque T_L is set to 4.0 N-m (half of rated torque). From these comparisons, the experimental results are very close to those of simulation. Therefore, the validity of proposed method is confirmed, except for high frequency ripples. The high frequency ripples of N^* and e_d^* are caused by PWM voltage control in experimental system. However, since the flux angle θ^* is obtained by integrating ω^* , the actual rotor speed has little ripples.

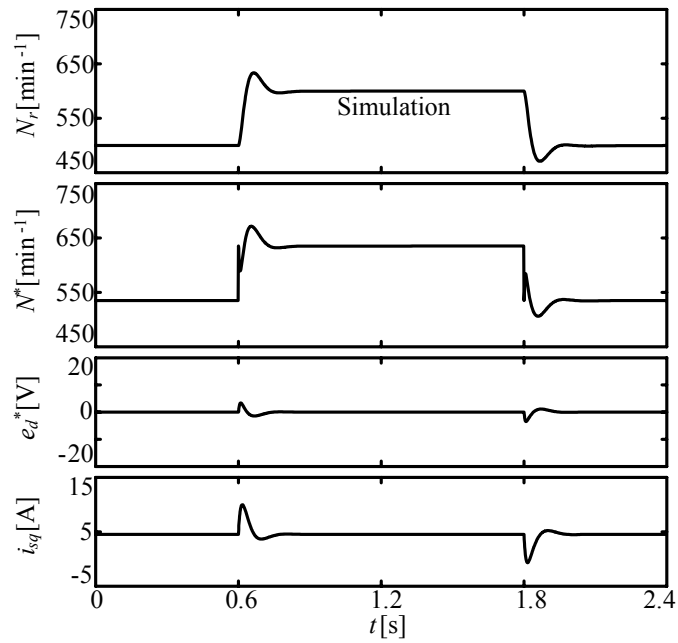


(a) Simulation

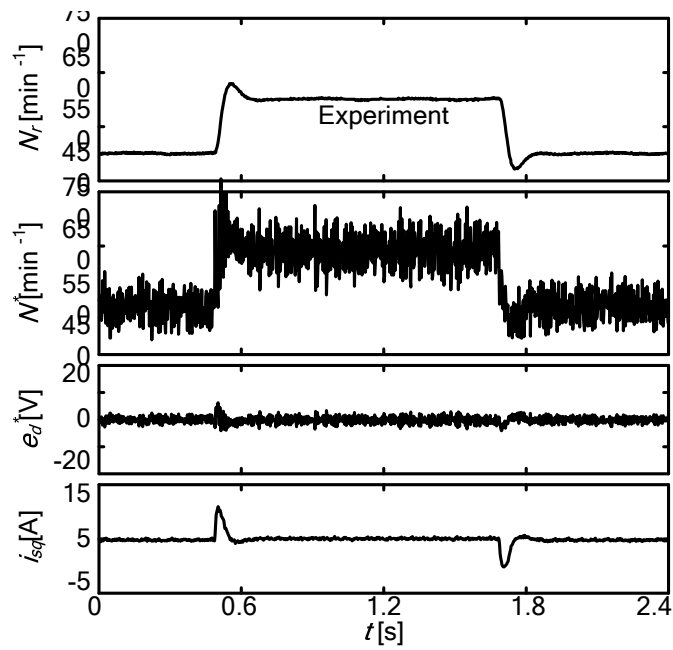


(b) Experiment

Fig.4.24 Transient response for the step change $50 \text{ min}^{-1} \rightarrow 150 \text{ min}^{-1} \rightarrow 50 \text{ min}^{-1}$ at $T_L = 4.0 \text{ N-m}$.

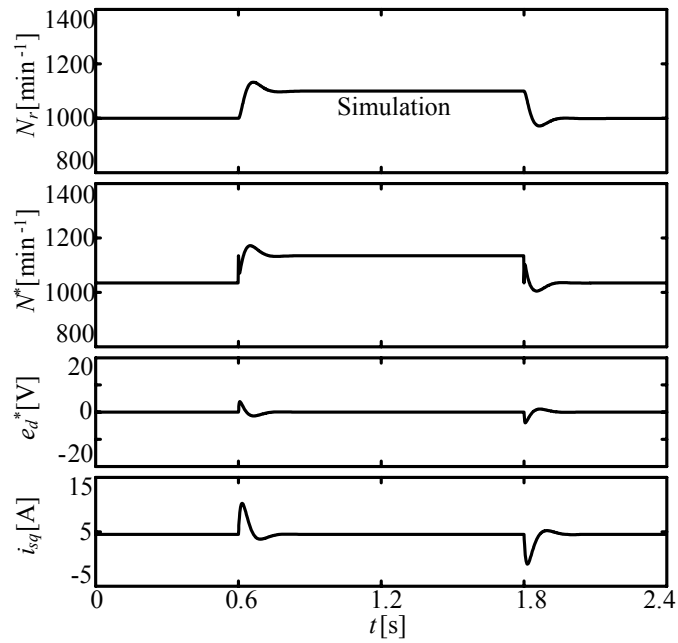


(a) Simulation

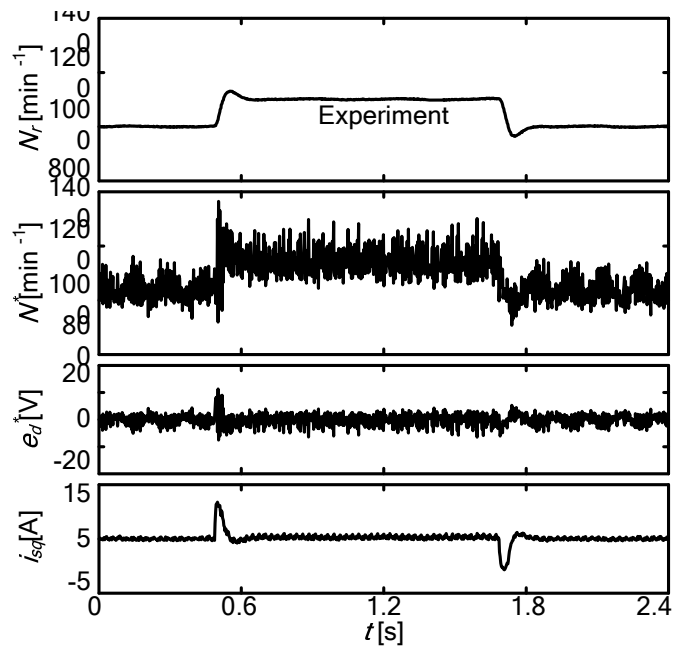


(b) Experiment

Fig.4.25 Transient for the step change $500 \text{ min}^{-1} \rightarrow 600 \text{ min}^{-1} \rightarrow 500 \text{ min}^{-1}$ at $T_L = 4.0 \text{ N-m}$.



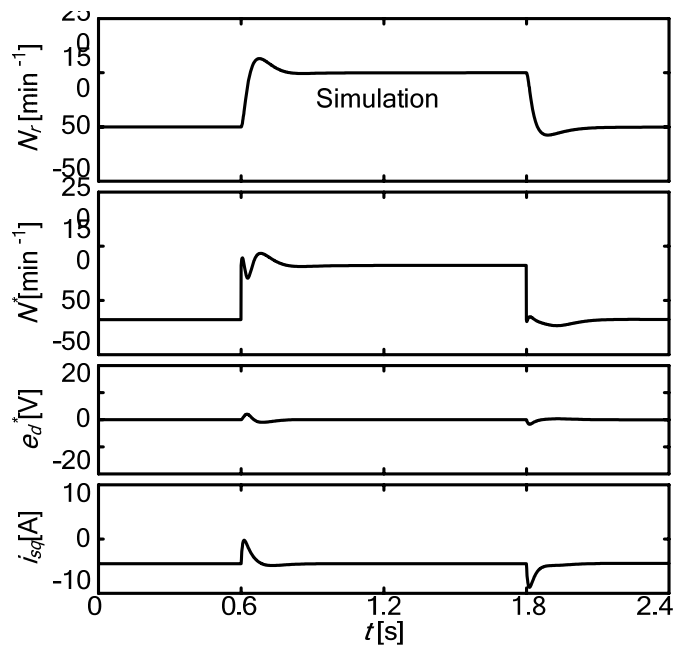
(a) Simulation



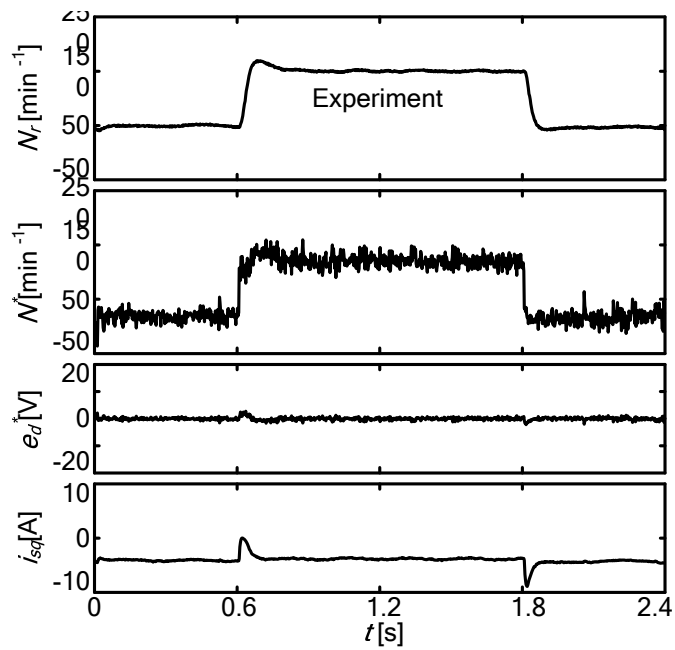
(b) Experiment

Fig.4.26 Transient response for the step change $1000 \text{ min}^{-1} \rightarrow 1100 \text{ min}^{-1} \rightarrow 1000 \text{ min}^{-1}$ at $T_L = 4.0 \text{ N-m}$.

Figures 4.27, 4.28 and 4.29 shows the simulation and the experimental result in regenerating operation. Same change of speed command are tested under the load torque $T_L = -4.0$ N-m for low, medium and high speed respectively. In any cases, quick responses of N_r are obtained. The high frequency ripples of N^* in Figs. 4.27, 4.28 and 4.29 are smaller than those in Figs. 4.24, 4.25 and 4.26. The reason for this difference can be considered that the amplitude modulation ratio of regenerating operation is smaller if the voltage control has allowance under limited DC-bus voltage; the distortion of stator currents is reduced. The larger we choose the gain $|K_\omega|$, the larger high frequency ripples of N^* are induced.

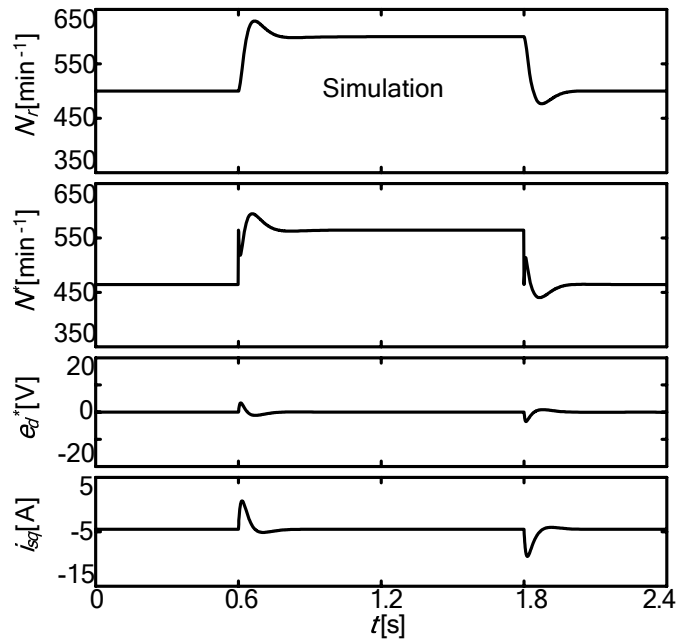


(a) Simulation

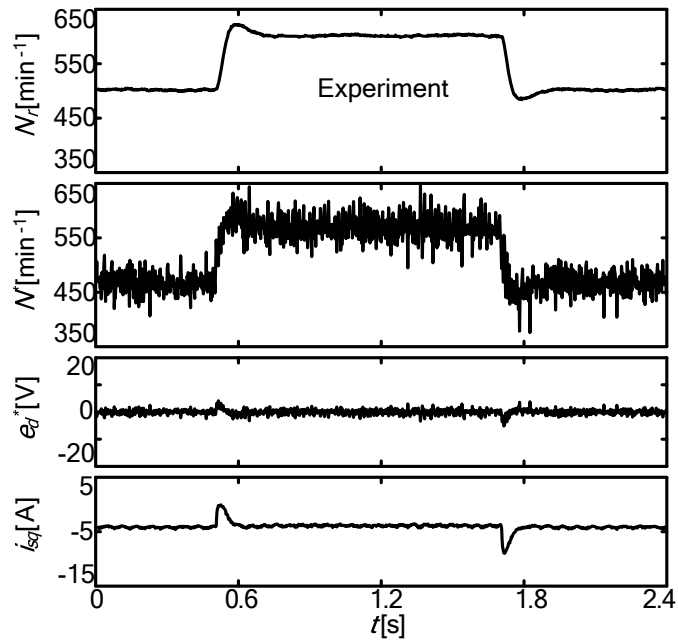


(b) Experiment

Fig.4.27 Transient response for the step change $50 \text{ min}^{-1} \rightarrow 150 \text{ min}^{-1} \rightarrow 50 \text{ min}^{-1}$ at $T_L = -4.0 \text{ N-m}$.

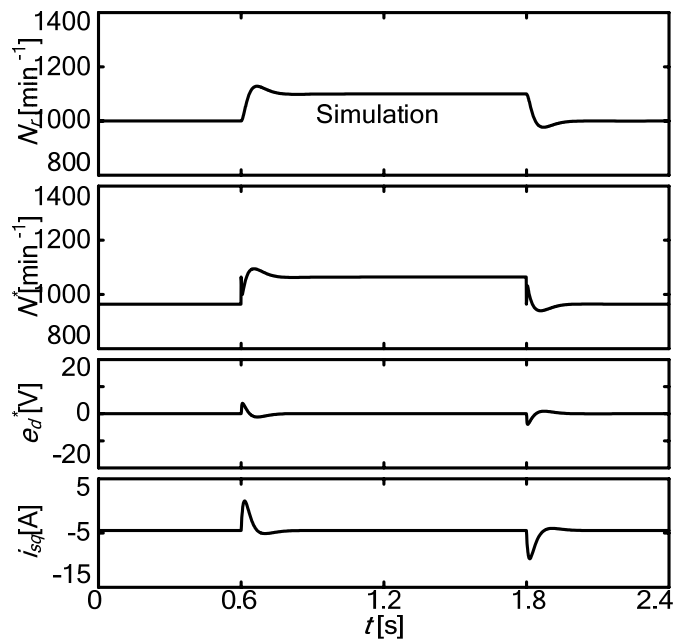


(a) Simulation

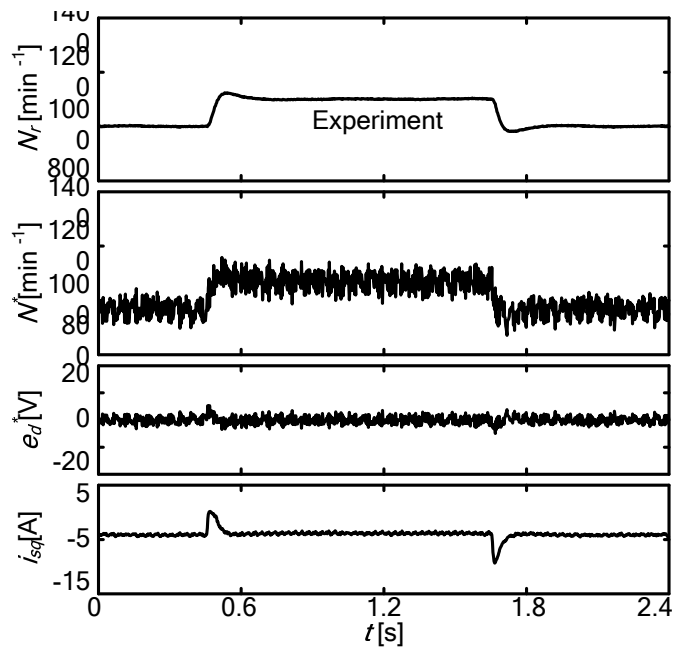


(b) Experiment

Fig.4.28 Transient for the step change $500 \text{ min}^{-1} \rightarrow 600 \text{ min}^{-1} \rightarrow 500 \text{ min}^{-1}$ at $T_L = -4.0 \text{ N-m}$.



(a) Simulation



(b) Experiment

Fig.4.29 Transient response for the step change $1000 \text{ min}^{-1} \rightarrow 1100 \text{ min}^{-1} \rightarrow 1000 \text{ min}^{-1}$ at $T_L = -4.0 \text{ N-m}$.

Figure 4.30 shows the transient responses of experiment for the step change of speed command from 100 min^{-1} to -100 min^{-1} and back to 100 min^{-1} . In this figure, the motor is driven between the operating points of motoring and regenerating through the unstable plugging region. It is observed that the system is operated stably. The control parameter $K_{pc} = 1.0$ is set for the following experiments.

Figure 4.31 shows the experimental results when the speed command is changed from 100 min^{-1} to 5 min^{-1} . In these case, the system can be operated stably. On the other hand, in Fig. 4.32, the speed command is changed from 100 min^{-1} to -25 min^{-1} . The system becomes unstable at plugging region and is operated using speed sensor for the protection after $t = 0.98\text{s}$. This experimental result can prove the unstable region of Fig.4.15.

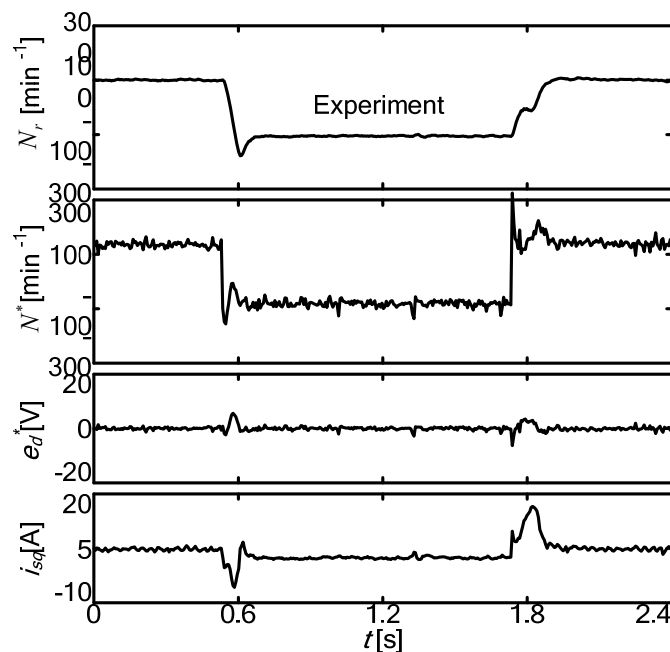


Fig.4.30 Transient response for the step change $100 \text{ min}^{-1} \rightarrow -100 \text{ min}^{-1} \rightarrow 100 \text{ min}^{-1}$ at $T_L = 4.0 \text{ N}\cdot\text{m}$.

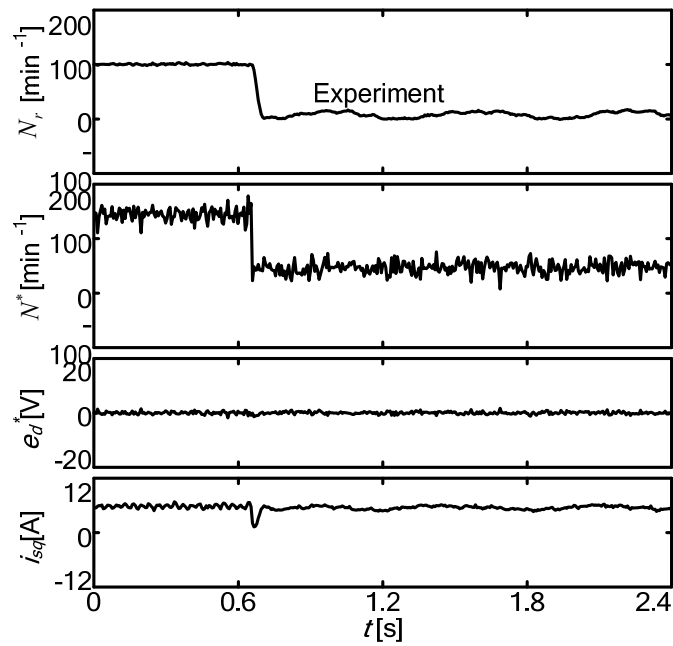


Fig.4.31 Transient response for the step change $100 \text{ min}^{-1} \rightarrow 5 \text{ min}^{-1}$ at $T_L = 5.0 \text{ N-m}$.

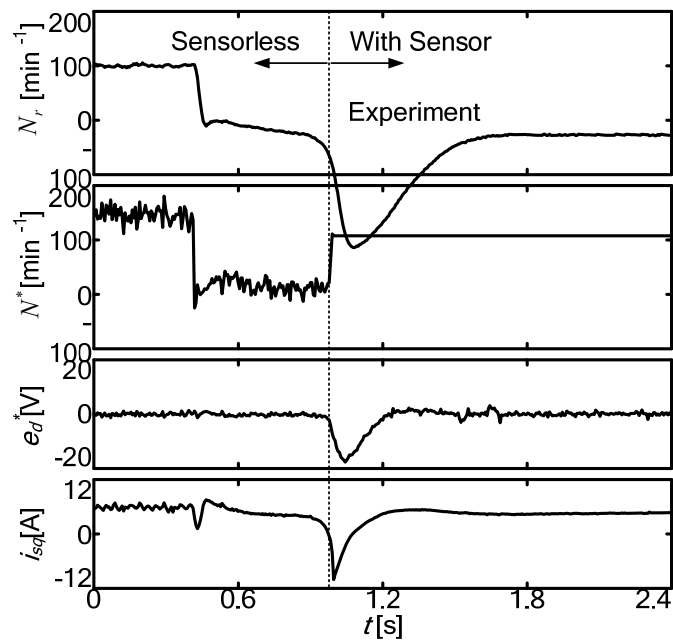


Fig.4.32 Transient response for the step change $100 \text{ min}^{-1} \rightarrow -25 \text{ min}^{-1}$ at $T_L = 5.0 \text{ N-m}$.

Moreover, Figs.4.33 and 4.34 shows the experimental results for the step change of the speed command N_r^* with speed changed $50 \text{ min}^{-1} \rightarrow 150 \text{ min}^{-1} \rightarrow 50 \text{ min}^{-1}$ corresponding to Fig.4.18 (b) and 4.19 (b) in motoring and regenerating operation respectively. These figures can compare the responses of actual rotor speed N_r for control parameter $K_{pc} = 1.0$.

Figure 4.35 shows the transient response at no-load condition ($T_L \approx 0$), with speed changed $50 \text{ min}^{-1} \rightarrow 150 \text{ min}^{-1} \rightarrow 50 \text{ min}^{-1}$ corresponding to Figs. 4.33 and 4.34. The speed responses give almost the same characteristics for each load torque. However, the i_{sq} differs from each parameter of T_L .

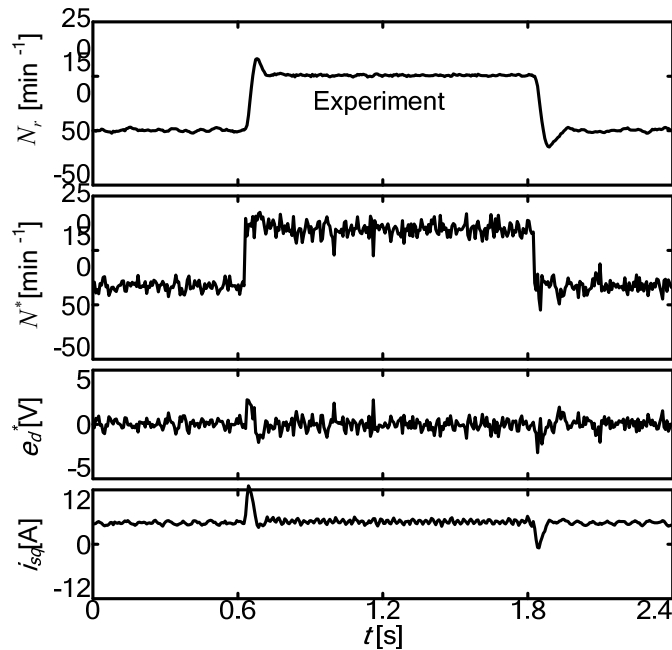


Fig.4.33 Transient response for the step change $50 \text{ min}^{-1} \rightarrow 150 \text{ min}^{-1} \rightarrow 50 \text{ min}^{-1}$ at $T_L = 4.0 \text{ N-m}$.

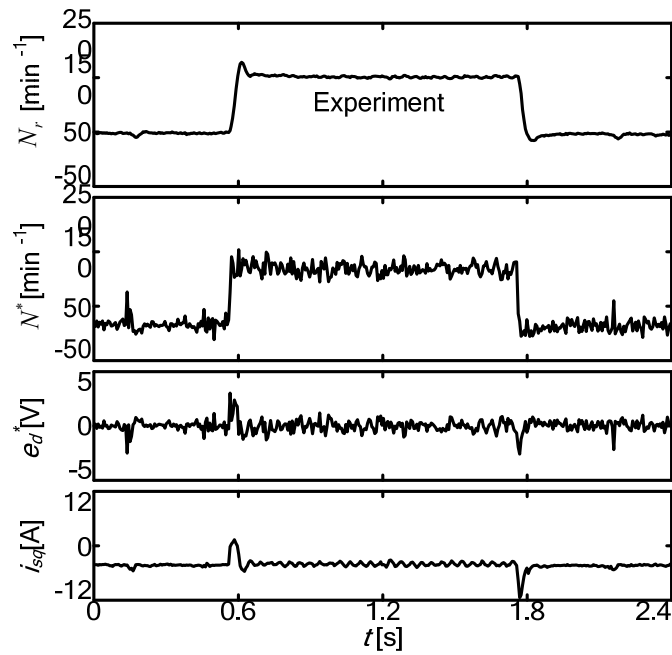


Fig.4.34 Transient response for the step change $50 \text{ min}^{-1} \rightarrow 150 \text{ min}^{-1} \rightarrow 50 \text{ min}^{-1}$ at $T_L = -4.0 \text{ N-m}$.

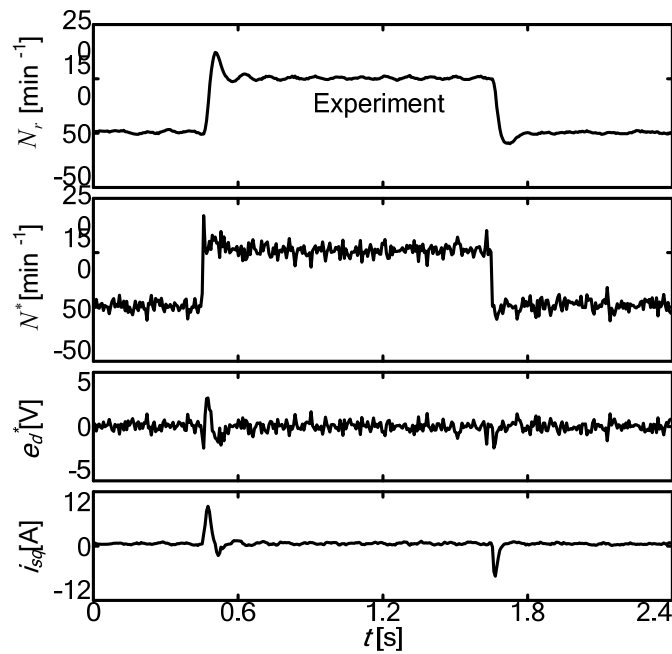


Fig.4.35 Transient response for the step change $50 \text{ min}^{-1} \rightarrow 150 \text{ min}^{-1} \rightarrow 50 \text{ min}^{-1}$ at $T_L \approx 0 \text{ N-m}$.

Chapter 5

Conclusion

Study on simplified speed sensorless vector control system for induction motors is described in this thesis. The results obtained from this study are summarized as follows:

- (1) New simplified speed sensorless vector control methods of IM based on rotor flux linkage are proposed. The two simplified sensorless systems are called as system A and system B. In both methods, the q – axis flux is obtained by the output voltage of d – axis PI current controller with a non-interference control.
- (2) In system A, the angular frequency of rotor flux is estimated to bring q – axis flux to zero by using PI controller. The flux angle is obtained by integrating the angular frequency. The rotor speed is computed by subtracting a slip speed from the angular frequency.
- (3) In system B, the computation of q – axis flux is as same as the system A. The angular frequency of rotor flux is computed by subtracting the q – axis flux from the speed command adding with a slip speed. The q – axis flux is also used to control the rotor speed by adjusting the q – axis flux. The flux angle is obtained by integrating the angular frequency.

- (4) In both systems A and B, the q – axis flux is obtained from voltage model, in which the derivative term of the d – axis flux is assumed zero because of constant magnetizing current command. A flux angle of a current model is aligned with the flux angle of voltage model by changing the angular frequency of current model. Since the output voltage of d – axis PI current controller is used for the flux angle estimation and speed control (q – axis voltage control), the system is simplified and stabilized at regenerating mode.
- (5) By choosing a reference frame which rotates synchronously with the computed flux angle, non-linear models are derived in both proposed systems A and B. From these non-linear models, linear models of the systems are derived in state space equations by considering a small perturbation around a steady-state operating point.
- (6) The performance of both systems A and B are compared by using linear models and non-linear models. Transient responses of linear models and non-linear models are computed and compared. Since both responses are almost same around a steady state operating point, the validity of the linear models are confirmed. By using the linear models, the system stability is studied by showing root loci.
- (7) In plugging mode of both systems, most of the poles of the root-loci are located on the positive real axis, it means the system becomes unstable. In motoring and regenerating operations of systems A and B, all poles are located in the left half plane. Therefore, the system is stable in both operations.
- (8) By virtue of the stability analysis, we can design the parameters of controller in both systems.

- (9) A digital signal processor (DSP) based PWM inverter fed IM system is equipped and tested. It is confirmed that the experimental results are very close to those of non-linear simulation except for high frequency ripples. Therefore, the effectiveness of the proposed methods are also demonstrated experimentally.
- (10) The nonlinear simulation and experimental results of the proposed system show stable and quick transient responses in both motoring and regenerating modes.
- (11) By using PI speed control (q – axis voltage control), the unstable region is improved comparing with the case of I control in system B.
- (12) It is considered that the system B is superior to the system A because its simple structure in the case of speed control applications.

References

- [1] C. Schauder, “Adaptive speed identification for vector control of induction motors without rotational transducers”, *IEEE Trans. Ind. Appl.*, vol.28, No.5, pp. 1054–1061 (1992)
- [2] H. Tajima, Y. Hori, “Speed sensorless field-orientation control of the induction machine”, *IEEE Trans.Ind. Appl.*, vol. 29, No.1, pp. 175–180, (1993)
- [3] H. Kubota, K. Matsuse, and T. Nakano “DSP-based speed adaptive flux observer of induction motor”, *IEEE Trans. Ind. Appl.*, vol.29, No.2, pp. 344–348 (1993)
- [4] J. Holtz, “Speed estimation and sensorless control of AC drive”, *Conf. Rec. IEEE-IECON*, pp. 649 – 654 (1993)
- [5] H. Kubota, K. Matsuse, “Speed sensorless field oriented control of induction motor with rotor resistance adaptation”, *Conf. Rec. IEEE-IAS Ann. Mtg.*, pp. 414 – 418 (1993)
- [6] T. Kanmachi, I. Takahashi, “Sensorless speed control of an induction motor with no influence of secondary resistance variation”, *Proc.of IEEE IAS Ann. Mtg.*, pp. 408 – 413 (1993)

- [7] M. Tsuji, E. Yamada, K. Izumi and J. Oyama, “A flux observer based vector control of a controlled current source-fed induction motor”, *Trans. IEE Japan*, vol.113-D, No.10, pp.1145 – 1153 (1993)
- [8] M. Tsuji, E. Yamada, K. Izumi and J. Oyama, “Stability analysis of a controlled-current source-fed induction motor vector control system without a speed sensor”, *Electrical Engineering in Japan*, vol.114, No.1, pp.78 – 87 (1994) (in Japanese)
- [9] C. Ilaş, A. Bettini, L. Ferraris, G. Griva, F. Profumo, “Comparison of different schemes without shaft sensors for field oriented control drives”, *Proc. of the 20th int. Conf. on Industrial Electronics, Control and Instrumentation, IEEE-IECON*, pp. 1579 – 1588 (1994)
- [10] H. Kubota, M. Tsuji, “Online tuning of induction machine parameters”, *National Convention Rec. IEE Japan IAS Symposium*, pp.s69 – s74 (1995) (in Japanese)
- [11] T. Kanmachi, I. Takahashi, “A secondary resistance calculation method for sensorless speed control of an induction motor”, *Proc. IPEC-Yokohama '95*, pp.1671 – 1676 (1995)
- [12] P. K. Kovacs, “Transient phenomena in electrical machine”, *Elsevier*, 1984
- [13] P. C. Krause, “Analysis of electric machinery”, *McGraw-Hill Book Company*, 1986

- [14] P. Vas, “Sensorless vector and direct torque control”, *Oxford University Press*, 1998
- [15] M. Tsuji, S. Chen, K. Izumi, T. Ohta, E. Yamada, “A speed sensorless induction motor vector control system using q -axis flux with parameter identification”, *Conf. Rec. IEEE-IECON*, pp. 960 – 965 (1997)
- [16] M. Tsuji, E. Yamada, F. Parasiliti, M. Tursini, “A digital parameter identification for a vector controlled induction motor”, *Proc. of EPE*, pp.4.603 – 4.608 (1997)
- [17] J. S. Lee, T. Takeshita, N. Matsui, “Stator-flux oriented sensorless induction motor drive for optimum low-speed performance”, *IEEE Trans. Ind. Application*, vol.33, No.5, pp. 1170 – 1176 (1997)
- [18] H. Umida, “The system configuration of speed sensorless vector control”, *Trans. IEE Japan*, vol.117-D, No.5, pp.541 – 543 (1997) (in Japanese)
- [19] M. Tsuji, S. Doki, “Advanced vector control for accurate torque control”, *National Conv. Rec. IEE Japan IAS*, pp.s3 – s8 (1997)
- [20] T. Noguchi, S. Kondo, I. Takahashi, “Field-oriented control of an induction motor with robust online tuning of its parameters”, *IEEE Trans. Ind. Applications*, vol.33, No.1, pp.35 – 42 (1997)

- [21] M. Tsuji, H. Li, K. Izumi, E. Yamada, "A generalized method of controlled voltage source-fed induction motor vector control using the observer theory, *Electrical Engineering in Japan*, vol.119, No.4, pp. 66 – 76 (1997)
- [22] H. Kubota, K. Matsuse, and Y. Hori, "Behavior of sensorless induction motor drives in regenerating mode", *Proc.PCC-Nagaoka'97*, pp.549 – 552 (1997)
- [23] K. D. Hurst, T. G. Habetler, G. Griva, and F. Profumo, "Zero-speed tachless IM torque control: Simply a matter of stator voltage integration", *IEEE Trans. Ind. Applicat.*, vol.34, pp.790 – 795 (1998)
- [24] M. Tursini, R. Petrella, and F. Parasiliti, "Adaptive sliding-mode observer for speed sensorless control of induction motors", *IEEE Trans. Ind. Appl.*, vol.36, No.5, pp.1380-1387 (2000)
- [25] T. Hamajima, M. Hasegawa, S. Doki, and S. Okuma, "Sensorless vector control of induction motor with stator resistance identification based on augmented error", *Proc. of Power Conversion Conf.(PCC-Osaka)*, pp. 504 - 509 (2002)
- [26] S. Suwankawin and S. Sangwongwanich, "A speed-sensorless IM drive with decoupling control and stability analysis of speed estimation", *IEEE Trans. Ind. Electron.*, vol.49, No.2, pp. 444 – 455 (2002)
- [27] M. Hinkkanen, "Analysis and design of full-order flux observers for sensorless induction motors", *IEEE Trans. Ind. Electron.*, vol.51, No.5, pp. 1033 – 1040 (2004)

- [28] M. Hinkkanen and J. Luomi, “Stabilization of regenerating-mode operation in sensorless induction motor drives by full-order flux observer design”, *IEEE Trans. Ind. Electron.*, vol.51, No.6, pp. 1318 – 1328 (2004)
- [29] M. Saejia and S. Sangwongwanich, “Averaging analysis approach for stability analysis of speed-sensorless induction motor drives with stator resistance estimation”, *IEEE Trans. Ind. Electron.*, vol.53, No.1, pp. 162–177 (2006)
- [30] C. Lascu, I. Boldea, and F. Blaabjerg, “A class of speed-sensorless sliding-mode observers for high-performance induction motor drives”, *IEEE Trans. Ind. Electron.*, vol.56, No.9, pp. 3394–3403 (2009)
- [31] L. Harnefors and M. Hinkkanen, “Complete stability of reduced-order and full-order observers for sensorless IM drives”, *IEEE Trans. Ind. Electron.*, vol. 55, No.3, pp. 1319 – 1329 (2008)
- [32] M. Hinkkanen, L. Harnefors, and J. Luomi, “Reduced-order flux observer with stator-resistance adaptation for speed sensorless induction motor drives”, *IEEE Trans. Power Electron.*, vol.25, No.5, pp. 1173–1183 (2010)
- [33] T. Okuyama, N. Fujimoto, H. Fujii, “Simplified vector control system without speed and voltage sensors – effects of setting errors in control parameters and their compensation –”, *Trans. IEE Japan*, vol.110-D, pp. 477 – 486 (1990) (in Japanese)

- [34] S. Ishida, T. Endo, H. Fujii, H. Tomita, N. Fujimoto, “Sensorless vector control with quick response for general purpose inverters” *Proc. of Power Conversion Conf. (PCC-Yokohama)* pp. 467 – 472 (1993)
- [35] H. Tajima, Y. Matsumoto, H. Umida, and M. Kawano, “Speed sensorless vector control method for an industrial drive system”, *Proc. of International Power Electronics Conference (IPEC-Yokohama)* , pp.1034–1039 (1995)
- [36] K. Kondo and K. Yuki, “Study on an application of induction motor speed sensorless vector control to railway vehicle traction”, *Trans. IEE Japan*, vol.125-D, pp. 1–8 (2005) (in Japanese)
- [37] N. Yamamura, K. Aiba, Y. Tsunehiro, “Primary flux control for induction motor drive”, *Trans. IEE Japan*, vol.113-D, pp.859 – 864 (1993) (in Japanese)
- [38] N. Yamamura, I. Yasuoka, N. Nanato, Y. Tsunehiro, “A method for improving the performance characteristics of induction motor with primary flux control”, *Trans. IEE Japan*, vol.119-D, pp. 371 – 376 (1999) (in Japanese)
- [39] M. Tsuji, S. Chen, K. Izumi, and E. Yamada, “A sensorless vector control system for induction motors using q -axis flux with stator resistance identification”, *IEEE Trans. Ind. Electron.*, vol.48, No.1, pp. 185–194 (2001)

- [40] M. Tsuji, S. Chen, T. Kai, S. Hamasaki, “Q-axis flux-based sensorless vector control of induction motor taking into account iron loss”, *IEEJ Trans. IA*, vol.126, No.12, pp.1645–1651 (2006)
- [41] M. Tsuji, G. M. C. Mangindaan, Y. Kunizaki, R. Hashimoto and S. Hamasaki, “A New Simplified Sensorless Speed Control of Induction Motor using d -axis Voltage”, *Proc. of The 15th International Conference on Electrical Machines and Systems (ICEMS)*, 6 pages (2012.10)
- [42] G. M. C. Mangindaan, M. Tsuji and S. Hamasaki, “Transient Characteristics of a New Simplified Speed Sensorless Vector Control for Induction Motors”, *Proc. of The 16th International Conference on Electrical Machines and Systems (ICEMS)*, 6 pages (2013.10)
- [43] M. Tsuji, G. M. Ch. Mangindaan, Y. Kunizaki and S. Hamasaki, “Simplified Speed-Sensorless Vector Control for Induction Motors and Stability Analysis”, *IEEJ Journal of Industry Applications*, Vol.3, No.2, pp.138 – 145, (2014.3)
- [44] G. M. Ch. Mangindaan, M. Tsuji, S. Hamasaki, ”Stability Comparison of New Simplified Speed Sensorless Vector Control System for Induction Motors”, *Journal of International Conference on Electrical Machines and Systems*, Vol.3. No.2, pp.126 – 131, (2014.6)
- [45] H. Sugimoto, M. Koyama, S. Tamai, ”AC Servo System no Riron to Sekkei no Jissai”, *So-Go Den-Shi Syuppan* (1990) (in Japanese)

Acknowledgment

I used this opportunity to express my gratitude to my supervisor, Professor Mineo Tsuji, for the supervision and guidance that inspired me to realize this thesis. His enthusiasm, encouragements have been extremely helpful. He was always available for my questions and he spent generously his time. He always advised me to discover the solution while leading me to the right basic, concept, and perception. My thankful also to Assistant Professor Shinichi Hamasaki for his contributions, assistance and provision.

I would like to express my honest thank to my committee members of the dissertation, Professor Tsuyoshi Higuchi and Professor Takahiko Yamashita for their assessment, instruct and valuable criticism.

I would also like to thank Ms.Yurika Kunizaki for her contribution, support and guidance.

I received financial support from BPPLN-governmental Higher Education of the Republic of Indonesia.

Last but not least are my family, my wife Susan Marlein Mambu, my daughters Keensy Aimee Hendrika Mangindaan and Jeska Queency Javelin Mangindaan. They are supporting me spiritually all through my life to work for my Ph.D. in engineering.

Glanny Martial Christiaan Mangindaan

Nagasaki University